A STUDY OF HIGH TEMPERATURE TENSION AND COMPRESSION CREEP BEHAVIOUR

A SUMMARY OF THE THESIS SUBMITTED BY C.A. WALKER, B.Sc., FOR THE DEGREE OF DOCTOR OF PHILOSOPHY IN THE FACULTY OF ENGINEERING OF THE UNIVERSITY OF GLASGOW.

The origins of thermal fatigue are first considered, with reference to the turbine blades of jet turbine aero-engines. The relationship between this problem and the investigation described in the thesis is then explained. A detailed descriptio follows of the development and structure of the alloy to be tested - Nimonic 105.

To enable a systematic understanding of the creep curves produced experimentally, the theory of creep in two-phase alloys is reviewed, and in view of the high test temperatures involved, an examination is included of the time dependent changes occurring in two-phase systems produced by precipitation from a supersaturated solid solution. The literature review is conclude with a survey of previous relevant creep investigations, in particular those carried out to compare tensile and compressive creep behaviour.

The development of tensile and compressive creep apparatus is described, including detailed consideration of the design of compressive loading devices, and of a creep furnace made in two halves specially designed to suit the type of compressive creep machine chosen.

Details/

ProQuest LLC.
789 East Eisenhower Parkway
P.O. Box 1346
Ann Arbor, MI 48106 – 1346

Details of the experimental procedure are discussed at some length since they explain the small scatter obtained in the creep data. As well as the sequence followed in the creep tests, a description is included of the metallographic examination of specimens after creep testing.

The results of the creep testing programme are given as a series of graphs of creep strain versus time. Since the tests were carried out at constant load, a procedure is developed for correcting the constant load creep curves to constant stress curves. A knowledge of the strain-rate dependence upon stress is necessary for this correction. This dependence has been measured, and its significance is discussed. Since the theoretical discussion showed that the strain rate dependence upon temperature varied from one nickel alloy to another, the activation energy for creep was measured, both in tension and compression. The resulting values are discussed, both in relation to each other, and to the values found by other workers. The discussion of results ends with a critical comparison between the creep curves measured in tension and compression, which involves a detailed consideration of the nucleation and growth of cracks during creep deformation.

The relevance of the Bauschinger effect to thermal fatigue prediction, is pointed out, and the present state of understanding of this effect in two-phase alloys is outlined. The development of a device to measure this effect at high temperature is described.

The final chapter draws together the conclusions from the rest of the Thesis and discusses their more general significance in the experimental and theoretical investigation of time-dependent deformation.

A STUDY OF HIGH TEMPERATURE TENSION AND COMPRESSION CREEP BEHAVIOUR

by

COLIN A. WALKER, B.Sc.

A Thesis submitted for the Degree of Doctor of Philosophy in the Faculty of Engineering of the University of Glasgow.

Engineering Laboratories
University of Glasgow
Glasgow, W.2.

October, 1967.

ACKNOWLEDGEMENTS

The author wishes to thank the University of Glasgow for the provision of laboratory facilities, and Rolls-Royce Limited, Aero-Engine Division, Derby., for financial and technical support.

Acknowledgement is also made here of the assistance received from Professor J.D. Robson, Dr. P. Hancock, and other members of the staff of the Faculty of Engineering. Due note is taken of the help, both spiritual and physical, received from the research students and technical staff of the Materials Laboratory.

TABLE OF CONTENTS

CHAPTER ONE

CHAPTER ONE

INTRODUCTION

1.1 The Problem of Creep and Thermal Fatigue.

At temperatures considerably below half the absolute melting point (T_m) of a metal, the assumption may be made that stress and strain are uniquely related. This assumtion no longer holds at temperatures approaching and in excess of half T_m. It is found that a test piece impressed with a constant tensile stress extends with time. This phenomenon is known as creep, and during the past hundred years, creep has commanded ever increasing attention from engineers and metallurgists as the working temperatures of machinery have been increased. Typical temperatures encountered in high temperature environments are the 3000°C encountered by space vehicles re-entering the atmosphere; 1000°C in a gas-turbine aero-engine and 600°C in a steam turbo-generator. Since the long-range purpose of this investigation is to assist the economic usage of aircraft engines the temperature of interest here is the second of these.

The general mode of operation of all jet engines is the same in that air is drawn in and compressed, prior to burning and rearward ejection, in an axial flow compressor, which derives its power from a turbine driven by the outflowing gases. The combination of high temperature and centrifugal stress produces an extremely testing environment for the turbine blades. In this situation creep can be a limiting factor in the life of a blade, either due to the loss of dimensional tolerance, or to actual failure.

In/

In recent years the development of cooled turbine blades, in which air is blown down cooling holes in the blade, has reduced the problem of creep. The life limiting factor which is now of most importance is the thermal fatigue induced by thermal shocks at the beginning and end of each period of engine use(1).

Thermal shock is produced during the start-up of an engine, when cold turbine blades are suddenly exposed to a high speed flow of hot gas. The outer surfaces of a blade are heated immediately to a temperature many hundred degrees higher than the blade core. Thermal expansion in the hot surface is restrained by the core, and so the surface is held in a state of compression; if the thermal shock is of sufficient severity, plastic flow will occur. As the temperature gradients lessen, the core expands, so that the surface is now in tension, and further creep relaxation can occur. As will be understood, a similar shock is experienced on shut-down, when the hot blades are exposed to a cool stream of gas. The heating shock is usually held to be more damaging, since the thermal stresses are developed at a higher temperature(2).

The result of repeated thermal shocks is that the deformation accumulates as fatigue damage, and results in cracking of either the leading or trailing edge of the blade. Once a crack is present, the blade life is severely limited, since the centrifugal stress tends to profugate the crack across the whole cross-section.

For safety reasons, the life of a blade must be known with a certain degree of accuracy. If the life were simply creep limited, blade life could be defined as a certain amount of running time. Since thermal shock is now the main cause of damage to blades, the number of shocks as/

as well as the amount of running time must be included. Since relaxation of the thermal stresses will occur during high temperature running time, the incorporation of running time in a blade life criterion is not irrelevant.

The object of thermal fatigue analysis is to calculate how many cycles of heating, holding at high temperature, and cooling, a particular blade configuration will withstand. By using modern high speed computers, the problem has been tackled in the following manner(3).

Knowing the temperature of the exhaust gas, a distribution of temperature over the surface of the blade is assumed. The blade cross-section is then divided into an array of square elements and the temperature of each element is calculated. From known thermal expansion data, the stress regime at each element can be calculated. To find the plastic strain at each point, the stress-strain-time behaviour must be known at each temperature for the material in question. An additional complication arises from the fact that the temperature distribution throughout the blade is changing rapidly during the first few seconds of the thermal shock.

The main obstruction to a complete solution of the problem is the lack of precise knowledge of material behaviour. As a result of the extensive creep testing which has been carried out, the tensile properties of some nickel base alloys are sufficiently well known. A solution has been computed on the assumption that the unknown compressive creep properties were identical to the tensile ones. This solution could be inaccurate due to two factors.

1) Compression and tension creep are not necessarily identical.

2)/

2) The material may exhibit a Bauschinger effect[4]. This effect appears as a drop in the flow stress after prior straining either in the same or the opposite direction. The importance of this effect in thermal fatigue is apparent, since the blade alloy is stressed successively in opposite directions. Thus the presence of a Bauschinger effect could powerfully affect the amount of plastic strain experienced by a blade.

The programme of research described in this thesis is designed to shed light on these factors, by measuring the compressive creep properties of Nimonic 105, one of the nickel alloys in common use in British jet engines. The information required is the strain-time relationship for a test piece at various temperatures and uniaxial stresses, both in compression and tension. The advantages of this type of data over that collected from tests which more nearly duplicate actual blade conditions are:

1) The uniaxial creep test is well established and accepted both as a means for collecting useful engineering design data, and for investigating deformation mechanisms in metals.

2) The apparatus required for such a test is relatively simple, and usually consists of a lever loading device, a furnace with suitable temperature control, and an extension measuring device.

3) The results of these tests are fairly easy to interpret and are used as a means of comparison between one alloy and another.

4) Dislocation theories of creep can be used to predict the creep rate in a simple stress system. The validity of the theory can be evaluated by comparing the prediction with the creep rate measured in a uniaxial creep test.

As a second line of research, it was intended to measure the high temperature Bauschinger effect of Nimonic 105. Although this alloy is known to have a Bauschinger effect at room temperature[5], no reliable information on any metal or alloy appears to be available for the magnitude of the effect at high temperature. A more complete account of the Bauschinger effect, and the progress made towards its measurement, is given in Part Two of this Thesis (Chapter Six).

1.2 The Structure and Development of the Nickel Base Alloy Nimonic 105.

Before describing the present theories of creep in metals, the composition and structure of the alloy in question will be discussed. This is necessary, since the theory applicable to a particular alloy is decided by the microstructure. During this discussion the reasons will be outlined for the resistance of this alloy to the extreme conditions experienced by an aircraft-engine turbine.

Composition.

The composition of Nimonic 105 is given in Table 1 below[6]. As can be seen this is not a simple binary or even ternary alloy. It is the purpose of this section to rationalise the presence of each of the nine elements nominally present.

Table 1.

Element	Weight Percent
Nickel	Balance
Carbon	0.8
Chromium	15
Cobalt	20
Molybdenum	5
Titanium	1.2
Aluminium	4.7
Boron	< 0.01
Zirconium	< 0.04

The Strengthening of Metals.

A successful alloy for service at temperatures of the order of 1000°C, must possess a combination of properties. Strength, corrosion resistance and toughness are of prime importance, but ease of forming and the cost of the constituents must also be considered. Of the commonly available structural metals, nickel has better oxidation resistance than iron, and is much more ductile than chromium, but like all pure metals is fairly weak. After suitable alloying the properties of the resultant metal can be improved very considerably.

At 950°C, under a stress of 2,000 lb in , a pure nickel test piece ruptures after 8 hours(7), while a Nimonic 105 specimen, under similar conditions, would remain unbroken for 30,000 hours.

This remarkable strengthening is achieved basically by two structural mechanisms - solid solution hardening and precipitation hardening.

Solid Solution Hardening.

The principle which governs all attempts to make stronger alloys is the restriction of the movement of crystal dislocations. These are the imperfections which allow a metal lattice to be permanently deformed(8). By introducing atoms of a different atomic size into a lattice, irregularities are introduced in the form of strain fields which surround each solute atom. These strained areas retard the easy glide of dislocations, and hence the alloy is stronger than the pure metal.

As the temperature is increased, thermal agitation helps the dislocations to overcome the barriers of the strain fields, and the yield stress of the alloy falls. The general structure of a true solid solution, however, does not change to/

to any great extent after heating at high temperature[9].

For maximum hardening, large differences between solute and solvent atomic size are desirable. However, for a misfit greater than 15%, the solid solubility is restricted[10], and once this level of solute concentration is reached, the solute precipitates as a second phase, and no further solid solution hardening accrues.

Since the effect of a second additive is independent of the first, further hardening can be obtained by increasing the number of alloying additions, provided the solute atoms do not combine chemically to give an intermetallic compound.

Precipitation Hardening.

Although solid solution hardening has been known in the form of bronze and the iron-carbon alloys, for many centuries, precipitation hardening was unknown till 1906, when it was accidentally discovered by Wilm[11]. But no explanation of the phenomenon was given until 1919, when Merica and his co-workers[12] enunciated the principle that hardening depended upon a solid solution whose solubility decreased with decreasing temperature. An originally homogeneous alloy could thus decompose into a two-phase mixture when the temperature was lowered.

The second phase is usually precipitated as a dispersion of fine particles. For a variety of reasons, discussed later, these particles are effective dislocation barriers.

To produce the desired effect, a two-stage heat treatment is usually necessary. A single phase solid solution is produced by exposure at high temperature, above the solution temperature, and by quenching to ambient temperature. An aging treatment at a lower temperature results/

results in the beneficial dispersion of second phase particles. The aging temperature is chosen as a compromise between the short time required, but low amount of precipitate, of a high temperature, and the uneconomically long, but large amount of precipitate, of a lower temperature.

The operating temperature of this type of alloy is limited severely by the solution temperature of the precipitate phase. On the other hand, substantial strength is retained even at temperatures fairly close to the solution temperature, since even a small amount of second phase has a large strengthening effect.

With a knowledge of the strengthening mechanisms involved, the effect of individual alloying additions can now be discussed.

Chromium has been recognised as a useful addition to nickel since 1906, when Marsh[13] realised its beneficial effect both upon corrosion resistance and upon strength, as a solid solution strengthening agent. Chromium itself has excellent corrosion resistance due to its adherent impermeable oxide, and in solution, chromium imparts this property to the alloy.

Since chromium is available at a reasonable cost in relation to its ability in improving these properties, it has been added almost universally to nickel base alloys and in particular, to Nimonic 105.

The most spectacular strength increment observed in nickel alloys is derived from the precipitate phase based upon Ni_3 Al. Since 65% of the aluminium atoms can be replaced by titanium without changing the lattice structure from face centred cubic (Ni_3 Al) to hexagonal close packing (Ni_3 Ti), the formula is usually written Ni_3(Ti, Al), and is known as the/

the gamma prime phase. Although the h.c.p. eta phase is also beneficial to the creep strength the gamma prime is preferable. In its equilibrium form eta exists as long thin needles, incoherent with the matrix. Such incoherent particles are less effective as dislocation barriers than the spheroidal, coherent gamma prime particles (see section 1.4).

As will be shown later, the best strengthening effect is obtained from a large volume fraction of closely spaced precipitates. This has led to an increase in the amount of titanium and aluminium added to nickel alloys, with the aim of increasing the volume fraction of gamma prime.

The amount of gamma prime present, however, is not limited to the stoichiometric $Ni_3(Ti, Al)$ composition. The phase has extensive solubility for atoms such as chromium and cobalt, especially in the early stages of precipitation when the phase change reaction proceeds most rapidly[14]. It has been shown[14] that during high temperature exposure some of these foreign atoms are rejected from the gamma prime lattice. A refining process takes place so that the precipitate composition approaches the expected $Ni_3(Ti, Al)$ formula.

Hence the most recently developed of nickel alloys have up to 8% by weight titanium plus aluminium. After suitable heat treatment, the volume fraction of gamma prime precipitate which results is over 50%.

The effectiveness of the gamma prime precipitate can be extended to higher temperatures by the addition of cobalt, which raises the solution temperature. A cobalt bearing alloy can thus operate at a higher temperature than a non-cobalt-bearing alloy[15,16]. Cobalt is also an effective/

effective solid solution strengthening element, though because of the similarity in size between the nickel and cobalt atoms, the strengthening obtained is less marked than that from the addition of chromium. By comparison with Russian superalloys which contain no cobalt, and most American ones, which do contain some, Nimonic 105 with 20% cobalt makes greatest use of this metal as an alloying addition.

Since the molybdenum atom is almost twice as heavy as the nickel atom, it diffuses more slowly through the nickel lattice, and so slows down diffusion rates generally, in particular at the interface between the gamma prime and the parent matrix[16]. The presence of molybdenum in Nimonic 105 thus slows down the precipitate agglomeration process. As do most alloying additions, molybdenum fulfils a multiple function, since it also acts as a solid solution strengthener and forms a carbide of the form Mo C_6. This type of carbide is desirable, since the alternative M_{23} C_6, where M is a metal ion, has been associated with brittleness especially in welded structures[16].

The improvement of ductility was given unexpected help when it was found[17] that accidental additions of boron and zirconium improved the elongation of nickel base alloys. These original additions were made as contamination from the walls of the crucible in which the alloy was melted. Decker, Rowe and Freeman[17] have carried out a systematic investigation into the reasons for the improvement. They concluded that the boron and zirconium atoms segregated to grain boundaries. The reason proposed is that the atomic sizes of these atoms, 1.7 A.U. and 3.16 A.U. for boron and zirconium respectively, are markedly smaller and larger than the major constituents of nickel alloys, for which the substitutional atomic diameter has been given as 2.53 A.U.

For/

For this reason, it is claimed, the boron and zirconium atoms tend to segregate to regions of great lattice misfit, such as the grain boundaries. The distortion creates lattice sites of unusual size, which would be unfilled if these elements of odd atomic size were not present. Such vacant sites would act as imperfections which under the influence of a stress could grow into a cavity, which could eventually lead to failure.

In present practice these elements are added in controlled quantities, since the amounts required are minute (see Table 1). The presence of too much boron gives rise to the formation of complex, brittle borides in the grain boundaries. These reduce the ductility and hot workability of the alloy both by their brittleness and their low melting point.

Despite being a minor constituent, carbon plays a major role in preventing brittleness in nickel alloys. By means of suitable heat treatment, the formation of carbides can be induced in the grain boundaries. Since the main carbide-forming element is chromium, a region depleted of chromium forms along grain boundaries. Now, the solubility of aluminium and titanium in the matrix has been shown to be decreased by presence of chromium[15]. Hence in the region depleted of chromium there is an absence of gamma prime particles. This weakened region has high ductility, and so the initiation of cracks is retarded. In support of this, several observations[18,19] show that an absence of grain boundary carbides leads to low ductility and short creep life. The direct effect of the carbides is to act as precipitation hardening agents in the grain boundaries, retarding grain boundary sliding, and preventing grain growth by boundary migration.

As/

As has been mentioned above, the final properties of a precipitation hardened alloy depend crucially upon the heat treatment given to it. The first stage for Nimonic 105 is[6,15] a solution treatment at 1150°C for 4 hours which takes into solution all but the most refractory particles. A further 16 hours at 1050°C allows carbon to diffuse to the grain boundaries and form carbides. A final treatment at 700°C for 16 hours converts a large volume fraction - up to 50% - of the alloy to gamma prime. By continuing the treatment long enough for the particles to grow to a few hundred angstrom, the precipitate is better able to resist dissolution at high temperature than when the particles are very small.

1.3 Theory of Creep in Two-Phase Alloy Systems.

Curve Fitting.

The earliest attempt to systematise creep data was the fitting of mathematical expressions to creep curves. The equation proposed by Andrade[20] is probably the best known example of this approach. The strain, ϵ, during a test, is given, at time t, by

$$\epsilon = \epsilon_0(1 + B\, t^{\frac{1}{3}}) \exp k\, t, \quad \text{where}$$

ϵ_0, B and k are constants.
As Andrade points out, for small values of B and k, this can be written $\frac{d\epsilon}{dt} = \epsilon_0(\frac{1}{3} B\, t^{-\frac{2}{3}} + k + \text{smaller terms})$ giving the well known transient ($\frac{1}{3} \epsilon_0 B$) and steady state ($\epsilon_0 k$) components of the creep curve.

Many other equations such as this have been devised[21], and while all may be useful in practice to represent actual behaviour, none help to indicate the fundamental mechanism of deformation.

It has long been the dream of the metallurgist to predict the creep rate in a metal, without recourse to experiment, knowing only the stress and temperature involved, and one or two parameters defining the material structure. When dislocation theory gained general acceptance, it became possible to advance particular atomic interactions to account for the behaviour of metals under stress. In the case of pure metals and solid solution alloys many arrangements of dislocations and atoms have been proposed[22] as creep mechanisms. In any particular case it has proved extremely difficult to identify the deformation process which is controlling the rate of strain. Hence the complexity of the problem has caused slow progress towards the prediction of creep rates.

Two-phase alloys of the precipitation or dispersion hardened type are, despite their structural irregularity, more simple to treat theoretically, since the rate controlling process can be assumed to be the interaction of dislocations with precipitates[23]. Both single- and poly-phase systems have been treated by Weertman[24,25,26], who, almost alone, has had success in developing theoretical expressions for steady state creep rates.

Since the ideas and assumptions used in Weertman's analysis are of great interest, the detailed argument is given in an Appendix. Suffice it here to say that the assumed rate controlling mechanism is the climb of dislocations around precipitate particles.

The following expressions result a) at low stresses

$$\frac{d\epsilon}{dt} = \frac{\pi \sigma b^3 D}{2k T h^2} \qquad (1)$$

where/

where $\frac{d\varepsilon}{dt}$ is the rate of strain

σ is the resolved shear stress

b = the Burgers vector

D = the coefficient of self diffusion

$= D_o \exp(-Q/RT)$

Q = activation energy for self diffusion

k = Boltzmann's constant

T = temperature

h = the average second phase particle diameter.

At higher stresses, given by

$$\sigma > \frac{\mu b}{\lambda}, \quad \text{where}$$

μ = shear modulus

λ = interparticle spacing,

the creep rate is given by

$$\frac{d\varepsilon}{dt} = \frac{2\pi \sigma^4 \lambda^2 D}{h \mu^3 k T} \qquad (2)$$

This equation is valid up to stresses such that

$\frac{2\sigma^2 \lambda}{\mu k T} b^2 > 1$, and at higher stresses,

$$\frac{d\varepsilon}{dt} = \frac{\pi \sigma^2 \lambda D}{\mu^2 b h} \exp\left(\frac{2\sigma^2 \lambda b^2}{\mu k T}\right) > 1 \qquad (3)$$

The following points of interest arise from these equations for the steady state creep rate.

1) At low and medium stresses, (equations (1) and (2)) the predicted stress dependence is a power law, while at the highest stresses, the creep rate depends upon $\sigma^2 \exp\left(\frac{2\sigma^2 \lambda b^2}{\mu k T}\right)$. Similar expressions have been found for creep in single phase alloys[26]. A great deal of experimental data has been fitted to a power law dependence[9,27].

2)/

2) Equations (1) and (2) predict a temperature dependence of the form $\exp(-Q/RT)$, and since Q is the activation energy for self-diffusion, the measured creep activation energy should be close to this value.

3) The creep rate depends explicitly upon the structural parameters h and λ. Changes in these during a test should affect the creep rate.

Comparison of Predicted and Observed Creep Behaviour.

Despite the existence of Weertman's equations for some eight years, no great mass of experimental evidence has been accumulated to confirm the accuracy of Weertman's ideas. To this author's knowledge, the only readily available published information is the following: two studies of dispersion hardened alloys - sintered aluminium powder[28] (S A P) and thoria dispersed nickel[29] (T D nickel), and an investigation on two precipitation hardened nickel alloys - M252 and Inconel 700[30].

The experiments of Ansell and Lenel[28] on S A P alloys showed that the steady state creep rate obeyed, to a high degree of accuracy,

$$\frac{d\epsilon}{dt} = K\sigma^4 \exp(-Q/RT)$$

where Q was found to be 37,000 k cal/mole. This, then shows excellent qualitative agreement with Weertman's equation (2), since the activation energy for creep is in excellent agreement with the figure for self-diffusion, and the derived stress exponent is 4, also in agreement with the experimental value.

Despite a knowledge of the structural parameters, it proved impossible to predict the creep rates. In general the observed creep rates were much lower than those predicted by equation (2). The conclusion is drawn that the number of mobile/

mobile dislocations in a dispersion hardened alloy is much lower than in a single phase alloy. In a single phase alloy, there exists a continuous three-dimensional network of dislocations, the development of which may be prevented by the particles of Al_2O_3 in S A P.

Similar results have been obtained for T D nickel[29], in that the creep rate depended upon the stress according to a power law, with an exponent 7 and the creep activation energy was 64 k cal/mole, in full agreement with the activation energy for self-diffusion.

The stress exponent of 7 is somewhat higher than the calculated value of 4, and it is difficult to explain the difference. The main structural difference between S A P and TD nickel is that the Al_2O_3 particles are flat platelets, while the thoria particles are spheroidal. Both types are incoherent with the pure metal matrix surrounding them.

In the T D nickel alloy, the creep rate was found to depend upon the structural parameter λ^2/h, in agreement with the prediction of equation (2), which is the appropriate equation for the stress levels discussed.

The experiments carried out to determine the relation between structure and creep rate in precipitation hardened alloys are more difficult than similar experiments on alloys strengthened with dispersions of oxide particles, since the size and number of precipitate particles is continuously changing. While the oxide particles are insoluble due to their large energy of formation, the gamma prime particles have been observed by Rowe and Freeman to agglomerate into larger particles[30] at the test temperature of 871°C. The course of the agglomeration was followed by interrupting creep tests after suitable fractions of the creep rupture life, so that the structure could be examined by electron microscopy.

Such a structural survey was carried out on the M252 alloy which contains approximately 2% of gamma prime, and a linear relationship was found between Weertman's structural parameter λ^2/h and the steady state creep rate.

On the other hand, Inconel 700, with 40 vol% of precipitate, proved to be insensitive to structural alteration, insofar as could be ascertained. It would appear that at the higher volume fraction of precipitate, λ^2/h is not as sensitive to the variations in λ and h which undoubtedly took place.

On this evidence it may be concluded that Weertman's equations, while still unable to predict absolute creep rates, are probably based upon sound assumptions, and further work is required to define their limitations.

There are, however, several observations which do not entirely agree with Weertman's scheme. Wilcox and Clauer[31] measured creep rates in T D nickel which had an asymmetric, acicular grain structure. Although their results for temperatures in excess of 0.5 Tm fitted an equation of the usual form

$$\frac{d\varepsilon}{dt} = A\,\sigma^n \exp\left(\frac{-Q}{RT}\right)$$

where A is a constant, the values measured for n and Q were 40 and 190 k cal/mole, compared with the expected values of 4 and 68 k cal/mole respectively. These do not fit into any theoretical formulation, nor has any deformation process been associated with them.

An even higher value for the activation energy of creep in a nickel alloy has been published by Dioguardo and Lloyd[32] who found Q = 215 k cal/mole in Rene' 41. This is far in excess of other observations of the activation energy in nickel base superalloys[33,34] which have generally/

generally found values between 80 and 120 k cal/mole. Likewise, no explanation exists for these apparently anomalous results.

Since all these studies have been carried out on polycrystalline material, it can be argued that grain boundary effects are causing this lack of complete agreement. With the improvements in techniques of directional solidification, it would seem feasible to produce single crystal test pieces with which to test further the validity of Weertman's equations, which take no cognisance of the presence of grain boundaries. Such experiments would have to be carried out on suitably oriented crystals, so that a particular set of slip systems could be made to operate under a known shear stress.

Other Theories of Creep in Two-Phase Alloys.

Although prominence is given here to the ideas developed by Weertman, other theoretical treatments of the two-phase system have been published recently. In particular, Webster and Piearcey[76] have considered the multiplication of mobile dislocations with increasing strain, and produced an equation which fits the creep curves measured in the nickel-base alloy D.S.-200. No detailed mechanism is assumed in this treatment, and the values of the constant terms in the creep equation are found by fitting the equation to the experimental curves.

Unlike Weertman's theory, this treatment does not make useful predictions about the probable dependence of creep rate upon structure and stress. It does, however, forecast that the measured activation energy for creep should be twice the activation energy for self-diffusion in the alloy, and indeed, experiment shows that the activation energy for creep in this alloy is twice the activation energy/

energy for self-diffusion in pure nickel. This must be regarded as satisfactory agreement.

Another theory which makes no explicit predictions of stress and structure dependence has been developed in the Soviet Union by Roitburd, Usikov and Utevskii.

After examining thin sections of a Ni-Cr-Ti-Al alloy by transmission electron microscopy, Roitburd[35] and his co-workers conclude that the dislocation structure present after creep cannot be explained by any accepted dislocation motion e.g., glide, cross-slip or climb. They propose that the rate controlling process in creep is the movement of helical dislocations, which can proceed by means of short range diffusion flows from one segment of dislocation to another of opposite sign.

On this basis, an expression for the steady state creep rate has been developed:

$$\frac{d\epsilon}{dt} = A \frac{D}{kT} \left(\frac{h}{a}\right)^2 b^3 \sigma p$$

where A = constant
h = pitch of the helix
a = radius of the cylinder enclosing the helix
p = dislocation density.

By inserting values of the experimental parameters, an excellent approximation to the observed creep rate was obtained. It is concluded that the non-conservative motion of helical dislocations can take place at a sufficient rate to give observable plastic flow.

In this theory no explicit account is taken of the precipitate dispersion. Presumably the dislocation density p is restricted by the presence of the particles, as is suggested by the creep tests on S A P - type alloys[36].

As/

As the authors comment, the stress dependence of the creep rate in this theory is more complex than the explicit linear relationship, since p will depend, in some manner, upon the applied stress.

Before this theory can be generally accepted, further experimental work is required, since the only evidence at present depends upon the creep of one alloy at one temperature and stress, and upon a dislocation density assumed to be of the right order of magnitude rather than measured directly.

1.4 The Effect of Precipitate Particles on the Mechanical Properties of Metals.

Weertman's analysis of creep in two phase alloys assumes that the second phase particles resist penetration by dislocation segments. While this may seem readily acceptable for refractory, incoherent particles of Al_2O_3 in pure aluminium, it is not so for the gamma prime precipitate, which has a crystal lattice similar to the parent matrix, and a lattice parameter which differs by only 0.5%[37]. It is the intention of this section to set out reasons for the undoubted hardening which the presence of the gamma prime accomplishes. The several effects will be examined separately as follows.

1) Even a small difference in lattice parameters will induce strains in a particle, and in the matrix surrounding it. Such strains have been detected both by X-ray and electron microscopy methods[38]. A dislocation encountering a region of disturbed lattice, surrounding either a solute atom or a precipitate particle, is retard in its motion and Mott and Nabarro[39] have calculated that the stress necessary to move a dislocation through such a strain field is/

is

$$\sigma = 2 G \epsilon f$$

where σ is the shear stress acting on the dislocation slip plane

G the shear modulus of the matrix

ϵ a function of the difference in lattice parameters

f the volume fraction of precipitate.

This formula can be used to calculate the yield stress of a metal, and estimates have been made[40] for the yield stress in several aluminium alloys. In most cases the calculation was fairly successful in its prediction.

The most efficient distribution of precipitate particles can be seen to be, both from this expression, and from Weertman's calculated structural parameter to be a large volume fraction of particles, whose interparticle distances are so small that the adjacent strain fields overlap.

2) A totally different type of strengthening effect arises when the precipitate has an ordered structure. The gamma prime precipitate has an ordered structure, whose unit cell is based on the f.c.c. lattice with nickel atoms occupying all the face centre sites, and titanium or aluminium atoms filling the corner sites. The passage of an ordinary dislocation through such a structure will destroy order along its slip plane, leaving behind a so-called anti-phase boundary (A P B). This is a high energy interface whose energy of formation may be calculated. from the analysis given by Marcinkowski[41], to be 400 erg/cm^2 for the octahedral planes - the usual slip planes in an f.c.c. lattice. In a disordered alloy the analogous defect is a stacking fault, which as an energy of around 100 erg/cm^2 , much smaller than that of an A.P.B.

In/

In addition to the energy of disordering, new surface is created between the particle and matrix. By considering the work done in moving a single dislocation through a particle, the stress required can be calculated[40] to be

$$\sigma = \frac{f\,\gamma_p}{b} + \frac{3}{\pi}\left(\frac{2}{3}\right)^{\frac{1}{3}}\frac{f\,\gamma_s}{r}$$

where γ_p = the energy of a disordered interface in the particle

γ_s = the energy of the particle-energy interface

f = the volume fraction of precipitate

b = the Burgers vector

r = the particle radius.

Assuming γ_p to be much greater than γ_s, we have

$$\sigma > \frac{f\,\gamma_p}{b}$$

Inserting $f = 0.5$

$\gamma_p = 400$ erg/cm^2

$b = 2.5 \times 10^{-8}$ cm

we obtain $\sigma > 80$ kg/mm^2

$= 51$ ton/in^2,

which shows that very appreciable strengthening results from the internal ordering of the precipitate, especially when it is realised that this is a lower limit for the yield strength. This figure of 51 ton/in^2 is a resolved shear stress, and compares with 0.6 ton/in^2 for the critical resolved shear stress of a pure nickel single crystal[42].

However, it has been found[41] that dislocations can move through superlattices in pairs, separated by an anti-phase boundary. The equilibrium spacing of the dislocations is decided by a balance between the mutual repulsion of the dislocations, and the energy of formation of the/

the A.P.B. The Burgers vectors of the components of such a superdislocation are so related that the disorder created by the leading dislocation is repaired by the second of the pair. The stress required to move such a configuration is less than that calculated above. Superdislocations have been observed in the matrix of Nimonic alloys(37). The presence of titanium and aluminium apparently induces some long range order in the matrix.

It has not yet been proved that the motion of superdislocations plays a major role in the deformation of Nimonic 105. Even if such dislocations were the only mobile types in a lattice, creep would be slow, due to the comparatively low density of such dislocations.

3) The proposal has been made by Fleischer(43,40) that when a dislocation is moved into a second phase particle, interface dislocations must be created, with a Burgers vector equal to the difference between the vector in the matrix, and that in the particle. The assertion is made that even though this difference may be small, the effect is physically significant. Since no quantitative evidence is available for the size of the effect in nickel alloys, it must remain a matter of conjecture as to whether or not this effect is of use in Nimonic 105.

4) When a dislocation approaches a region of different elastic modulus, it experiences a repulsive force(43). Since Fleischer has shown that the Guinier-Preston zones in an Al-Cu alloy give rise to appreciable strengthening by this means, it may be assumed by analogy that gamma prime in Nimonic can act in a similar fashion.

There is thus good reason for the assumption that gamma prime particles resist penetration by dislocations, as/

as required by the dislocation climb model for creep. This does not mean that dislocations never cut through these particles, since it is known that the yield stress in alloys with a dispersion of small coherent particles is decided by the stress required for dislocation cutting of the precipitates(40).

1.5 Time Dependence of Precipitate Size Distribution.

An alloy with a dispersed second phase produced by precipitation from a supersaturated solid solution has a particle size distribution which covers up to an order of magnitude from smallest particle to largest. During high temperature exposure, this distribution changes with time as the solute rearranges itself into a configuration of lower surface energy. The net result is that the smaller particles diminish in size, while the larger particles grow at their expense.

This effect has serious consequences for alloys of economic importance, since their creep resistance falls with the coarsening of the precipitate. Continuous high temperature use (e.g. steam turbines) is obviously more damaging in this respect than intermittent periods of exposure (short-range-aircraft engines), since in this latter case further precipitation will take place during each cooling cycle.

When an attempt is made to calculate the rate of agglomeration a serious difficulty arises in characterising the problem. Essentially a mathematical function is required to describe the shape, size and spatial distribution of the particles. The concentration gradients which lead to overaging could then be computed, and a precise solution calculated.

In/

In the absence of such a complete analysis. several approximate calculations have been made, and will now be discussed.

Ham(44) divided the material into an array of cubic elements, with a particle at the centre of each cube. The size of the particle was assumed insignificant compared to the size of the cube. His results, though interesting, cannot be considered to have a more general application, especially in the situation of interest, where particle spacing/particle diameter ratios are not greatly in excess of unity.

A possible, and elegant, description of the system of precipitate particles is a Fourier series. Cahn(45) has used this technique to describe the magnitude of compositional fluctuations, as well as their arrangement in space, in a theoretical discussion of spinodal decomposition.

For a fair degree of success to be achieved the use of such a sophisticated technique has, however, not been necessary. The most concentrated theoretical effort has been upon liquid-solid systems, by workers such as Greenwood(46), Lifshitz and Slyozov(47,48) and Wagner(49). Of these the most explicit and useful treatment is that of Wagner, and only his results will be considered. Wagner avoids the problem of specifying the spatial relationships of particles by assuming that the particles are far enough apart for a region of equilibrium concentration to surround each particle. This proviso is not as restricting as Ham's condition on the size of the particles in relation to their spacing, and is justifiable in view of the success of Wagner's theory. The size distribution may be defined by any suitable expression e.g., a Gaussian curve.

For/

For the situation in which the parent solution has been depleted down to the equilibrium concentration, Wagner derives for the average particle radius, $\bar{r}$,

$$\bar{r} = \frac{8 \gamma D C_o V_m}{9 R T} t^{\frac{1}{3}} \qquad (4)$$

where t = time

C_o = the equilibrium solubility of a particle of infinite radius

γ = the interfacial energy between the parent phase and a particle of molar volume V_m

D = the diffusivity of the particle species in the matrix at temperature T

R = the gas constant = 2 cal/mole.

One disadvantage of this approach is that no consideration is given to the effect of elastic strains, both in the matrix and in the particles. Lifshitz and Slyozov[47,46] examine how the elastic stress field created by a difference in lattice parameter might affect the diffusivity and solubility in a solid matrix, but do not make it clear how important they adjudge this effect to be.

Oriani[50], however, considers this a minor effect compared to the restriction placed upon the system by the coupling of diffusion processes. This can be visualised by considering a volume containing a coherent precipitate particle. Then the flux of atoms entering the volume for the formation of the particle must be balanced by an equal flux of different atoms leaving. For a non-coherent particle the situation is more complex, since the number of lattice sites present within a volume changes with the size of the particle. The limitations this places on the diffusion processes has, in principle, been calculated by Oriani[50].

Another serious limitation upon equation (4) is the demand that the concentration of the precipitate constituents in the parent phase has the equilibrium value so that it is independent of time. During the high temperature exposure of Nimonic 105 at temperatures higher than the aging temperature, the amount of precipitate falls considerably (see fig. 25). In consequence the concentration of gamma prime constituents rises in the matrix as the amount of precipitate diminishes and agglomeration proceeds. Only after long aging times does the volume fraction of gamma prime reach equilibrium level. A complex situation thus exists, in which, although the average particle size is increasing, the volume fraction of gamma prime is diminishing.

In view of this, it is surprising that such good agreement has been obtained between measurements of the growth of particles and equation (1).

Mitchell[51] followed the course of agglomeration in six commercial nickel base alloys. All his results fit a $t^{\frac{1}{3}}$ time dependence for the average particle size. Wagner's law was obeyed over a range of temperatures from 600°C to 1100°C. From Mitchell's data the activation energy for the clustering process will now be calculated. To this author's knowledge, this calculation has not been completed before, and no activation energy has been reported for the clustering process in any other alloy.

If equation (4) is now differentiated

$$\frac{d\bar{r}}{dt^{\frac{1}{3}}} = \frac{8\ \gamma\ V_m\ D\ C_o}{9\ R\ T}$$

an expression is obtained for the rate of agglomeration. Since this rate is diffusion controlled, a knowledge of the activation energy should supply information about the mechanism of formation.

Now/

Now C_o has been shown to be[21]

$$C_o = \exp(-H/RT)$$

where H = heat of formation of precipitate
$\doteq$ 2 k cal/mole for Ni_3Al[21]

And $D = D_o \exp(-Q/RT)$

where Q is the activation energy for the diffusion of the precipitate species.

$$\text{Hence } \frac{d\bar{r}}{dt^{\frac{1}{3}}} = \frac{8\,\gamma\,V_m\,D_o}{9\,R\,T} \exp\frac{-(Q+H)}{RT}$$

Now, from Mitchell's data[37], the slope of the plot of $\log\left(\frac{d\bar{r}}{dt^{\frac{1}{3}}}\right)$ versus $1/T$ can be measured to give

$$Q + H = 29.6 \text{ k cal/mole}$$

$$\text{Thus } Q = 27 \text{ k cal/mole.}$$

This figure should compare with the activation energy for the diffusion of aluminium or titanium in nickel. However, the work of Sherby and Simnad[52] and Swalin and Martin[53] on the diffusion of molybdenum in iron and tungsten in nickel indicates that the activation energy for diffusion of solute atoms is not greatly different from that of self-diffusion, which is 66 k cal/mole for pure nickel.

The value mentioned above for Q holds for a range of titanium and aluminium concentrations, and since it is known[14] that other atoms than those given by $Ni_3(Ti, Al)$ are present in gamma prime, it is difficult to assign any physical significance to the measured activation energy.

Further evidence has been reported in agreement with the time dependence given in equation (4). The copper-cobalt system, for alloys containing from 0.7% to 2% by weight of cobalt, has been examined by Livingston[54,50]. In/

In this case a magnetic technique was used to follow the change in particle size with time.

Bannyh and his associates[55,50] followed the agglomeration of Fe_3C in α-iron at 700°C over a 60-fold increase in average particle size. Using an electron microscope technique, they found that their results showed a $t^{\frac{1}{3}}$ time dependence for the average particle radius, in agreement with Livingston and Mitchell.

The agreement of these investigations is encouraging but this satisfaction must be tempered by the realisation that no success has been reported in predicting, from equation (4), the absolute rate of coarsening. This is due largely to ignorance of the appropriate values of γ, the surface energy.

In an alloy undergoing deformation, large numbers of vacancies are produced by the deformation processes. It is to be expected that these vacancies would raise the diffusion rates in the alloy. High diffusivity paths also exist along dislocation cores. These effects may well combine to raise the rate of agglomeration. From the evidence presented above, and in the next paragraph, these higher diffusion rates do not result in a change in the time dependence of $\bar{r}$.

The Effect of Stress on Precipitation.

So far no allowance has been made for the presence of stress upon the precipitating system. No difference has been noted between agglomeration produced under stress, in a creep test, and the unstressed behaviour[56,51], and so this effect can be taken to be negligible.

From the calculation, by Mott and Nabarro[57], of the elastic energy of the strain field surrounding a precipitate/

precipitate particle, Oriani[50] has shown that the elastic energy, per atom of precipitate, is independent of the particle size. This implies that once the equilibrium fraction of precipitate has been attained, surface energy is the sole driving force for precipitate agglomeration.

In conclusion it may be said that while the derived $t^{\frac{1}{3}}$ time dependence has been shown to be accurate, further work is required before rates of agglomeration can be predicted on purely theoretical grounds.

1.6 Review of Relevant Previous Studies.

Despite the difficulties involved in testing, the subject of compression creep has aroused interest from time to time. Sully[54] has recommended compression creep testing as a means of testing small samples of material. Such limited samples might arise in the investigation of experimental alloys, or in the testing of specimens taken from engineering structures. Despite this advocacy, the technique does not seem to have gained wide acceptance, probably due to the difficulties of compression testing and previous investment in tensile equipment.

Super-alloys.

Of particular interest is the extensive study of high temperature alloys carried out by the Marquardt Corporation[59,60,61]. These alloys were the iron base N-155, cobalt base L-605 and nickel base René 41. The first two of these are solid solution hardened, while the third is strengthened by the gamma prime precipitate. During the above investigation, several types of test were used, including short time tensile and compressive creep tests, in which the maximum test time was limited to 15 minutes. In spite of the differences in structure between the/

the alloys, the creep data for each alloy has been shown[9] to obey a relationship such as

$$\frac{d\epsilon}{dt} = \frac{A\sigma^n}{T} \exp\left(\frac{-Q}{RT}\right),$$

in agreement with Weertman's equation (see 3.3). In this case $n = 4 - 5$, in fair agreement with the predicted values of $4 - 5$ for a pure metal and 4 for a dispersion hardened alloy. However, the measured values for Q were always far in excess of the appropriate figures for self-diffusion.

In general, the conclusion was that compression creep rates were lower than the corresponding tensile ones. The Rene' 41 data at 982°C is particularly interesting, since at very short times - less than 100 seconds, the tensile curve at each stress lay below the compressive one. Thereafter tensile creep strains exceeded the compressive by progressively greater amounts.

Since all these tests were carried out on sheet material, a bracing device to prevent buckling was essential to the test equipment. Any specimen which tended to buckle would not then be under simple uniaxial compression. The criticism may also be made that the specimen was heated by passing a large electric current through the specimen. This might affect the material in two ways 1) Since it is known that dislocation cores can be electrically charged, such a dislocation would experience a force due to the presence of the electric field, in addition to the applied mechanical stress. 2) The electrons passing through the material are scattered, in particular by solute atoms. The electrons transfer their momentum to these atoms, which are moved through the lattice by this "electron wind".

No/

No attempt was made to explain the differences between tensile and compressive creep on a theoretical basis, and so the main conclusion from this work is that for design purposes the assumption that tensile and compressive creep rates are the same is a safe one. Since the range of experimental parameters was very large - strain rates from 10^{-5} to 1.0 sec^{-1} temperatures from 871°C to 1204°C - the correlation of the data with Weertman's equation is powerful support for the concept of dislocation climb as the dominant rate controlling mechanism of creep.

Stainless steel.

Manjoine[62] has reported the results of tests on stainless steel at 565°C and 595°C, which showed the tensile creep rate to be always greater than the compressive.

Another investigation showed[63] that the creep rates differed, but in a more complex manner which depended upon the temperature.

Aluminium and its alloys.

The available results on pure aluminium and its alloys show even greater complexity, and even disagreement. The data of Heimerl and Farquar[64] shows general agreement between tensile and compressive creep rates. The exceptions are at low temperatures, around 150°C, where the effects of precipitation and prestrain were most marked and tensile creep was greater than compressive.

On the other hand, Carlsson[63] et al. conclude after tests on sheet aluminium alloys that compressive creep was generally different from tensile. Depending upon the stress and temperature, these workers found either the tensile or compressive creep could be greater.

Pure/

Pure nickel.

The results on pure nickel differ[94] from the rest in that they show a compressive creep rate decidedly higher than the tensile one. A tentative explanation is given on the basis of the grain boundaries acting as sources or sinks for vacancies. Since no evidence appears to have been published confirming the postulated grain boundary behaviour, this theory must await further evidence before being accepted.

From these investigations into the creep properties of various alloys, the following conclusions may be drawn

1) In general, tension and compression creep are different.

2) The magnitude of the differences depend in a complex way upon stress temperature and structure.

3) In the face of an almost complete lack of theoretical speculation, an explanation does not exist for those differences which have been measured.

4) This is understandable since the resolved shear stress on a slip plane is the same, whether produced by a tensile or compressive force. The stress experienced by a dislocation segment should therefore be the same in tension and compression.

T.D. nickel.

Recently, interesting results have been published[29,65] on the tensile creep of nickel-thoria alloys which contained from 1% to 4% of ThO_2 particles. When recrystallised by cross-rolling and annealing at 1200°C, these alloys showed behaviour in fair agreement with the theoretical predictions of Weertman. The activation/

activation energy for creep was measured as 66 k cal/mole, compared with a range from 63 - 66.8 k cal/mole for the self-diffusion activation energy in nickel. Also the creep rate depended upon the stress according to

$$\frac{d\epsilon}{dt} \propto \sigma^n$$

at constant temperature, where $n = 7$, compared with Weertman's predicted value of 4.

A similar alloy, swaged and tested without subsequent recrystallisation had an activation energy three times that for self-diffusion and a value for n of 40.

The differences between the two types of material lay in thetangled dislocation structure and elongated grains of the as-swaged material, compared with the annealed, equiaxial grains of the recrystallised material.

These results illustrate the caution with which creep data in complex alloy systems must be viewed, since the composition of the alloy, in this case, gave little clue as to the expected creep behaviour.

1.7 Conclusions.

For the purposes of this present study, the following conclusions are drawn from the theoretical and experimental work described in the Introduction.

1) The steady state creep rate varies with stress according to a power law, with an exponent determined by the alloy structure.

2) Creep is diffusion controlled, and measured activation energies are, in the case of nickel alloys, in the range 80 - 120 k cal/mole.

3)/

3) The steady state creep rate depends upon the structure of a two-phase alloy according to Weertman's structural parameter λ^2/h, where h is the particle diameter and λ the interparticle spacing.

4) At high temperature, h depends upon time according to a $t^{\frac{1}{3}}$ law, as derived by Wagner.

The precise values for the stress exponent and activation energy must thus be determined for each material separately, since these have not been predicted theoretically, nor can values measured for other materials be assumed to be applicable. The values of these parameters were therefore measured for Nimonic 105, and are tabulated in Chapter Four.

CHAPTER TWO

CHAPTER TWO

DEVELOPMENT OF CREEP TESTING EQUIPMENT

In view of the requirements outlined in the Introduction, the apparatus necessary for the experimental part of this investigation had to fulfil the following functions.

1) To apply accurately known tensile or compressive stresses to a specimen of Nimonic 105.

2) To maintain this specimen at a temperature of about 1000°C, this temperature to be known and constant,

3) To measure the ensuing deformation with sufficient accuracy. These requirements are not mutually compatible, since the accurate measurement of deformation usually requires direct assess to the specimen. This access is precluded by the specimen temperature being of the order of 1000°C, and so the use of remote sensing extensometry is essential.

2.1 Compressive Creep Rig.

As has been stated before, the reason for the lack of compressive creep data is the difficulty of applying an axial load to the specimen when it is hot and of maintaining axiality during deformation. With this in mind, a suitable rig for creep testing in compression was first designed. For the comparative tensile creep tests, the tensile equipment was copied, as far as possible, from the compression rig. The aim in this was to maintain testing/

testing conditions identical in the two sets of tests, except for the state of stress.

Since so few compressive creep investigations have been carried out, no standard form of apparatus has evolved. It is possible to classify the different design philosophies as follows

1) A method which does not require the accurate guidance of a compressive force on to a column test piece is the three- or four-point bending test. For this test the specimen is a simple flat bar, and the load can be applied by a more simple guide than that required for axial compression. However, for calculations of stress and strain to be made from the applied load and measured deflection, a knowledge of uniaxial behaviour is required. Although opposite sides of the bar are in tension and compression respectively, the creep behaviour in both states of stress cannot be derived from one experiment. Thus two sets of tests are required, and any analysis of the bending test would be rendered inaccurate in the presence of cracking. This type of test has been used for plastics at ambient temperature[66] and for ceramic materials at very high temperature[67].

2) The most simple compression rig for a cylindrical specimen consists of an interlocking shackle which converts a tensile full into a compressive one. This shackle can be small enough to fit inside a normal tube furnace and can be mounted in a tensile creep machine. This system has been used successfully with aluminium alloys at temperatures up to 350°C[63]. For application to this study of Nimonic 105, such a reverse/

reverse-loading shackle has the disadvantage that the guidance surfaces would be susceptible to oxidation and wear at the higher temperatures, even if made of the most corrosion and wear resistant alloy available. After a few tens of hours the alignment would no longer be sufficiently accurate to guarantee the accurate loading required for a successful compressive creep test.

3) The method which appeared to be most capable of development for use at the high temperatures required, was a rig designed at the National Engineering Laboratory(68). This rig uses a cylindrical specimen, which sits on a massive anvil of heat resistant material, while a compressive force is applied by a rod which is guided from outside the furnace (Figure 1). The accuracy of these guiding surfaces is crucial to the success of the machine. All three holes in the main frame were drilled in line on one machine without disturbing the alignment of the frame between the drilling of each hole. The size of the frame was decided by the minimum furnace size necessary to heat the specimen accurately. The load is derived from the lever arm of a tensile creep machine (4) by hanging the main frame (1) from the lever arm, and shackling the loading rod (2) to the foot of the machine.

By guiding the loading rod from outside the furnace, the oxidation problem encountered in method (2) above is avoided. A close tolerance fit between the loading rod and its hole in the main frame can be maintained permanently. In practice, this bearing was lubricated with a film of "Molyslip" grease.

For use in this study, certain alterations were made to the original design, in view of the temperatures involved. Because of its superior strength and oxidation resistance, Nimonic/

Nimonic 105 was used for the load bearing plattens (2, 3) in the hot zone. Although at first sight it would appear to be bad design to use the same alloy for test piece and loading rams, this was necessary since no better alloy was available for the structural members. The stress on the loading rams was a factor of 10 lower than that on the specimen due to their greater diameter. The maximum temperature experienced by the loading rams was also lower, if only by a few degrees, than that at the specimen. The spherical bearing caps (4) were made of Stellite 4 as before, due to its superior hardness. These caps were used as final alignment devices to accommodate any small defect in the machining of the specimen ends. The lubrication of the bearing surfaces proved to be a problem of some difficulty. Two factors were involved: (see Figs. 1, 1b).

1) To act as a true spherical bearing, the stellite caps have to be able to slide freely on the Nimonic female surfaces.

2) The specimen ends will be restrained from deforming by the unyielding Stellite cap. This leads to a "barrelling" of the specimen, with consequent overall lowering of the observed creep rate. This barrelling can be avoided by lubricating the interface between the specimen end and the Stellite cap.

The two most common high temperature lubricants, powdered graphite and molybdenum disulphide are both inadequate in this application on account of thermal instability, their useful temperature limits being 400°C and 700°C respectively. The manufacturers of "Molyslip" suggested that this lubricant should be applied, and degraded to molybdic oxide at high temperature. This procedure has been found to give some lubrication above 700°C. The decomposition of $Mo S_2$ would release sulphur in rather high local concentrations. This sulphur would then attack the Nimonic parts, and the specimen, since nickel alloys are particularly prone to attack by sulphidation/

sulphidation. In addition the MoO_2 is volatile, and so would not provide long-term lubrication. For these reasons, this procedure was discarded.

A few tests showed that a proprietary antiseize compound "Grade 516", made by Moly-Paul was effective, but analysis showed the compound to contain quantities of sulphur, and so this method had to be discontinued.

The most efficient lubricant which was tested was semi-colloidal glass suspended in iso-propyl alcohol. Such glass lubricants have been developed for hot rolling and forging processes, and have been reviewed by Alder and Phillips(69). The particular glass chosen softened at about 900°C, and had a useful range of temperature up to 1100°C. Despite its excellent qualities as a lubricant, this glass had its drawbacks, since when hot it reacted with the Stellite, and corrosion pits were formed. In addition, because it hardened on cooling, this substance bonded together the specimen, the Stellite spherical caps, and the Nimonic push rods. Before the caps would be aligned for another test. they had to be heated to break the glass bond, and reground to remove the glass and corrosion pits. Because of these practical considerations, colloidal glass was ruled out as a possible lubricant.

A possible lubricant would have been gold, or silver, plated on the opposing faces. Although no data was available on the performance of these metals as lubricants, two factors seemed to discount any possibility of their being used: they would probably have seized the mating surfaces on cooling, in the same way as colloidal glass did: and, because of this, the plating would have to be renewed before each test. On the other hand, silver bearings have been used in jet engine applications with apparent success(70).

In view of the lack of a suitable lubricant, tests were carried out to see if a lubricant as such was essential. Satisfactory/

Satisfactory antiseize properties were obtained using a preoxidation treatment on the Stellite and Nimonic bearing surfaces, with a thin film of powdered chromic oxide interposed. Since satisfactory creep tests could be completed using this simplified procedure, it was adopted and used throughout the testing programme. Since the specimens were given an aging heat treatment after being machined, a sufficient film of oxide was present on them without further treatment.

2.2 Tensile Loading Rig.

The technique of tensile creep testing has been developed over many years, and so the basic principles are well known, and have been reviewed recently by Penny et al[71]. The usual type of machine employs a lever arm pivoting on top of a rigid framework (Figure 2). The specimen is attached to the base of the machine and the lever arm, by means of universal joints, and a force is applied by hanging weights from the long arm of the lever. Such a machine was available in the University of Glasgow at the start of this work - the 3 ton High Sensitivity model made by the Mand Engineering Company. In view of the length of time occupied by creep testing, a second machine was built, similar to the Mand machine, and, in particular, with the same lever ratio of 17:1. The tensile tests were carried out on one machine and the compression tests on the other. By this means, two tests could proceed at the one time. Work was begun on two more creep machines, but these were not completed in time. This was no real loss, since two creep tests proved to be sufficient to occupy the full time attention of the author.

The shackles used to carry the load to the specimen in the hot zone were machined from 7/8 in. bar "Nimonic 105". These were attached via universal ball joints to the creep machine base and the lever arm (Figure 2). The specimen was screwed into these rods, which were preoxidised before use to ensure/

ensure that the specimen threads would not seize.

2.3 Specimen Design (Figure 3).

Under ideal conditions, a specimen for a compression test would experience a perfectly axial load. The length of the specimen could be set at almost any value, limited only by elastic buckling. However, due to inevitable machining and assembling errors, some bending moment is always present. The length-to-diameter ratio of a creep specimen must hence be restricted. For the purpose of obtaining a measurable creep rate for a given applied load, a long thin creep specimen is obviously more desirable than a short fat one. The former is also more unstable as far as buckling is concerned. As a compromise, a specimen size of 1.3" in length and 0.1 in^2 in cross section was chosen. This gives a length to diameter ratio of 3.65:1.

A frequent criticism made of compression tests is that the end restraints on the specimen are severe, even when a cylindrical test piece is compressed between flat plattens. Such criticisms ignore the end restraints placed upon all tensile specimens by the threaded portion of enlarged cross-section. It would be possible to carry out compression tests on specimens with similar enlarged threaded ends. Despite this, the right cylinder was chosen as the compression test piece, to minimise the end restraints (see Figure 3). The length-to-diameter ratio of 3.65:1 was large enough for any end effects to result in little change in the creep rate measured over the whole specimen.

The size of the gauge length of the tensile test piece was dictated by that chosen for compression, since otherwise unknown effects due to specimen size would have been present. The specimen for tensile creep tests was thus more massive than is normally employed, and consisted of a gauge length/

length 1.3 in. long and 0.1 in^2 cross-section (0.357 in. diameter) with a suitably enlarged portion on either end to carry a 0.625 in. B.S.F. thread (see Figure 3).

These specimens were machined in the solution-treated condition from one heat of Nimonic 105 by Rolls-Royce Limited, Derby, who also carried out the post-machining heat treatment. To check that the tensile and compressive material had identical initial properties, specimens for testing in a Hounsfield tensometer were machined out of two tensile and two compressive untested creep test pieces. Room temperature tensile tests showed that the Ultimate Tensile Strengths of all four specimens lay between 84.4 and 88 ton/in^2. This agreement is satisfactory evidence that the two types of specimen have the same properties before creep testing.

2.4 Furnace Design and Temperature Control (Figs. 4, 4a).

One disadvantage of this type of compression rig is that the frame restricts the size of furnace which can be used. This is particularly serious for the length of the furnace, since any furnace which utilises the full space available has to be made in two parts.

Consideration was given to the use of a furnace short enough to be slipped down off the test piece, so that a new one could be put in place. This would have restricted the length of the furnace to 4 in., which was too small to provide an adequate constant temperature zone over the length of the specimen. Hence a split furnace was deemed necessary.

Since the requirement for a split furnace is somewhat unusual, no suitable furnace was commercially available. The original furnace designed at the National Engineering Laboratory had its heater windings cemented to shells cast from refractory concrete. These shells were then mounted/

mounted in casings packed with insulating powder. After many trials, this design was found to be impractical due to the frgility of the refractory shells. When a more suitable material to support the windings was sought, it was realised that porous firebrick offered a useful combination of properties. By a change of design, a greater thickness of firebrick could be used; the firebrick was easy to machine, and porous, so that the cement, used to hold down the windings, could form a powerful bond by seeping into the holes in the firebrick.

The required internal tubular shape of the furnace was hollowed out oversize in two firebricks clamped together. Each brick was mounted in a casing (see Fig. 4) packed with Morgan "Tri-Mor Kaowool" insulation. The furnace was completed by cementing the windings in place and securing the wires to terminals on the furnace casing. The cementing was carried out last so that the windings would not be damaged during mounting.

Each winding consisted of a coil of wire wound on a 0.25 in. mandrel. This coil was stretched to separate neighbouring turns of the coil, and bent into three parallel straight sections. Two such windings were cemented symmetrically in each brick, with a gap of one inch between the windings (Figure 4).

Initially, the resistance wire used was the nickel-chromium "K" alloy made by British Driver-Harris. The use, later, of Kanthal A.1. improved the life of the furnace, partly because of its higher temperature capabilities and partly because of its higher specific resistance. This latter property permitted the use of less wire, so that the spiral coils could be extended further before being cemented. Because the pitch of these spirals was greater than that of the nichrome ones, there/

there was less likelihood of hot spots occurring, and producing premature failure of the furnace.

The restriction on the size of the furnace left insufficient room for insulation. Thus the heat losses were higher than would have been desired. Large heat losses also occurred by conduction through the heavy push rods. The effect of these heat losses was to raise the temperature of the main frame to 150°C in places. This affected the design of the extensometry, as will be shown. Despite these losses, the average rate of power consumption during a test at 1000°C was only 900 watts.

In a cylindrical enclosure such as that defined by the inner walls of the furnace convective currents are always present, carrying a flux of heat upwards. This becomes a serious problem when a zone of constant temperature is desired. The problem can be tackled on two fronts: the convection currents can be reduced and their effect can be counteracted. Towards the first aim, the ends of the furnace were plugged with "Kaowool", and a set of annular stainless steel heat shields was placed in the upper part of the furnace (Figure 1). The second aim was achieved by supplying more power to the bottom set of windings, by including a variable resistance in parallel with the top pair of windings (Figure 4a). The ratio of power supplied to top and bottom could thus be adjusted until the required temperature distribution was achieved. Vital to this aim was the correct spacing between the two sets of windings in each half of the furnace. The spacing was determined by trial and error to be just over 1 inch.

To obtain a constant temperature independent of room temperature and random mains voltage fluctuations, the power of the furnace was regulated by a "Sirect" controller. This is an electronic unit which senses the furnace temperature by means/

means of a platinum resistance thermometer held against the inside of the furnace wall. According to the temperature sensed, the "Sirect" controller makes the necessary adjustment to the furnace power (see Figure 4a).

Over periods of 100 hours, this system proved to be capable of maintaining the temperature constant to within ± 1.0 C° of the desired temperature. Tests with three Pt-Pt. 13% Rh (platinum-rhodium) thermocouples wired to the specimen showed that the temperature variation over the gauge length was ± 0.5 C°.

As testing proceeded, expertise was gained which allowed temperature variations to be reduced to very small values, especially in the short time tests. The effect of temperature excursions away from the desired value will be discussed in the next section.

The only difference in furnace design between tensile and compressive apparatus was that the bore of the tensile furnace was 0.5 in. smaller. This was possible because of the smaller diameter of the tensile loading shackles compared with the more massive rams used in the compressive rig. The smaller bore permitted the use of more insulation; less power was required to maintain a given temperature, and so longer furnace life was obtained.

A useful change in the control system was the use of graded balance resistors, with a maximum resistance of 2000 Ω, and a maximum current rating of 2 amp. At maximum resistance these drew only a small current, but within a few seconds their resistance could be reduced to the level of 20-40 Ω required for furnace control (Figure 4a).

2.5 Measurement of Creep Strain (Figures 1,1a, 2,2a).

The measurement of changes in specimen dimensions during/

during high temperature testing is a problem which has yet to be solved in an ideal form. Briefly stated, a method of measurement must be found which does not interfere with the stress system on the specimen, or with the temperature distribution within the furnace.

Until very recently, all methods envisaged a sensing element outwith the high temperature region. Advances in the design of strain gauges indicate that high temperature strain gauges can be developed with sufficient range to be of use in creep testing. Such gauges would be close to a perfect solution, since they are small, and only require two electrical leads to enter the furnace[72]. As yet, no report of their use, in this application, has been found.

Systems of extensometry in actual use have been reviewed before[73], and much research has been devoted to improving their sensitivity. The choice of a particular system is dictated by the accuracy required and the length of the tests.

For tests involving large deflections in times of an hour or two, measurement of crosshead movement by a dial gauge has proved adequate. It is assumed that all the movement measured represents specimen deformation, and that temperature fluctuations are small, since expansion in specimen and shackles could swamp the deformation.

For long time high-accuracy creep testing, the Martens mirror and roller system has been extensively used, in conjunction with legs projecting from the furnace from each end of the specimen. This system is less sensitive to temperature deviations, and possesses great long term stability and it has been used in tests lasting for years.

Kanter/

Kanter and Spring[58,63] have developed a method which does not require mechanical contact with the specimen. These workers used twin telescopes attached to vernier scales to observe opposite ends of a gauge length, through a window in the furnace. The use of this approach at the temperatures of interest here is limited due to the difficulty of defining a gauge length accurately on a body glowing hot.

The systems discussed so far are not inherently automatic. This is no drawback for short or very long tests. However, when tests last for a few minutes, or some tens of hours, difficulties arise, in the first case due to the inability to take sufficient readings and in the second to the large gaps in measurement occasioned by the intervening nights. In an investigation such as this present one, which is interested in the range of time indicated above, a system of automatic data collection is attractive, if not essential.

With the advent of electronics which are stable over long periods of time, a range of electronic displacement measuring devices has become available, suitable for automatic use. Such an instrument was chosen for the measurement of creep displacements in this study - the Recording Extensometer manufactured by C.W.S. Instruments. A differential transformer transducer is used as the sensing element. Changes in specimen length are converted linearly into a d.c. voltage, suitable for printing out on a potentiometric recorder.

The long-term accuracy of the C.W.S. instrument was claimed to be 5 micro-inches. It was found in practice that the accuracy obtainable was limited by radiation from the coils of the furnace, which were inductively wound. It was found that when power was applied to the furnace, a "noisy" output was obtained on the most sensitive ranges. When the transducers were removed from their position below the furnace,/

furnace, the stability of the output was as good as claimed in the specification. Attempts to filter out the interference did not meet with success. Since a non-inductive winding for the furnace is impractical for lack of space, the limiting discrimination of the system is 50 micro-inches.

Since the maximum operating temperature of the transducers is 40°C, they cannot be attached directly to the specimen gauge length. Deformation in the specimen was transmitted to the transducers by means of a system of rods and rollers.

Compressive Extensometry. (Fig. 1a, 1b)

It was intended that the extensometer rods should be clamped directly to the test piece, using three or four cone-ended screws for each pair of rods. However, during heating, the clamps consistently became loose at around 500°C, due to differences in the thermal coefficient of expansion between the specimen and the clamps, which were machined out of "Brightray" alloy. Compression tests without extensometry showed that specimen end effects were small - no barrelling of the specimens was measured. The points of attachment were thus moved outside the gauge length to positions on the loading rams above and below the specimen. The first tests were carried out with one leg on each side of the specimen, spring loaded against the top ram. Since no plastic deformation was expected in the lower ram, or the main frame, measurement of the movement of the top ram gave the specimen deformation directly. The "Brightray" legs experienced the same temperature regime as the ram, hence only a small error could arise from any temperature fluctuation.

When consideration was given to the measurement of activation energy, which necessitated measurement of the creep rate/

rate before and after an abrupt temperature change, it became clear that this single leg design must be modified. The large thermal capacity of the lower ram prevented the ram and extensometer leg from staying at the same temperature after an abrupt change of 20 C°. Until the temperature became stable throughout the furnace, further measurements of the creep rate could not be made. A second leg on each side of the specimen was added, this one hanging from the top of the lower ram, but held clear of it so as not to be in thermal contact. With this arrangement (Figure 1a), measurement of creep rate was possible 5 minutes after a temperature change, as compared with 45 minutes with the single leg arrangement. By this means the structural changes, in the specimen, taking place between the two measurements of creep rate, were minimised.

Each transducer body was held in a brass block screwed to the leg connecting with the upper ram; the core rested on a block attached, in the first instance, to the main frame, and in the later arrangement, to the leg connecting with the lower ram. This lower block was provided with a micrometer thread, so that the transducer core could be reset in any desired position.

Since it was imperative that no deformation should take place in the extensometer legs, the forces in them were kept to a minimum. The tension in the supporting springs was adjusted to a value just sufficient to hold the upper leg in position. The rollers were placed in line with the springs, so that no bending moments should be induced in the legs.

As mentioned above, heat lost from the furnace raised the temperature of the main frame to as much as 150°C. This was taken into consideration in positioning the transducer mountings. It was found that sufficient convective cooling occurred when the transducers were placed 6 in. below the main frame.

Tensile Extensometry. (Fig. 2a)

In view of the arrangement decided upon for the compressive extensometry, the tensile specimens were altered, by machining a groove on the enlarged portion at each end, so that the legs could be firmly clamped in this position (Figure 3).

Since more room was available on the tensile machine, micrometer barrels were used for resetting the transducer cores. During a period of three months, when a malfunction in the Recording Extensometer rendered it unusable, these micrometers were used as the extension measuring devices. A reliable contact device for use with the micrometers was constructed from a battery and light bulb, which lit up when the micrometer made contact with the upper leg. The accuracy of this system was 100 micro-inches, with excellent stability.

A better solution to the problem of attaching the extensometer legs is described in a recent review[71]. The specimen is machined with small ridges defining the gauge length and the extensometer legs are clamped to these. Unfortunately, the production of specimens had been completed before this method was discovered, but the reproducibility of the data obtained showed that the methods adopted introduced no perceptible error.

2.6 Constant Stress Creep Machines.

Nearly all creep tests are carried out at constant load rather than constant stress. In a tensile test, the stress increases with increasing strain, and many creep machines have been devised to counteract this tendency[58,21, 74,75]. In the main, these machines are fairly complex, and limited in the strain and gauge length they can accommodate. Since/

Since the maximum strain anticipated was 20%, and since strains derived from thermal shock are expected to be much smaller than this, the use of a constant stress device was not thought necessary. As will be shown, allowance for the changing stress can be made, given a knowledge of the stress-strain rate relationship.

2.7 Conclusions.

1) The problems associated with developing the N.E.L. design of compressive creep machine for use at temperatures up to 1000°C have been solved.

2) A furnace of unusual and novel design has been developed, and shown to meet the requirements for creep testing. Despite an overall length of only 10 in., this furnace gives a zone 1.3 in. long of temperature constant to within ±0.5 C°.

3) A tensile creep testing apparatus has been developed compatible with the compressive creep machine, so that tests can be carried out under conditions as nearly identical as possible.

CHAPTER THREE

CHAPTER THREE

EXPERIMENTAL PROCEDURE

3.1 The Testing Programme.

The actual tests carried out during this programme were decided by considering their application to thermal fatigue problems. When the details of the programme were decided, no preliminary analysis of the thermal fatigue problem was available. Hence the testing parameters were derived with a certain amount of surmise.

Since most deformation seemed likely to take place at high temperature, the main experimental programme was confined to the range of temperature between 950°C and 1000°C. A few tests were conducted at lower temperatures to indicate the general trend of the creep behaviour.

The stress levels were chosen to give rupture times on tension from a few minutes up to 150 hours. The maximum stress used at 1000°C was equivalent to 80% of the Ultimate Tensile Strength, and the lowest, 30% of the U.T.S. This stress range is large enough for useful conclusions to be drawn about a general stress-strain rate law. A complete list of the tests carried out is given in the accompanying Table.

Creep Tests on Nimonic 105

Test Number	Temperature °C	Stress + = Tension - = Compression LB. IN^{-2}	Length of Strain Test HOURS	Strain %	Remarks (except where stated otherwise)
T24	1000	+20,400	17 min.	17	
C32	1000	-20,400	24 min.	1	
C37	1000	-20,400	25 min.	4	
T21	1000	+17,000	80 min.	25	
C31	1000	-17,000	60 min.	0.7	
T23	1000	+13,600	$5\frac{1}{2}$	19	
C30	1000	-13,600	$3\frac{1}{2}$	0.5	
T30	1000	+10,200	25	10	
C33	1000	-10,200	24	0.7	
T31	1000	+ 8,500	50	1.7	
C34	1000	- 8,500	50	0.7	
T15	950	+20,400	11	2	
T16	950	+20,400	11	2	Fracture.
T20	950	+20,400	4	0.3	Test stopped at onset of tertiary creep.
T22	950	+20,400	$18\frac{1}{2}$		Fracture.
C27	950	-20,400	19	1.5	
C29	950	-20,400	27	2	
T12	950	+17,000	50	8	
T13	950	+17,000	50	8	Fracture.
T14	950	+17,000	48	7	
T19	950	+17,000	41	4	
C20	950	-17,000	42		Preliminary test No extensometry.
C21	945	-17,000	38	0.5	
C23	950	-17,000	36	0.6	
C24	950	-17,000	18	0.5	Specimen buckled.
C25	950	-17,000	90	4	Controller failed. Furnace temperature rose to 1100°C.

Creep Tests on Nimonic 105

Test Number	Temperature °C	Stress + = Tension - = Compression LB.IN^{-2}.	Length of Test HOUR	Strain %	Remarks
T 6	950	+13,600	150	8.5	Fracture.
T10	950	+13,600	130	4	
T11	950	+13,600	110	2	
C26	950	-13,600	125	1.5	
T33	930	+20,400	41	4.5	Fracture.
C36	930	-20,400	64	1	
T34	800	+61,200	26	4.5	
T35	800	+61,200	33	6	Fracture.
C38	800	-61,200	35	1.7	Pre-aged 2 hours at 950°C prior to testing.
C39	800	-61,200	27	0.8	
T28	1000	+13,600-20,400			Strain-rate sensitivity determination.
T26	950-1000	+13,600			Activation energy determination.
T27	950-1000	+17,000			Activation energy determination.
C35	950-1000	-17,000			Activation energy determination.
T18	950	+13,600-20,400	103		Fracture.

C in the test number signifies a compression test.

T in the test number signifies a tensile test.

Since a scatter of experimental data is usually expected in creep testing, it was anticipated that at each stress and temperature, several tests would be carried out, to obtain reliable results. Tensile tests at 950°C were repeated several times (see Figs. 16-18). The scatter of the creep curves was much smaller than anticipated and it was found that scatter between tests was much smaller than the differences measured between tensile and compressive creep rates. In some cases it was thus felt that after one test sufficient accuracy had been obtained for no repetition to be necessary.

This, however, is modified for the compression tests, for which there is the ever present problem of the buckling of the specimen. After each test, each specimen was examined for signs of misalignment, which showed up as oxidation of the ends. In most tests the ends were completely free from oxidation. A test for buckling was then carried out, by placing the deformed test piece on a flat surface beside an undeformed one. Any buckling showed up clearly when the deformed specimen was rotated. Tests which resulted in buckled specimens were discarded, and another test carried out under the same conditions, until a satisfactory test was produced.

The effect of buckling on the creep curve was seen as a large increase in creep rate (Figure 19). The fact that some specimens did buckle with the above result can be used to show that the low compression creep rates reported later are not due to buckling effects. The result of a creep test in which the specimen buckled is shown in Figure 19, along with two other tests carried out under the same conditions. It can be seen that the effect of the buckling causes much larger differences than the scatter between successful tests.

3.2/

3.2 Assembly of Compression Creep Tests.

The alignment of the specimen was the first and most crucial step in the assembly of the compression test an approximate positioning was carried out by eye. Aligning clamps were then screwed round the top and bottom loading rams (Figure 1a). These clamps held the specimen parallel to the loading axis, and co-axial with the rams. A light load was placed on the load platform so that the specimen should be held firmly in place.

The loading and aligning systems were tested by cementing three strain gauges to the specimen, parallel to the long axis, and spaced at 120° intervals round a diameter. Weights were added to the load platform, and at each increment of load all three strain gauges were monitored by a "Peekel" strain gauge meter with a resolution of 10^{-7} in. The measured elastic modulus agreed precisely with the published value, taken from the "Nimonic Handbook" published by Henry Wiggin and Company[6]. This was satisfactory, since it implied that losses in the load transmission system were negligible.

The outputs from the three strain gauges were compared to detect bending in the specimen. After each loading cycle the specimen was dismounted and realigned. Over six repetitions the maximum difference in strain amounted to 10% of the mean value. The average difference in strain was less - of the order of 5%. Anything short of the most careful alignment produced very large differences, with one side of the specimen in tension, the other in compression. In view of these results, it was concluded that the alignment system was accurate enough to warrent extended trial during high temperature creep.

With the specimen held firmly, the aligning clamps were removed. Two Pt-Pt, 13% Rh thermocouples were wired to the/

the specimen, with the thermocouple beads pressed tightly against the specimen. Tests showed that shielding the beads of the thermocouple from direct furnace radiation made no difference to the temperature measured. Of much greater importance was adequate contact between the thermocouple and specimen. One disadvantage of wiring-on the thermocouples was that the soft platinum limb became deformed, and after repeated straightenings, became weak. At this point the thermocouple was scrapped and a new one used in its place.

After mounting the extensometer legs, the furnace was put in its place, before the transducers were locked in their holders. Exposure of the transducers to dust and grit from the furnace was thus kept as small as possible.

At this stage it would be natural to balance the loading lever to allow for the weight of the main frame hanging from it (Figure 1). To do so would have necessitated removing the load from the specimen. In this condition, it would have been possible for the specimen alignment to have altered. The beam was thus balanced before the specimen was aligned, an allowance being made for the weight of the upper loading ram, by adding a few pounds weight to the loading and carrying out the final adjustment by means of the moveable balance weight on the crosshead (Figure 1).

During the initial heating period the balance resistors were excluded from the circuit to keep the output current from the "Sirect" below the 13-ampere capability of the mains supply. Heating was rapid-within 20 minutes of switching on it was possible to reach 1000°C. Normal procedure was to bring the furnace temperature to 40°C below the required test temperature, and to adjust the temperature distribution at this level. When the difference between top and bottom thermocouples was less than 5 C°, the furnace temperature/

temperature was raised to the test requirement and final balancing carried out.

Because of the long term stability required in the creep tests carried out at 950°C, at this temperature a 24 hour period of stabilisation was allowed before loading. This time fulfilled a second purpose in that the material was given the same amount of aging before testing at 1000°C, by loading these tests 3 hours after reaching temperature. This shorter period of stabilisation at the higher temperature was possible due to the expertise gained during the tests at 950°C and to the, generally, shorter length of the tests at 1000°C. It is felt that these precautions to ensure identical material structure at the start of each test is a major factor in increasing the accuracy of the experimental results.

Just prior to loading the extensometry calibration was checked. The weights were then applied during a period of 30 seconds, so that the last weight was added just before the extensometer output was printed or the chart recorder - a Kent "Multilec", Mark III. This point was taken as the zero for measurements of creep strain. It may be noted here that the effect of the impact of a weight being placed on the load platform was checked with the strain gauged specimen. The maximum excess load due to the impact of a weight was measured as 0.5 lb., that is, less than 1% of the total load. In addition, no long lived transient vibrations were recorded.

During the course of each test the temperature was monitored continuously, either by applying the thermocouple outputs to a Kent Multilec recorder, or by direct measurement on a Cambridge potentiometer. On the recorder, a discrimination of 0.5 C° was possible. With the potentiometer, changes of 0.1 C° could be detected.

In/

In compression the creep experiments were invariably ended by switching off the power to the furnace, while leaving the specimen loaded until cool. By this means, the dislocation structure developed during creep was preserved for future examination by transmission electron microscopy. However, due to the lack of an electron microscopy until the closing stages of this investigation, no such transmission studies were in fact carried out.

3.3 Tensile Creep Tests.

These tests were much more easily assembled than the compression tests, since no specimen alignment was necessary. Otherwise, the procedure was as outlined in the previous section for the compression tests. The exception related to the action at the end of a test. After those tests in which the specimen was allowed to break, the falling weights were caught by a shock-absorber of expanded polystyrene, and the furnace switched off immediately after.

3.4 Calibration of Thermocouples.

Before use all the thermocouples were calibrated for the temperatures of interest against a thermocouple calibrated at the National Physical Laboratory. The accuracy of the calibration of this standard was $\pm 0.3\ C^{\circ}$ above $800^{\circ}C$.

For checking, each thermocouple was connected to its own length of compensating lead, and the junction placed in a furnace along with the standard thermocouple. When the thermocouples reached the furnace temperature, the e.m.f. from each was measured. Repeatable results were not obtained until a satisfactory method was found for maintaining thermal contact between the two thermocouple beads. Despite the fear of damage to the standard, the only useful method was to wire the beads firmly together.

Each/

Each thermocouple was calibrated for all the temperatures at which it was used, and in fact, all the tests showed agreement between the standard and the creep test thermocouple within the limits of the original calibration of the standard. For these calibration tests, as for the creep tests the thermocouple cold junctions were maintained at zero degrees Centigrade by immersion in a well-stirred mixture of ice and water.

3.5 The Effect of Temperature Variations on the Creep Rate.

We now consider the effect of small temperature variations on the creep rate. According to the arguments advanced in the Introduction, the creep rate follows an exponential temperature law, i.e.,

$$\dot{\epsilon} \quad \alpha \quad \exp\left(\frac{-Q}{RT}\right)$$

If now the temperature changes from T to T + δT, we have, when δT is small compared to T.

$$\ln \frac{\dot{\epsilon}_{T+\delta T}}{\dot{\epsilon}_T} = \frac{-Q}{R(T+\delta T)} + \frac{Q}{RT}$$

$$= \frac{Q\,\delta T}{RT^2}$$

If now numerical values are inserted

$$Q = 100 \text{ k cal/mole}$$

$$T = 1000^{\circ}C = 1273^{\circ}K$$

a table can be drawn up as follows, to show the effect of δT on the creep rate

δT °C	$\dot{\epsilon}_{T+\delta T}/\dot{\epsilon}_T$
0.1	1.003
0.5	1.02
1	1.07
2	1.15
5	1.41

From this table it can be concluded that temperature fluctuations of more than one degree cannot be tolerated for a large fraction of the duration of the test. Cyclic variations in temperature of about a degree or less, with a period much shorter than the duration of a test, would have a negligible effect on the final creep curve. For this reason, almost constant supervision was given to the temperature of each creep test, so that any drift from the required temperature should not go undetected for long. Such drift was usually caused by abrupt changes in the ambient conditions, such as those due to the opening of the windows of the laboratory in which the creep tests were carried out. One of the most important factors in obtaining accurate temperature measurement was found to be adequate stirring of the ice-water mixture used as a standard cold junction for the thermocouples. A desirable feature for any creep testing facility is a thermostatically controlled room for the creep machines. This assists in maintaining constant temperatures at the test pieces. Although the room used in this investigation was not so controlled, the temperature remained fairly constant due to the continuous use of several furnaces which maintained room temperature above that of the surroundings.

3.6 Consideration of Errors.

The variations in temperature discussed above are the most important source of error in the determination of creep curves. Several other errors must be considered before the overall accuracy of the creep tests can be assessed.

The weights used in the loading of the creep machines were of two kinds. Those used for nearly all of the test were a set of 40 lb. and 20 lb. iron weights, calibrated accurately/

accurately to within 1 part in 7,000 of their stated weight. Another set used occasionally were 10 lb. weights calibrated to within 0.5% of their stated weight. In no case did these 10 lb. weights comprise more than 20% of the total load, so that any effect due to their less accurate calibration should be minimised.

The calibration of the transducers was carried out prior to each test by means of a barrel micrometer with a 4 in. diameter, incorporated in the C.N.S. Recording Extensometer. This was used to move the core of a transducer whose performance matched exactly that of the external transducers. A typical calibration would thus be that 10 mV. on the Kent recorder chart represented .025 in. ± .0002 in. When the chart record was processed so that the creep curve could be plotted on a convenient scale, one side of the dotted line was consistently read.

Time was measured during the test by two means. The recorder drove the chart at a known speed e.g. 4 in./hour. This was used routinely to measure time, and the speed was checked by noting the time on an electric clock periodically. The chart drive system in fact proved itself to be extremely accurate, and was never found to be in error.

In the absence of sufficient tests at any one temperature and stress to estimate the accuracy statistically, it is estimated that the final accuracy obtained was ±10%, although better agreement than this was obviously obtained in such tests as the tensile ones in Figure 15.

3.7 Metallography.

After testing, a portion from the gauge length of each specimen was sectioned longitudinally by grinding, and polished, first on wet silicon carbide papers, starting with 220/

200 grit, and finishing with 600 grit, then on "Selvyt" cloth or a Struers "Nol" polishing pad, impregnated with diamond dust and lubricated with "Marcon" polishing lubricant. At first all the polishing was done by hand, but later an automatic polishing attachment was obtained for the diamond polishing stage. Although slow, this device produced a very fine polish.

When a scratch-free polished surface had been produced, an etching treatment in a mixed acid etch revealed the microstructure for examination in the light microscope. The composition of the etch is given below. The etch was applied either by swab or immersion for 7-10 seconds, and was followed by a hot water wash, and drying in a blast of compressed air.

Composition of Chemical Etch	
Nitric acid, concentrated	15 ml.
Hydrochloric acid, concentrated	85 ml.
Anhydrous ferric chloride	5 gr.
Cupric chloride	5 gr.
Water to make up to	200 ml.

Very late in the course of this investigation, an electron microscope was installed in the Engineering Department of the University of Glasgow. A few of the specimens were repolished and etched electrolytically to leave the gamma prime particles standing clear of the surface. The etchant used was an aqueous solution containing 10% glycerol and 5% hydrofluoric acid, using a nickel-chrome cathode at an etching voltage of 2-4 volt. Replicas of these specimens were examined in the electron microscope, and the resulting photographs were measured to detect differences in the amount of gamma prime present after tensile or compressive creep. Lack of time prevented extension of this investigation/

investigation to include detailed analysis of all the specimens and, of particular interest, examination of dislocation arrangements in thin sections of deformed material.

The main metallographic study was thus carried out by light microscopy, and consisted of an examination of the visible damage caused by creep deformation. In particular the incidence of grain boundary voids and cracks was investigated by scanning the surface at right angles to the stress axis, using a magnification of 400 X. The cracks and voids were counted, and classified according to their position: either at a triple point, elsewhere on a grain boundary, or within a grain (see Figures 27-42).

A further subdivision was made according to whether or not the cavity was associated with a large grain boundary particle, e.g. a massive carbide or a cyanonitride particle (see Figures 34-37). The smallest cavity detectable was about 1μ across its smallest dimension (see Figure 30).

On all the tensile specimens a careful comparison was made between the gauge length, and the undeformed threaded end. This was useful in showing that the intragranular cavities were not due to deformation, since equal numbers were present in the gauge length and the enlarged ends.

The effect of oxidation on the surface of the specimens was routinely examined, to ensure that no gross changes in gauge diameter due to this cause should go undetected. However, no oxidation was ever observed to penetrate deeper than about half a grain diameter (see Figure 44).

3.8/

3.8 Conclusions.

1) A reliable creep test procedure has been developed, and the scatter observed was very small, especially after the first few tests during which expertise was developed (Compare the tensile tests in Figures 15 and 18).

2) This accuracy was thought to be due to the attention given to ensuring that the material at the start of each test had the same amount of aging, and to the supervision given to the temperature measurement and control systems.

3) A method of crack analysis has been developed which should enable the growth of cracks to be followed.

CHAPTER FOUR

CHAPTER FOUR

DISCUSSION OF THE RESULTS OF THE CREEP TESTS

Introduction.

This chapter is devoted to the exposition and discussion of the results of the creep testing, and the subsequent metallographic examination of specimens. Since not all the creep tests had the same purpose - from some were produced strain-time curves, while from others values for the activation or stress exponent - the discussion is of necessity somewhat complex. First the effect of strain upon strain rate is discussed, and constant stress curves are computed from the constant load creep curves plotted in Figures 6 to 15. The reason for this is that comparison between tensile and compressive creep curves produced under constant load is not possible at large strains, as shown in section 4.1.

As was pointed out in Chapter One, the stress exponent, and the activation energy should be measured for the particular alloy under test. The results of these tests are discussed next, in that order.

Before comparing the creep behaviour in tension and compression, those factors which may change the creep rate are investigated. Firstly, cracking, and so included in this section are the results of the optical metallography; secondly precipitate changes, and the results of the small amount of electron metallography carried out.

Finally, the creep behaviour in tension and compression is compared, and likely causes for the differences are discussed in terms of the theoretical treatment developed in Chapter One.

4.1 The Effect of Strain on the Applied Stress.

As extension or compression proceeds, the cross-section of the test-piece is constantly changing. In consequence, despite the fact that the load is constant, the stress impressed upon the specimen changes. During a tensile test the stress progressively increases. This leads to the observed creep rates being higher in a constant load test than in a constant stress test. Andrade first pointed this out, and devised a method for applying a constant stress[20]. Because of these changes in cross-section, it is not realistic to compare the creep curves in tension and compression until allowance has been made for this effect. The following calculation shows how such allowance may be made.

It is assumed that during the course of a creep test the test-piece maintains a constant volume. Since the elastic strain is small compared with the plastic creep strain, both the longitudinal and lateral elastic strains can be neglected.

For a test-piece of gauge length ℓ and cross-sectional area A, the constant volume condition implies

$$\ell A = \text{constant} = \ell_o A_o \qquad \text{where}$$

ℓ_o and A_o are the values of ℓ and A at the start of a test i.e. at zero time

$$\text{hence} \qquad A = \frac{\ell_o A_o}{\ell}$$

Thus the stress on the specimen,

$$\sigma = \frac{\text{load (L)}}{A}$$

i.e./

$$\text{i.e.} \qquad \sigma = \frac{L\ \ell}{\ell_o A_o}$$

Now, at a point in the test where the strain is ϵ,

$$\ell = \ell_o(1 + \epsilon),$$

where ϵ is positive in tension, negative in compression

$$\text{so} \qquad \sigma = \frac{L}{A_o}(1 + \epsilon)$$

$$= \sigma_o(1 + \epsilon), \qquad \text{where}$$

σ_o is the stress at the start of the test.
To determine the effect of this change in stress upon the creep rate, a strain rate dependence upon stress is assumed of the type derived by Weertman's analysis

$$\text{i.e.} \qquad \dot{\epsilon} = k\sigma^n, \qquad \text{where } k \text{ is a constant,}$$

and, in the next section, n will be shown to be 9 for these tests.

For a constant load test, we thus have

$$\dot{\epsilon} = k\sigma_o^{\,n}(1 + \epsilon)^n \qquad (1)$$

This can be integrated to give the strain-time relationship in a constant load test

$$(1 + \epsilon_o)^{-n+1} - (1 + \epsilon)^{-n+1} = (n - 1)k\sigma_o^{\,n}(t - t_o) \qquad (2)$$

where ϵ_o is the strain when $t = t_o$. If the primary creep strain is subtracted away from the creep curve, the condition could be $\epsilon_o = 0$, at $t = 0$. This is the equation of the creep/

creep curve under a constant load which would be measured if no structural changes took place. Since it is known that the precipitate size distribution does change during a high temperature creep test, the condition of no structural change is not met. This equation (2) is, hence, of no great value in correcting constant load curves to constant stress. Equation (1) is more useful in this respect, and, in fact, was used in the following manner.

Each creep curve was approximated by a series of chords. Each chord represented ½% or 1% of strain, centred on a particular value of strain, say, ϵ. For the purpose of discussion, let us call the strain interval $\delta\epsilon$. If the stress were constant, then in the same time interval, the amount of deformation would not be $\delta\epsilon$, but $\delta\epsilon/(1+\epsilon)^9$. This follows since the creep curve can be approximated by a series of sufficiently small chords, and since the creep rate in constant stress can be derived from that measured in constant load by means of equation (1) above, i.e.,

$$\text{strain rate at constant stress} = \frac{\text{strain rate at constant load}}{(1+\epsilon)^9}$$

Each new increment $\delta\epsilon/(1+\epsilon)^9$ is fitted to the previous one, to produce a new creep curve, as shown in Figures 6 - 15.

It may be argued that this process of normalising the curves to constant stress is invalidated by the creep damage caused at the higher stresses. Such increased creep damage may be present, but all the important effects can be shown to happen during the first few percent of strain when the stress is essentially constant, as can be seen from the following table, giving values of $(1 + \epsilon)^9$ in tension and compression.

ϵ (percent)	$(1+\epsilon)^9$ Tension	$(1+\epsilon)^9$ Compression
1	1.1	0.9
1.5	1.14	0.88
2	1.2	0.83
2.5	1.25	0.8
3	1.3	0.77
3.5	1.36	0.74
4	1.42	0.7
4.5	1.5	0.67
5	1.55	0.65
6	1.7	0.59
7	1.84	0.54
8	2	0.5
9	2.2	0.45
10	2.36	0.42
15	3.5	0.28
20	5.2	0.19
25	7.5	0.13

It can thus be seen that only a small effect will operate below 2% strain, while, in fact, no great difference appears until strains in excess of 4% are reached (see, e.g. Figures 6 and 14).

The constant load and constant stress curves are shown together in Figures 6 - 15, along with the corresponding compressive creep curves. Since the strains observed in compression were very small - usually less than 2%, no correction was required to convert these to constant stress curves.

As/

As will be seen, the amount of correction to the tensile curves is not large except at large values of strain, and, indeed in the case of Figure 10, no correction was applied, since the total strain measured was 1.5%. On the other hand, the tensile curves shown in Figures 6 and 7 reduce to straight lines, and have undergone large amounts of correction.

It is possible that constant-stress rupture times could be derived using this method, and extrapolating the curves to the same total extension as is measured in the constant load tests. Since this ductility does not change much with stress, the value obtained from the constant-load tests could be used. Rough estimates from the available data indicate that such rupture times would exceed the constant-load rupture times by as much as 50%. This procedure could be inaccurate due to the voids which develop as strain proceeds. Much of the extension takes place just prior to rupture, and so the constant-stress rupture life might not be much longer. An approximate determination could be carried out with the present apparatus by progressively reducing the load as the strain increases.

4.2 Dependence of Strain Rate on Stress.

The stress dependence of the creep rate was measured by carrying out a creep test at various loads. The amount of strain required at any one load to establish the creep rate was very small - about 0.1%, and the total strain over a stress change test was not more than 0.5%, hence no correction to the stress was required on account of the changing cross-section. Assuming a stress law of the form

$$\dot{\epsilon} \propto \sigma^n,$$

a/

a plot of log $\dot{\epsilon}'$ versus log σ should give a straight line with a gradient n. The results of these tests are shown in Figure 20. Stress-change tests were carried out in tension at 950°C and 1000°C. The values of the minimum creep rate measured in constant stress tests at 1000°C are plotted on the same graph. These are included in the estimation of n, although the material in the different tests has had slightly different aging. The values of n calculated from Figure 20 are shown below

Test Type	Temperature	Stress Range ($LB.IN^{-2}$)	n
Compression, constant stress	1000°C	20,400- 8,500	8.5
Stress change, Tension	1000	20,400-10,200	10.1
Stress change, Tension after 100 hour creep	950°C	20,400-13,600	10.2

Another method of measuring n is to use the change of stress in a constant load test. From the analysis in the previous section $\dot{\epsilon}' = k \sigma_o^n (1 + \epsilon)^n$.

Hence by plotting log $\dot{\epsilon}'$ versus log $(1 + \epsilon)$, the value of n can be obtained from the slope of the resulting graph (Figure 24). This applies so long as k is constant i.e. that the structure is constant during the test. From the information given in the paper by Mitchell[51], it can be calculated that only a small overaging effect takes place during the tests shown in Figures 6 and 7. In fact the precipitate size should change only by a factor of 1.1.

The further objection may be made that, since a small amount of cracking is observed, this will vitiate any value of n derived in this way. Since the amount of cracking must increase with increasing strain, it would be expected/

expected that the value of n so derived would be high. In fact the average value derived in this way from Figure 24 is 8.3. Thus, although this value is, if anything, high, it is in reasonable agreement with the values derived, by other means, above. For the stress exponent required for the analysis of the previous section, an average value of 9 was taken.

Although this is much higher than the value of 4 derived by Weertman, it is not out of line with other stress exponents measured in two-phase alloys. These range from 4.5 in René 41[9] through 7.7 for Mar M-200[76] to 40 in T.D. nickel[29]. This large range of values is not covered by the estimated errors in these investigations, and so it must be concluded that the stress exponent is a property of the particular material used in any series of tests.

The fact that the stress exponent measured in compression agrees well with that in tension is powerful support to the argument that this high value is not due to cracking. Large variations in the value of the stress exponent have been observed in other systems. A series of gold-nickel alloys has been investigated, and values of n from 2 to 5.5 have been measured, depending upon the concentration of nickel[77].

4.3 The Temperature Dependence of the Creep Rate.

In line with the widely held view that creep is diffusion controlled, creep tests at constant load but changing temperature were used to measure the activation energy of the creep process. The results of these tests are shown plotted as log $\dot{\epsilon}$ versus $1/T$ in Figures 21 to 23, and in the table below.

Stress $LB.IN^{-2}$	Temperature Range ^{o}C	Measured Activation Energy k.cal./mole
13,600 tensile	950-1000	203 ± 20
17,000 tensile	950-1000	190 ± 20
17,000 compressive	950-1000	250 ± 25

The values for the activation energy tabulated above agree well with the figure of 210 ± 30 k.cal/mole reported for Rene 41[9], although they are much higher than those reported for several other nickel base alloys of different composition, which span a range from 80-133 k.cal/mole[33,34,77]. For comparison, the activation energy for self-diffusion in nickel is 66 k.cal/mole[78]. The wide spread of activation energies for creep, and the disagreement between predicted and measured activation energies, have not yet been explained in any satisfactory manner.

It can be said, however, that the measurements of Conrad et al[9] on René 41 and the present investigation share the feature that they are very high temperature studies in which the activation energy was measured by recording the creep rate a very short time after the attainment of the test temperature. This feature is not shared by the other investigations quoted above[33,34,37] in which the creep rate was measured some longer time after the change in temperature. In this latter instance, relatively small changes in the amount and size of precipitate particles would occur during this measurement.

These considerations render plausible the proposal by Conrad et al[9] that a) the higher activation energy is due to the changes in precipitate structure which are known to take place at high temperatures or b) there is an energy of/

of interaction between a solute atom and a precipitate which leads to an increased activation energy for climb, and hence for creep.

The distinction between these becomes blurred when it is realised that both imply that the structural ordering and compositional changes, involved in the formation of gamma prime particles, hinders the climb of dislocations round these particles. Since the phase boundary is highly coherent, it is unlikely to be a prolific source or sink of vacancies. There will hence be a flow of vacancies towards or away from the climbing dislocation. Diffusion within the precipitate particles has not been considered as affecting the rate of climb, but given that such vacancy flows do exist, a possible explanation for the magnitude of the activation energy could be found in this effect. This idea is developed below.

As stated before, the gamma prime particles have a fully ordered structure based on the f.c.c. lattice, and in such systems, very high activation energies for diffusion have been measured[79]. For Ni_3Al, a value of 164 k.cal/mole is quoted. This figure would, presumably, be modified by the titanium, chromium and cobalt present in the gamma prime of Nimonic 105, but in such a two-phase system the activation energy as measured in a creep test should be some combination of the activation energy in Ni_3Al, with that in pure nickel. In the absence of a complete understanding of the diffusion processes involved, a value for the creep activation energy cannot be predicted. Two considerations of which give added force to this argument are

a) the large amount of gamma prime present in modern nickel heat-resistant alloys.

b) the observation of superdislocations in the matrix of a nickel alloy[37] which indicate that some long range ordering is present. This ordering would increase the activation energy throughout the alloy.

4.4 The Stress Dependence of the Activation Energy.

The difference between activation energies measured in tension (see table, section 4.3) and compression was not unexpected, since the creation of a vacancy should be assisted by a tensile applied stress, and hindered by a compressive stress. The compressive activation energy should, therefore, be the higher, since, in essence, this energy is compounded of two parts: the energy to produce a vacancy, and the energy required to move it from one atomic rate to a neighbouring one. We can express this approximately as

$Q = Q_o + A\ p\ V_v$

where Q is the measured activation energy in k.cal/mole

Q_o is the activation energy, at zero stress, in k.cal/mole

p is the applied stress

V_v is the volume of a vacancy

A is Avogadro's Number = 6.02×10^{23}.

The term $p\ V_v$ is simply the work done by the external forces when a vacancy is created in the lattice.

For the present case, a value of $10(A.U)^3$ was used for V_v, giving

$$Q = Q_o + A\ p\ V_v$$
$$= Q_o + 6\ \sigma \times 10^{-5} \quad \frac{\text{k.cal/mole}}{\text{lb.in}^{-2}}$$

where σ is the applied stress in lb.in^{-2}.

If we take $\sigma = \pm 17{,}000\ \text{lb.in}^{-2}$.

we have $Q = Q_o \pm 1.02$ k.cal/mole.

The difference in activation energies should thus be of the order of 2 k cal/mole. This is an order of magnitude smaller than the measured difference of 50 k.cal/mole. The experimental error associated with the measurement of activation energy is $\pm 10\%$, hence the actual difference in Q may be much smaller than the figure quoted, but still appreciably larger than that predicted from the above analysis.

Since all the tests were carried out in identical fashion, with the temperature reduced from 1000°C in steps of 10-15 C°, the possibility of systematic error was minimised. The decreasing temperature method was adopted to minimise the effects of structural changes during the tests. After a comparatively brief period of time at 1000°C, the equilibrium volume fraction of precipitate would not have been reached, so that when the temperature was reduced very little further precipitation would occur. During the alternative, increasing temperature method, the amount of precipitate would tend to decrease as the temperature was increased, so that structural change would certainly take place between successive measurements of the creep rate.

In an extensive series of measurements of Q in Nimonics 80A and 90, Heslop[33] observed no stress dependence, but a slight increase with temperature an increase of 30% being observed over the temperature range from 700°C - 900°C. On the other hand, Murray and Choubey[34] obtained a strong stress dependence over the same stress range, but since the measurements were spread over a wide temperature range, it is likely that the effect is due to temperature rather than stress. Indeed, these authors ascribe the changes in Q to a change in the mechanism of creep deformation, from cross-slip to climb.

From these several observations, it is concluded that at the stress levels discussed the activation energy for creep is little affected by stress - induced changes in the energy of formation of a vacancy. This effect is certainly much smaller than that which increases the activation energies to 200% more than the value for self-diffusion in pure nickel.

Also, from the limited observations made, the activation energies in tension and compression are different. Further experiments would verify this point and determine more accurately the magnitude of the difference. An indication that/

that the stress should affect the activation energy is given by the work carried out by Butcher[80,22], who found that the activation energy for creep in a constant shear stress test was linearly dependent upon the applied hydrostatic pressure. A smaller effect should probably be expected from the present experiments, in which the applied stress is uniaxial, hence Butcher's work cannot be compared directly with this present study.

4.5 Changes in Precipitate Size and Amount, and their Effect on Creep Behaviour.

The discussion of section 1.5 showed that a system of precipitate particles tends to a more coarse size distribution as it is exposed at high temperature. The creep resistance of precipitation hardened alloys is further reduced by the fall in the volume fraction of precipitate. For Nimonic 105 the final aging treatment at 700°C converts about 50% by volume of the alloy to the gamma prime phase. From Figure 25 which is derived from the data given in the paper by Rowe and Freeman[19], it can be seen that the equilibrium volume fraction of gamma prime falls with increasing temperature, so that at 1000°C, only about 20% gamma prime will remain after long aging times.

Together these effects reduce the number of precipitate particles and increase the spacing between them. Quantitative expression can be given to this weakening effect by considering Weertman's derived structural parameter, λ^2/h, where λ = the average interparticle spacing

h = the average particle diameter.

For a given volume fraction of gamma prime, V,

$$V = \frac{h}{\lambda+h} ,$$

since/

since the volume fraction of precipitate is measured by summing the intercepts of precipitate particles on a line drawn on a micrograph of a plane section of the specimen. V is then given by the ratio of the sum of the intercepts to the total length of the line.

$$\text{Hence} \qquad \frac{\lambda^2}{h} = h\left(\frac{1}{V} - 1\right)^2$$

Using Wagner's law (section 1.5), this can be written

$$\frac{\lambda^2}{h} = (A + B\, t^{\frac{1}{3}})\left(\frac{1}{V(t)} - 1\right)^2$$

where A, B are constants, and V(t) gives the variation of the volume fraction of gamma prime with time.

If V(t) were constant, the structural parameter would vary directly as h. As can be seen from Figures 45 and 46, the amount of gamma prime present after 60 hours at 950°C is 25% in fair agreement with Figure 25. The effect of this decrease in the amount of precipitate from the 50% initially present can be seen from the following table, in which the variation of the factor $\left(\frac{1}{V} - 1\right)^2$, with changes in V is shown

Volume fraction of gamma prime (V)	Factor $\left(\frac{1}{V} - 1\right)^2$
0.5	1
0.4	2.25
0.3	5
0.2	16

If the factor $\left(\frac{1}{V} - 1\right)^2$ was substantially constant over the observed range of V, the variation of λ^2/h with time would be predictable. But, from the table given above, $\left(\frac{1}{V} - 1\right)^2$ changes by an order of magnitude in the range of V which is of interest.

Hence/

Hence without a specific knowledge of V(t), the relationship derived by Wagner is of only limited use in the prediction of creep rates. This lack of information could be remedied by a comparatively simple electron microscope investigation, but no such study has, to this author's knowledge, been published.

The effect of precipitate changes can be seen clearly in the compression tests plotted in Figures 6 - 15 as an increase in the compression creep rate with time. The shape of these compression curves follows a pattern consistent with the changes in precipitate size. At short times, that is less than two hours testing at 1000°C, or less than four hours at 950°C, the compressive creep rates show no tendency to increase with time. At longer times, however, what appears to be a phase of tertiary, or accelerating, creep, is found. This behaviour was unexpected, since the stress is decreasing throughout these compression tests, even if only slowly at these low strains, and so the creep rate should have become smaller as the strain increased, in accordance with the equations developed in section 4.1. That this tertiary creep should be ascribed to overaging seems certain, since changes in cross section due to cracking can be ruled out in compression, both intuitively, and on the grounds that no cracking was observed in specimens which had undergone compression creep. Another alternative which must be rejected is the possibility that the tertiary creep is due to specimen buckling. As described previously, careful precautions were taken to prevent buckling, and to detect it if buckling did occur. The onset of tertiary creep can occur at small strains, as in Figure 10, but does not necessarily appear at larger strains, as in Test No. C 37, which reached 4% after 75 minutes.

Temperature/

Temperature °C	Stress LB.IN^{-2}	Strain %	Time hour	Increase in $\dot{\epsilon}$ over minimum value
1000	20,400	4	1.25	1.5
1000	8,500	1.5	50	20

For ease of presentation a comparison of the two tests is made in the table above. The high stress test, No. C 37, was corrected to constant stress in the same way as the tensile tests, this time using a factor of $(1 + \epsilon)^{-9}$ to multiply the creep rate. Were the tertiary creep due to buckling, it would be anticipated that the effect would be larger at high strains. This is not so, and in line with the postulate that the tertiary creep is due to agglomeration, after a long time at high temperatures - 50 hours at 1000°C - the creep rate increased by a factor of 20 over the minimum value, measured early in the test.

The compression creep tests at 800°C confirm the pattern of behaviour at higher temperatures. The rate of agglomeration at 800°C is much lower than at 1000°C, and so it can be said that the amount of aging taking place is proportionately lower.

The test carried out under normal conditions showed no tertiary creep (Figure 15). Another test at 800°C, and the same stress was carried out, but the specimen was given an overaging treatment of 2 hours at 950°C in the creep furnace, before testing began. As expected, the creep rate in this test was higher (Figure 15) than the previous one, and once again, when even less agglomeration was expected, no tertiary creep took place. It is worth while to mention here that the stress in the tests at 800°C was 61,200 lb.in^{-2}, three times higher than the highest stress used at more elevated temperature. In these tests the effects of buckling should have been most obvious,/

obvious, yet no tertiary creep was seen. It is anticipated that, given long enough at any high temperature level, tertiary creep would be observed due to the changes induced in the precipitate size distribution.

4.6 Grain Boundary Cracking and the Results of the Metallographic Examination.

The discussion in this section will be devoted to the incidence of cracking during a creep test. At the high temperatures of interest in this investigation, failure occurs by the growth and coalescence of grain boundary cracks. This holds as a general rule for metals and alloys, and the inhibition of crack growth is a major objective in the heat treatment of Nimonic 105, as indicated in Section 1.2.

The precipitation of carbides in the grain boundaries produces a zone free from gamma prime precipitate. This zone is quite naturally, weaker than the matrix, and also more ductile, so that stress concentrations around the carbide particles, which are potential crack initiations, are relieved by flow in the ductile zone. The mechanism of crack nucleation and growth has been a subject of speculation and discussion for some years, and this previous work has given rise to the following conclusions.

1) In general, two types of cracking have been distinguished[81] cavitation cracks, which appear as round or oval holes (Fig. 29) and triple point cracks, which have a characteristic wedge shaped appearance, and occur at the meeting of three grain boundaries (Figure 40). The growth of cavitation cracks is generally attributed to the agglomeration of vacancies[82]. This accounts for their abundance on grain boundaries at right angles to the stress axis, where a tensile force is most effective in producing an excess of vacant lattice sites.

Several/

Several detailed accounts for the rate of growth of such cavities have been published[82,83,84], and together with experiments on the change in density of a metal undergoing creep[85], these have shown that the number of cavities grows steadily throughout a test[86].

2) While the growth of cavitation cracks is susceptible to mathematical treatment, the nucleation of these cracks is still a controversial matter. McLean[87] proposed that all cracks are nucleated by the action of grain boundary sliding at points of stress concentration, either at triple points, or at ledges on the grain boundary. The difference between the two types of cracks is that ledge-nucleated cracks require vacancy diffusion for their growth, while those at grain corners can grow as sliding progresses without the addition of vacancies. In this model of crack initiation the type of crack is decided by the applied stress.

3) A development of this idea is due to Gifkins[88], who postulated that cavities could arise from a combination of boundary sliding and slip across the boundary.

4) McLean's ideas have been modified by Weaver[89], who found that the type of cracking was influenced by the grain boundary structure. An absence of carbides resulted in low ductility resulting from triple point cracks. The presence of even a few grain boundary carbides inhibited the growth of these cracks, and gave higher ductility.

This work was limited in its scope, since tests were carried out at one stress and temperature.

5) The most general conclusions is that of Heslop[33], who suggested that the type of cracking depended upon both stress and temperature for a given structure.

6)/

6) Rowe and Freeman[90] observed that the ductility at fracture in a creep test was lower for an alloy of superior strength. An explanation is proposed on the basis that most of the strengthening of the alloy, in the form of more gamma prime, operates on the matrix. This forces a greater proportion of the deformation to take place in the zones close to the grain boundaries. Less total specimen extension is thus needed to cause microcracks to grow and coalesce to the point at which failure occurs.

7) The shape of cavity cracks has been investigated by fracturing at low temperature specimens which had previously undergone creep[90]. The grain boundaries so revealed were examined in replica in an electron microscope. In agreement with expectation, the cavities were shown to grow as round discs.

8) The supersaturation of vacancies necessary for the growth of cavities would appear to be dependent upon the presence of a stress, since an annealing treatment has been shown to be capable of removing cavities produced by creep deformation[91]. This study is of particular interest since the material used was Nimonic 80A, with a structure similar to Nimonic 105.

These conclusions represent the background information against which the results of the crack studies, carried out in this present investigation, will now be discussed.

The primary object of the crack survey was to determine the fraction of specimen cross-sectional area which cracked during each test. As a secondary objective the distribution of crack types was investigated, to find the most likely sites for the initiation of cavitation cracks, and to follow the development of the cracking pattern adjacent to the fracture surface in broken tensile specimens.

The/

The effect of cracking on the cross-section of the tensile specimens is shown in the following table. No cracks were observed in any compressive specimen. The figures given are for the unnecked gauge length in the case of fractured specimens.

Test No.	Temperature °C	Stress lb.in^{-2}	Strain %	Amount of Cracking % of cross-section	Cracking Required*
T24	1000	20,400	17	1	20
T21	1000	17,000	25	5	20
T23	1000	13,600	19	3	20
T30	1000	10,200	10	1	20
T31	1000	8,500	1.7	0	10
T22	950	20,400	9	2	15
T20	950	20,400	0.4	0	0
T16	950	20,400	9	1	15
T15	950	20,400	2	5	10
T19	950	17,000	4	4	10
T14	950	17,000	7	2	15
T13	950	17,000	7	5	15
T12	950	17,000	4	5	10
T11	950	13,600	4	1	15
T10	950	13,600	1.5	1	10
T 6	950	13,600	9	1	20
T33	930	20,400	4	1	20

* These figures will be used in the discussion of section 4.6.

The/

The amount of cracking shown for specimen T11 is anomalous, since this was entirely due to four large cracks, two of which are shown in Figure 43. These cracks are very narrow in relation to their length, which is several grain diameters. Such cracks were found only in this specimen. The relevance of the information will be discussed in the next section, when a comparison of tensile and compressive creep curves is made.

The classification of cracks revealed several interesting features

1) No true wedge-type cracks were seen prior to fracture. All the cracks found in the unnecked portion of the gauge length had the typical rounded shape of a cavitation crack. (Figures 29-39).

2) Most cracks appeared to have nucleated in the grain boundaries at right angles to the stress axis, remote from either a triple point or a massive grain boundary particle (Figures 29-33). However, since many such large particles were associated with cavities, it is concluded that they are ideal nucleating sites (Figures 34-37).

A difficulty arises in assessing the importance of the triple points. Since each metallographic section is two dimensional, no account is taken of the position of the grain corners below the surface, or, indeed, above it, in the material which has been ground away. With this proviso, the grain corners were no more efficient crack initiations than any other stretch of grain boundary.

3) As the point of survey is moved into the necked region, and close to the fracture surface of a broken specimen, the number of cracks increased, their size grew, and nearly all became associated with triple points (Figures 28, 40, 41). It/

It is concluded that these wedge type cracks began as cavities, which grew very slowly until the onset of necking prior to fracture. Such a crack then grew very rapidly until it reached a triple point, where, because of the unfavourable orientation of the boundaries beyond, it stopped extending in that direction.

It is known that necking is a phenomenon occurring late in the creep-rupture life of a specimen. Tests stopped before the expected rupture time showed no sign of necking. Test T14 was stopped $\frac{1}{2}$ hour before rupture was anticipated, when the specimen had extended to 90% of the rupture ductility. This specimen was removed from the furnace and found to be necked, but not fractured. The conclusion is drawn that necking is a phenomenon of the last few moments of a creep test.

No difference was observed, in the appearance of the fracture surface at 930°C, 950°C or 1000°C, which depended upon the stress or temperature, Figure 28. However, at 800°C (Figure 42) there was no appreciable amount of necking, and few cracks were seen apart from the main fracture. Away from the fracture surface, a few isolated cavities were observed. A feature seen only in the specimen fractured at 800°C was the higher crack density in the surface, as compared with the interior. This observation may be explained by postulating that the higher rate of oxidation at the higher temperatures - 950°C and 1000°C - inhibited the growth of cracks either by the presence of a thicker oxide film, or by slowing down the growth of the crack tip, as suggested by Lemay[99]. The actual amount of cross section lost due to the surface cracking was, however, small - less than 1%.

In conclusion, this work has shown that one type of crack is not necessarily unique to one set of test conditions, and that while failure may be precipitated by the coalescence of voids, the high strain rates operating prior to failure develop/

develop cavities into wedge-type cracks. The observation, puzzling at first, of two types of crack in one specimen, has thus been satisfactorily explained.

4.7 Comparison of Creep Behaviour in Tension and Compression.

Inspection of the creep curves shown in Figures 6-15 show that even after the corrections applied to the tensile curves in section 4.1, the tensile creep curves are in general different from the compressive ones. As a general rule, as the stress and temperature are increased, the difference between tensile and compressive creep increases. The following specific points arise which are of interest.

1) The creep rates in tension and compression are in excellent agreement for the initial portion of some creep tests (Figures 9-14).

2) At high stresses and temperatures, the creep curves are markedly different from the earliest stages (Figures 6, 7, 8 and 15). In Figures 7 and 8 the primary creep stage is not visible on the main graph, and so the early stages of these tests are shown in greater detail in the upper parts of the figures.

3) Considering any one temperature, the stage in the creep test at which the curves diverge is moved to smaller fractions of the tensile rupture life as the stress increases (Figures 6-10 and 11-13).

4) For a single stress - 20,400 $lb.in^{-2}$, the tensile and compressive behaviour patterns become more alike as the temperature is reduced (Figures 6, 11 and 14).

5) The differences measured between tensile and compressive creep are much larger than the scatter in the repeated tests shown in Figures 15-19.

Since/

Since no evidence of grain boundary cracking was found in any compressive specimen, while cracks and cavities were found in tensile specimens, it is evident that the higher creep rates in tension should be thought of as caused by creep damage to the material. This implies that the compressive creep properties measured are the "true" creep curves for homogeneous material. The simple explanation of these creep results, outlined above, meets with two objections

1) Enough cracks were not observed in the crack survey to account for the observed tensile behaviour.

2) Since as indicated under item (2) above, at some test conditions the creep curves diverge from the first moments of the test, the cause of this cannot be cavities or cracks induced by creep deformation.

The first point is amplified by the table in section 4.5 which compares the amount of cracking required in each tensile creep test to produce the observed creep rate, with the amount actually seen under the microscope.

Since the amount of cracking required is always much greater than that measured, the question must arise whether a stress-concentrating effect could operate. Although stresses of the required magnitude could arise at the tip of a sharp crack, since the maximum stress is given by[91]

$$\sigma_m = \sigma_o \left(1 + 2 \sqrt{\frac{c}{a}}\right) \qquad \text{where}$$

σ_o = applied stress
c = crack half-length
a = crack end-radius,

it is difficult to understand how such localised stress could affect a large part of the matrix surrounding the crack. Also, at the high temperatures of interest the stress concentration should/

should relieve itself quickly.

Nevertheless, even for a crack, such as is seen, with an end radius $a = 0.25\ C$, say,

$$\sigma_m = 5\,\sigma_o$$

from the elastic stress concentration formula given above. Remembering that the strain rate follows a ninth power stress law, this is a very large effect.

Another possibility is that a large number of cracks are so small as to be discounted in the crack survey. Since the limit of observable crack size was about 1μ, this is a very real effect. The number of submicroscopic cracks would have to be very large, but since the critical size for a cavity crack to grow by agglomeration is 0.1μ, according to McLean[31], many cracks of this size could exist unseen.

Cavitation cracks have been studied by replica electron microscopy[31]. In T.D. nickel the limit of crack resolution was found to be at a diameter of 0.5μ. Since cracks were enlarged by the necessary electropolishing treatment, the original size of such small cracks was unknown, and so no great advantage can accrue from the use of the electron microscope.

Since the development of cavity cracks is diffusion dependent, they should grow with time at high temperature. To test the effect of high strain rates on these cracks, a test at 950°C and 13,600 lb.in^{-2} was interrupted by increasing the load to 17,000 lb.in^{-2} and 20,400 lb.in^{-2} for short periods. The results of this test are shown below

Time/

Time Hour	Strain %	Stress lb.in^{-2}	Strain Rate % per hour
73.5	1.5	13,600	0.016
75	2	17,000	0.16
76	2	20,400	0.74
77	2.5	13,600	0.017
78	3	17,000	0.16
79	3.5	20,400	0.92
81	4	13,600	0.024

The underlined values of the creep rate at 13,600 lb.in^{-2} before and after deformation at higher stress show that little change results from a small amount of strain at higher stress. The total deformation can be regarded as occurring solely at the higher stresses, since the strain rates in these instances are so much greater. Only after 2.5% strain at the higher stresses is any substantial change in the creep rate recorded. Since only cavitation cracks are observed before fracture at this temperature, the increased strain rate presumably promoted the growth of these cavities.

It can thus be seen that prolonged application of a higher stress is required to cause creep damage to the specimen. The instantaneous effect of a higher stress appeared to be small.

This being so makes it more difficult to understand the high stress results (Figures 6, 7, 8 and 15) where the creep rates in tension and compression are different from the start of the test. However, it should not be thought that two discrete modes of behaviour exist. It is thought rather that some discontinuity develops in the tensile specimen which appears earlier in the creep life as the stress is increased.

4.8 Conclusions.

From the results and discussion presented in this Chapter the following conclusions are drawn

1) Creep testing facilities have been developed for both tension and compression loading. The requirements for axial loading and constant temperature were met so that a low scatter on the experimental data was obtained.

2) Tests have been carried out over a range of stress and temperature, so that the general trends of the creep behaviour have been shown.

3) Compressive creep has been shown to be the same as tensile under certain circumstances. The differences arise when creep damage accumulates in the tensile specimens, so that the tensile creep rates become higher than the compressive.

4) A quantitative crack survey has shown that insufficient cracks are visible to account for the observed tensile creep behaviour. It is thought likely that the presence of stress concentrations, and small cracks invisible to the available optical microscopes account for the difference.

5) Tertiary creep has been observed in compression after extended times at high temperature. The acceleration in the creep rate is attributed to the overaging of the precipitate particles.

6) Preliminary micrographs show that precipitate aging characteristics are the same in tension and compression, and so are unaffected by stress. This electron microscope study should be extended to the rest of the specimens. Thin film transmission microscopy would reveal the dislocation configurations after creep. However, it has recently been pointed out by Hale[100] that the 100 kv electron energies available in present electron/

electron microscopes are insufficient to reveal fully the details of the precipitate-particle interactions. The use of higher energies - up to 1 M e v - gives greater resolution and penetrating power, so that thicker sections can be examined, which should have properties more closely related to the bulk material than the thin sections necessary for the present generation of electron microscopes.

7) The measured activation energies in tension and compression agree with those measured by other workers under similar conditions, although they differ significantly from each other.

8) Both tensile and compressive creep rates can be fitted to a power law stress dependence. The exponent measured in compression was 8.5, and in tension an average value of 9 was obtained.

9) The grain boundaries transverse to the tensile axis have been shown to be the source of cavities which eventually lead to failure. This has been appreciated before, and steps have been taken to eliminate grain boundaries, first by producing grains elongated in one direction, and later by growing single crystal material. These developments have been used in turbine blades[92] and have substantially raised the blade life. The method used was the casting of the final blade shape in a heated mould, which was cooled from one end at a controlled rate. The orientation of the resultant single crystal was approximate parallelism between the blade axis and the 001 planes. This is the desired orientation for optimum creep and fatigue properties.

CHAPTER FIVE

CHAPTER FIVE

INVESTIGATION OF THE BAUSCHINGER EFFECT

5.1 Review of the Bauschinger Effect.

As stated before in the Introduction, the Bauschinger effect appears as a reduction in the flow stress of a metal after straining in the same or the opposite direction. The most dramatic effect appears after straining in the direction opposite to the final one[95]. Reviews of the literature on the Bauschinger effect exist in a paper by Thompson[96], and the book by Lubahn and Felgar[95]. The mechanism generally visualised as causing the Bauschinger effect is the piling-up of dislocations against obstacles during the initial straining. When the direction of straining is reversed, these piled-up arrays move easily due to the mutual repulsion between parallel dislocations of the same type and on the same slip plane. The information given in the reviews mentioned above relates mainly to single phase material. However, studies of the Bauschinger effect in a precipitate-hardened aluminium alloy have recently been published[97,98]. These are particularly interesting since they cover both single- and poly-crystal material, and a range of precipitates which can be produced in the aluminium 4 wt.% copper alloy by suitable heat treatment.

The conclusions reached are that the Bauschinger effect in the alloys containing coherent precipitates does not differ from that in pure aluminium. When the precipitates are coherent, however, the Bauschinger effect becomes very large, due to the fact that the particles resist shear by the dislocations,/

dislocations, and so large dislocation pile-ups can accumulate around such incoherent particles. The internal stresses due to these pile-ups then produce plastic deformation at a small value of reversed stress.

These investigations were carried out at room temperature, and at 80°K. To this author's knowledge, no information has been published on the effect of high temperature on the Bauschinger effect of a precipitation hardened alloy. In the absence of precise knowledge, certain tentative proposals may be advanced about the Bauschinger effect in Nimonic 105 at high temperature.

Since the gamma prime particles in Nimonic 105 after a short time at 1000°C have a diameter in excess of 1000 Å these particles are much larger than the coherent particles in aluminium-copper alloys, which are disc shaped, with a diameter of, typically, 500 Å, and a thickness of a few angstroms(40). The gamma prime particles are hence much more resistant to deformation, and hence a large Bauschinger effect might be expected.

However, at high temperatures the dislocations can climb out of the piled-up arrays, as discussed in the Weertman theory of Creep in Chapter 1, and in the Appendix. Thus unless the stress reversal is applied very quickly, the dislocation pile-up will have relaxed, and only a small Bauschinger effect will be observed.

5.2 Requirements for a Bauschinger Testing Programme.

For the purposes of thermal fatigue analysis, the data required is the dependence of some parameter defining the Bauschinger effect upon the amount of prestrain, strain rate and temperature. Several such parameters are possible, examples being the strain occurring before the reverse of the pre-stress/

pre-stress is reached and the drop in flow stress after the reversal, where the flow stress may be defined either as an offset proof stress, or as the limit of elastic proportionality.

The temperatures and strain rates would be decided by those predicted to occur in the thermal fatigue cycle of turbine blades. There is no reason why the investigation should stop after one cycle of stress reversal, so that the Bauschinger studies could be regarded as the limiting case of a high-strain fatigue test. The short-time tensile and compressive stress-strain curves could also be used to predict the creep strain-time curves at very short times, using the method suggested by Lubahn and Felgar[95] to convert the stress-strain curves to strain-time curves. The effect of specimen aging, which are usually regarded as limiting the usefulness of this technique, could be minimised by pre-aging specimens for long times at the test temperature before testing, so that only a small amount of precipitate agglomeration would take place during the time of the test.

Because of delays in gaining access to the Instron Testing Machine, the time available for high temperature testing was very short, and so the projected testing programme was discontinued after the preliminary testing programme described in the following sections.

5.3 Requirement for a Bauschinger Testing Machine.

The requirements for a machine to measure the Bauschinger effect at high temperature are thus rather complex, but related to the measurements of compression creep. For similar reasons to those discussed in Chapter Two, tests carried out in uniaxial tension and compression are the most meaningful and acceptable. The high testing temperature gives rise to guidance problems, and the need for fast stress reversal/

reversal cannot be easily met, since most commercially available testing machines can drive their crosshead in only one direction. The construction of a complete, sophisticated testing machine was inhibited both by cost, and by the difficulty of obtaining an electronic load measuring device to measure both tensile and compressive loads.

As a preliminary measure a machine was built to strain both in tension and compression, using a proving ring as the load measuring device. Although the performance of this machine was not satisfactory, a brief consideration of it is held to be informative as to the difficulties encountered in building a testing machine for reverse straining.

During the time that the crosshead was being driven, the proving ring underwent large elastic deflection until the yield strength of the specimen was reached. It was thus almost impossible to control the strain rate impressed on the specimen, since this was decided largely by the elastic characteristics of the proving ring. This would be no drawback at low rates of strain, when many measurements of the specimen extension and of the load could be taken. Also, this large elastic extension caused a long delay between the reversal of the stress. At higher strain rates, necessary both to emulate thermal fatigue, and to reverse the stress before relaxation took place in the specimen, sufficient readings of the stress and strain could not be obtained from the dial gauges used on the load cell, and as the extension measuring devices. These dial gauges were photographed with a cine camera, and a combination of the vibration of the machine and the high speed of movement of the dial gauge needles caused blurring of the image on the film. Due to this blurring the exact position of the smaller of the hands of/

of the dial gauge could not be ascertained with any certainty.

These difficulties led to the decision to build a rig to fit the Instron Universal Testing Machine which had just been installed in the University of Glasgow, Department of Mechanical Engineering. This machine is specially designed so that the crosshead can be driven under load both up and down, and measures electronically both the load and the crosshead movement.

5.4 Development of the Bauschinger Machine.

It was decided that the principles successfully incorporated in the compression creep rig would be used in the design of a Bauschinger machine (see Figure 5). The heavy main frame was machined out of 2 in. thick mild steel plate, and the guide holes were accurately machined in line. The loading rams were made from Nimonic 105, but instead of the spherical bearings used in compression creep testing, threaded seatings were machined centrally to receive a specimen with threaded ends (Figures 5 and 3).

To prevent backlash in the seatings, nuts of Nimonic 105 were made with accurately flat faces to screw tightly against the faces of the loading rams (Figure 3). Similarly, precautions were taken to prevent backlash in the coupling to the load cell by means of a close-fitting, heavily tightened thread, and in the coupling between the main frame and the crosshead. The main frame sat on a spigot and was held in place by a press-fit steel pin. The lower ram was also held in place by a press-fit pin, and relied for accurate positioning both on the guide hole, and on the shoulders machined at right angles to the axis of the ram.

Since/

Since it was imperative to prevent the load cell being overheated, cooling coils were soldered to both sides of the main frame, both at top and bottom, and water flushed through them during the whole period of testing. By this means, that part of the upper ram above the main frame was kept cooler, in fact, than room temperature.

The heating and temperature control equipment were identical to that used in the creep testing. Because of the small size of the specimen, only one thermocouple could be attached. This was felt to be permissible both because of the known constancy of the temperature in the central zone of the furnace, and because of the small size of the specimen in relation to the zone of constant temperature. The specimen temperature was recorded continuously on a Kent single channel chart recorder, on which temperature variations of $0.1^{\circ}C$ could be detected.

A few tests were carried out at room temperature on specimens of aluminium, chosen because its tensile strength at room temperature is approximately that of Nimonic 105 at $1000^{\circ}C$, viz. 25,000 $lb.in^{-2}$.

The specimen extension was measured by recording the crosshead movement on the Instron chart record. The elasticity of the load cell is known, and no elastic deformation is expected in the massive loading rods. Hence crosshead movement should provide an accurate measurement of specimen deformation. This system was used by Ham and Abel[97], but since the strain rate these workers could use was very low (0.7% per minute) the magnification of the motion on the chart was correspondingly larger. Hence the strain resolution in their experiments was 0.05%. There are, however, well-founded objections to such an indirect method, such as the contribution to the apparent strain from bedding in of the threaded ends. This/

This can be minimised by heavy tightening of the nuts on the specimen prior to testing. Another objection is the large unknown effects from random temperature variations, which can be much larger than the specimen deformation at low values of strain. An extensometer clamped to the specimen itself is always preferable, and, as indicated later, should be incorporated in the next phase of development of the Bauschinger machine.

These tests enabled familiarity with the apparatus, and showed that with the specimen size chosen, 1/80 in^2. in cross-section and 0.25 in. long gauge length, the sensitivity of the strain measurement was 0.5%. This specimen size was chosen, since it was hoped to carry out Bauschinger tests all the way from room temperature up to 1000°C. The load capabilities of the tension-and-compression load cell would have been exceeded by a larger specimen diameter, and a different specimen size would then have been required for high and low temperature tests. In the event, since specimens of Nimonic 105 had been turned to the above dimensions, these were used.

For these preliminary tests the temperature chosen was 1000°C, and the strain rate 8% per minute. Because of thermal expansion the apparatus was completely assembled, then the pin holding the lower ram removed and the crosshead moved down about half an inch. When the test temperature was reached the crosshead was carefully returned to position and the pin slid into place. The test could now begin.

Since the strain resolution was not felt to be good enough for Bauschinger tests, tensile and compressive short-time tests were carried out. These showed that the limit of linear proportionality between stress and strain was the same in tension and compression, as expected. The stress-strain/

strain curves in compression showed no ultimate strength, because of the ever-increasing cross-section.

The backlash, seen as a kink in the stress-strain curve when the stress was reversed, was very small with the nuts in place, and large without them. The residual backlash was probably located in the load cell or crosshead coupling.

The friction in the bearing between the main frame and upper guide rod was investigated by driving the crosshead up and down after the specimen had fractured. A maximum force of 40 lb. was recorded. This was reduced to 20 lb. by applying "Molyslip" grease to the bearing surfaces. This frictional force was found to be repeatable both in tension and compression.

No gross buckling of the specimens was found below compressive deformations of 5%. Obviously the alignment in this case is not as good as that in the compression testing, so that a certain number of specimens will buckle, probably due to errors in machining their threads.

Several conclusions can be drawn from these tests, some of them indicating the developments necessary for successful Bauschinger testing.

1) In view of the agreement between the measured limits of proportionality in tension and compression it is felt that a machine capable of carrying out successful high temperature Bauschinger tests has been built.

2) The strain sensitivity should be increased, either by using a longer specimen or by attaching a system of extensometry to the specimen. The extensometer output would be used to drive the chart, and so produce directly the stress-strain curve. Such a system is being purchased from Instron Limited.

3)/

3) If the stress is reversed manually, then the strain rate must be slow enough for the moment of reversal to be chosen accurately by observation of the chart record. The strain rate is thus limited to about 10% per minute. This could be increased by using the fatigue loading cams available for use on the Instron. By means of these the load could be reversed at a value known to give any required amount of prestrain. The strain rate could be increased so that the stress reversal became almost instantaneous, as it is in thermal fatigue, instead of the 10 seconds required at present.

CHAPTER SIX

CHAPTER SIX

CONCLUSIONS AND SUGGESTIONS FOR FURTHER WORK

6.1 Conclusions.

The description of experimental procedures and results is now complete, and the work carried out during this investigation will now be reviewed in terms of the progress made towards achieving the aims set out in the Introduction, the contribution to the general understanding of the time-dependent deformation of metals at high temperatures, and the development of improved techniques for compression creep testing at high temperatures.

The major aim of this investigation has been to throw light on the creep behaviour of Nimonic 105 at temperatures experienced by jet turbine blades during thermal shock. In view of the fact that previously no such information existed, the situation is now much more clear since the general trend of comparative creep behaviour has been uncovered, for temperatures between 800°C and 1000°C. In general, the creep curves in tension and compression are different, and if a difference exists the tensile creep rates always exceed the compressive. In no instance was a compressive specimen observed to deform more quickly than the corresponding tensile one.

At any one temperature the difference between the curves decreases with decreasing stress, so that at a sufficiently low stress the creep rates in tension and compression are identical, at least during the initial part of the test. When structural defects, such as cavity cracks, develop,/

develop, the tensile creep rate increases. Since no such cavities are observed in compression, due to the unfavourable stress system, no such increase is observed in compression. After long times at high temperature, however, the unexpected phenomenon of tertiary creep in compression is observed, and results, it is thought, from the agglomeration of the strengthening second phase, to which Nimonic 105 owes its remarkable high temperature creep strength.

If a particular stress is considered, the difference between tensile and compressive creep diminishes as the temperature is reduced, so that even if at 1000°C the creep curves differed from the first instant of loading, at 950°C or less the two creep curves are observed to agree for a substantial part of the tensile rupture life.

These observations can now be used in the prediction of the life of turbine blades, and point the way to the improvement of the material for such applications. Since failure always is initiated in grain boundaries, especially those transverse to the stress axis, substantial improvements in performances should result from the elimination of such grain boundaries. The compressive creep properties. which are much better than the tensile ones from the point of view of creep resistance, give an indication of the improvement possible.

This investigation has improved on previous comparative studies in the extensive metallographic study of deformed specimens, aimed at elucidating the cause of the difference between tensile and compressive creep. A survey of the cracking in tensile creep specimens showed that grain boundary cavity cracks, of about 1μ diameter, could be observed after 2% tensile creep strain. These cracks grew and multiplied throughout the creep test, and during the necking/

necking of the specimen prior to fracture they develop into wedge-type cracks characteristic of high strain-rate deformation. The main features of the differences between the tensile and compressive creep rates are explicable in terms of this cracking behaviour.

The values measured for the stress exponent and the creep activation energies show fair agreement with other studies on similar alloys. The fact that they are not in agreement with the values predicted theoretically shows that the creep process is more complex than visualised in the present theoretical treatment. The large range of values obtained for activation energy values in nickel base alloys probably reflects minor differences in technique, although the methods used in various investigations may be nominally similar. In particular, no standard procedure has been adopted in the past for ascertaining the effect of changes in precipitate morphology on the activation energy, and of minimising it. The activation energies derived for creep in this investigation, and in that of the Marquardt Corporation[9], agree with each other, and disagree with that derived by other investigators in that they are much larger. The common factor would appear to be that both were measured during rapid changes in the precipitate size and amount, while the lower values were derived in circumstances which would tend to reduce the effect of the phase change.

A feature common to both tensile and compressive creep tests was the unusually small scatter between creep tests carried out under nominally identical conditions. The reasons for this small scatter were considered to be the care taken to ensure that all material had an equivalent amount of aging before being tested, the fact that the temperature was monitored continuously, and any small drift corrected, the fact that all the/

the tests were assembled and run by one operator, and that only two tests had to be supervised at the same time.

In view of the low failure rate of compressive creep tests due to buckling - 4 failures in 25 tests - the compressive creep machine is considered to have justified the choice of design. No gross deterioration of any component has been noted, after more than 1000 hours of high temperature testing. Vital to the success of this design is a split furnace which will provide an adequate constant temperature zone and a life of several hundred hours, if tests are not to be wasted by furnace failure. This problem has been solved in a novel fashion which has resulted in a furnace of exceptional mechanical durability and heat input capability, considering its small size. In addition, the simplicity of the design means that it can be quickly repaired, should a winding burn out, by cementing another in its place.

At the time of writing, the development of a machine to measure the Bauschinger effect is far advanced, and has reached the stage at which tensile and compressive loading are available in rapid succession, but the strain measurement is not yet sufficiently accurate to be satisfactory.

It is hence felt that comprehensive testing facilities have been developed for all the investigations originally envisaged. The creep testing equipment has had extensive trial and has shown itself to be capable of great accuracy in the measurement of creep curves.

Despite the large amount of theoretical effort expended on the problem of metallic creep, no convincing account has yet been developed to embrace more than a few of the experimental observations. The development of alloys and the prediction of creep properties will probably continue for/

for some time on a pragmatic basis. The discovery of precipitation hardening and of the beneficial effects of boron and zirconium additions to nickel alloys are two excellent examples of how a chance occurrence can assist the advance of the metallurgical frontiers.

Suggestions for Further Work.

It is felt that although this investigation has gone far towards a total knowledge of the comparative tensile and compressive creep behaviour in Nimonic 105 at high temperature, there are several directions in which the scope of the work could be extended. The following suggestions are intended to indicate what this author considers to be the most fruitful approaches.

1) The thermal fatigue analysis discussed in Chapter One has now indicated that the temperature range of interest extends as far down as 700°C. In addition to producing useful data, comparative tests at these lower temperatures would be interesting from a wider scientific standpoint, since they would be relatively free from the rapid changes in precipitate morphology which complicate an understanding of the creep behaviour at high temperatures. Also, since stress concentrations relieve themselves less rapidly at such temperatures, their effect should be more marked on tensile creep properties, and hence this reinforces the case for carrying out tests at lower temperatures.

2) Now that confidence in the apparatus has been established the investigation of creep phenomena could be continued at very short times - of the order of a few seconds. Since the transient phenomena are most important in thermal fatigue, particular attention could be paid to primary creep.

3)/

3) Further work would elucidate the role of cavitation, and its effect on the creep rate. It is possible that methods could be developed for detecting such cracks could be developed along the lines of the work by Crussard et al[90], which does not require any electropolishing.

4) A thorough investigation of the effect of stress on the activation energy for creep should be carried out, and should include precise determinations of the activation energy by means of very small temperature changes e.g. 1 or 2 C°, which would change the creep rate appreciably, without changing the precipitate structure. Long holding times at the test temperature prior to loading the specimen would ensure that interaction between the creep process, and the precipitate clustering is minimised.

5) As was stated before, an extended electron microscope investigation into precipitate effects, and precipitate-dislocation interactions was intended, but scarcely begun due to the lack of a microscope. Since all the specimens are available, this study could be carried to completion with great rapidity, and would correlate with the large research effort being expended on a world-wide scale to determine the role of precipitates and dislocation interactions in creep deformation.

APPENDIX

WEERTMAN'S DISLOCATION CREEP THEORY

Since it is the object of this Appendix to point out the main physical ideas used by Weertman, detailed calculations will not be included. These can be found in the appropriate references[25,26] or in a textbook of Physical Metallurgy (see Bibliography).

The model discussed envisages dislocation loops expanding under an applied stress until they meet obstacles. In the case of two-phase dispersion-hardened alloys these obstacles are the particles of the dispersed phase and their surrounding strain fields. It is assumed that the climb of dislocations is the rate-controlling process[23].

In general, then, the creep rate $\dot{\epsilon}$ is equal to

$$\dot{\epsilon} = M\pi L^2 bR \qquad (1)$$

Where M = the density of dislocation sources
L = the maximum radius a dislocation loop will grow to
b = Burgers vector of a dislocation
R = the rate of creation of dislocations at one source.

The maximum radius, L, may be calculated, since at this size the dislocation is assumed to be annihilated by combination with dislocations of opposite sign on neighbouring slip planes.

Thus $2M\pi L^2 d \doteq 3$

i.e. $L^2 \doteq \frac{1}{2Md}$

where/

where d is the distance climbed by a dislocation in order to be annihilated, and is assumed to be of the order of h, the particle diameter.

In reference (25) the velocity of climb is calculated for an edge dislocation some distance away from other dislocations

$$v \doteq \frac{\sigma b^2 D}{k T}$$

where v = the velocity of climb
σ = the resolved shear stress
k = Boltzmann's constants
T = Temperature in ^{o}K

Thus the term R in equation (1) can be calculated as

$$R = \frac{v}{h}$$

We thus have

$$\epsilon = \frac{\pi \sigma b^3 D}{2 k T h^2} \qquad (2)$$

This equation is valid for the range of σ from the stress required to activate a dislocation source up to the stress necessary to push a dislocation loop between two precipitate particles.

This latter stress is given by

$$\sigma = \frac{\mu b}{\lambda}$$

where μ is the shear modulus
λ is the interparticle spacing.

For/

For stresses higher than this dislocations are bowed out between particles, and the rate of production of dislocations is controlled by the climb of the cut-off dislocation loops surrounding particles. When such loops have climbed a sufficient distance away from the slip plane, a further dislocation can pass.

Weertman calculates this distance to be

$$H = \frac{\mu^2 b^2}{2\sigma^2 \lambda}$$

and the expression for the creep rate which results is

$$\dot{\epsilon} = \frac{2\pi \sigma^4 \lambda^2 D}{h \mu^3 k T} \qquad (3)$$

For stresses so high that $\frac{2\sigma^2 \lambda b^2}{\mu k T}$ is greater than unity, the velocity of climb is given by

$$v = \frac{D}{2b} \exp\left(\frac{2\sigma^2 \lambda b^2}{\mu k T}\right)$$

and the creep rate now becomes

$$\dot{\epsilon} = \frac{\pi \sigma^2 \lambda D}{\mu^2 b^2 h} \exp\left(\frac{2\sigma^2 \lambda b^2}{\mu k T}\right) \qquad (4)$$

for the highest stresses.

NUMERICAL LIST OF REFERENCES.

1. E. Glenny. "Thermal Fatigue" Metallurgical Reviews, 1961, 6 p. 387.

2. E. Glenny and T.A. Taylor. J. Inst. Met. 1960, 88 p. 44

3. Rolls-Royce Aero-Engine Division, private communication.

4. J. Bauschinger. Mitt. Mech.-Tech. Lab. Munch, 1886, 13 p. 1.

5. Henry Wiggin & Company Limited., private communication.

6. Henry Wiggin & Company Limited., "Nimonic Handbook" 1962.

7. R. Fletcher. University of Glasgow, unpublished work.

8. J. Freidel. "Dislocations" Gauthier-Villars, Paris 1964.

9. H. Conrad, E.C. Bernett and J. White. Joint International Creep Conference, 1964, 1 p. 9, Institute of Mechanical Engineers.

10. W.R. Hume-Rothery. Elements of Structural Metallurgy, 1961, Institute of Metals.

11. A. Wilm. Metallurgie, 1911, 8 p. 225.

12. P.D. Merica, R. Scott, and R.G. Wattenburg. U.S. Bureau of Standards Science Paper, 1919, 15 p. 271.

13. A.L. Marsh. British Patent 2129 (1906).

14. W.C. Bigelow, and J.A. Amy. Wright Air Development Centre Technical Report 58-406.

15./

15. W. Betteridge. The Nimonic Alloys, 1959, Arnold.

16. C.H. Lund. D.M.I.C. Report 153, 1961, Battelle Institute, Columbus, Ohio, U.S.A.

17. R.F. Decker, J.P. Rowe and J.W. Freeman. Report No. 1392. National Aeronautics and Space Administration, U.S.A.

18. C.W. Weaver. J. Inst. Metals, 1959-60, 88 p. 296.

19. J.P. Rowe and J.W. Freeman. Technical Note D-1325, National Aeronautics and Space Administration, 1962.

20. E.N. da C. Andrade. Proc. Roy. Soc. 1910, p. 1.

21. A.J. Kennedy. "Processes of Creep and Fatigue in Metals", Oliver and Boyd, 1962.

22. J.E. Dorn and J.D. Mote. Office of Naval Research, Third Symposium on High Temperature Materials and Structures, 1964.

23. G. Schoek. "Creep and Recovery", Seminar of American Society of Metals, Cleveland, 1957.

24. J. Weertman and G. Ansell. Trans. A.I.M.E. 1959, 215 p.838.

25. J. Weertman. Journal of Applied Physics, 1955, 26 p. 1213.

26. J. Weertman. Journal of Applied Physics, 1957, 28 p. 362.

27. J. Weertman and J.R. Weertman. "Physical Metallurgy" Chapter 16, North-Holland, 1965, R.W. Cahn, Ed.

28. G. Ansell and F.V. Lenel. Trans. A.I.M.E. 1961, 221 p. 452.

29. A.H. Clauer and B.A. Wilcox. Metal Science Journal, 1967, 1 p. 86.

30./

30. J.P. Rowe and J.W. Freeman.
Joint International Creep Conference, 1963, 1 p. 65, Institute of Mechanical Engineers.

31. A.H. Clauer and B.A. Wilcox.
Trans. A.I.M.E., 1966, 236 p. 580.

32. P.R. Dioguardo and R.P. Lloyd.
Aeronautical Systems Division Technical Report. Technical Report 61-499, 1962.

33. J. Heslop. J. Inst. Metals, 1962, 1 p. 28.

34. D.A. Murray and R. Choubey.
Metallurgia 1966, p. 243.

35. A.L. Roitburd, M.D. Usikov and L.M. Utevskii.
Soviet Physics Doklady 1965, 9, No. 11, p. 1022.

36. G. Ansell. Trans. A.I.M.E., 1959, 215 p. 294.

37. W. Mitchell. The Origins of Creep Resistance in Nickel-Base Alloys. International Nickel Co. Ltd., 1966.

38. Yu A. Bagaryatskii and Yu D. Tyapkin.
Soviet Physics (Crystallography) 1960, 5 p.p. 513 and 841.

39. N.F. Mott and F.R.N. Nabarro.
Report on the Conference on the Strength of Solids, Physical Society, 1948.

40. A. Kelly and R.B. Nicholson.
Progress in Materials Science, 1962, 10 p. 150.

41. M.J. Marcinkowski. Electron Microscopy and Strength of Crystals, Thomas and Washburn (Editors), Interscience, 1963.

42. P. Haasen. Phil. Mag. 1958, 3 p. 384.

43. R.F. Fleischer. Acta Met. 1960, 8 p. 32.

44./

44. J. Ham. J. Phys. Chem. Solids, 1959, 14 p. 183.

45. J.W. Cahn. Acta Met. 1966, 14 p. 1283.

46. G.W. Greenwood. Acta Met. 1956, 4 p. 243.

47. I.M. Lifshitz and V.V. Slyozov. J.E.T.P. 1958, 35 p. 479.

48. I.M. Lifshitz and V.V. Slyozov. J. Phys. Chem. Solids 1961, 19 p. 35.

49. C.M. Wagner. Z. fur Elektrochimie 1961, 65 p. 581.

50. R.A. Oriani. Acta Met. 1964, 12 (2) p. 1399.

51. W. Mitchell. Z. Metallkunde 1966, 57 p. 586.

52. O.D. Sherby, and M.T. Simniad. Trans. Amer. Soc. Metals 1961, 54 p. 227.

53. R.A. Swalin and A. Martin. Trans. A.I.M.E. 1956, 206 p. 567.

54. J.D. Livingston. Trans. A.I.M.E. 1959, 215 p. 566.

55. O. Bannyh, H. Modin and S. Modin. Jernkonter 1962, 146 p. 774.

56. Rolls-Royce Limited, Aero-Engine Division, private communication.

57. N.F. Mott and F.R.N. Nabarro. Proc. Phys. Soc. London, 1940, 52 p. 86.

58. A.H. Sully. Metallic Creep, O.U.P., 1953.

59. E.C. Bernett. Tensile and Short-Time Creep Properties of N-155 Alloy Sheet. Trans. Amer. Soc. Mech. Eng., J. Eng. Ind., 1960, 82, Series B, No. 4, p. 283.

60. P.R. Dioguardo and R.D. Lloyd, A.S.D. T-R 61-499, 1962.

61. H. Conrad. Mechanical Behaviour of Materials at Elevated Temperatures, p. 193, McGraw-Hill, New York, 1961.

62. M.J. Manjoine. Trans. A.S.M.E., J. Basic Eng., 1960, 82, Series D, No. 4, p. 880.

63. R.L. Carlsson, O.K. Salmassy and G.K. Manning. Technical Report No. 56-26, 1957, Wright Air Development Centre.

64. G.J. Heimerl and J. Farquar. Technical Note D-160 (18). National Aeronautics and Space Administration, U.S.A.

65. A.H. Clauer and B.A. Wilcox. Trans. A.I.M.E., 1966, 236 p. 580.

66. D.F. McNamee. University of Glasgow, unpublished work.

67. High Temperature Technology (Symposium), International Union of Pure and Applied Chemistry, Butterworths, 1964.

68. A.E. Johnston. Engineering, 1953, 176, p. 320.

69. J. Alder and V. Phillips. J. Inst. Metals, 1954, 83 p. 80.

70. Rolls-Royce Limited, Aero-Engine Division, private communication.

71. R.K. Penny, E.G. Wells and G.A. Webster. Materials Research and Standards, 1966, 6 p. 77.

72. Saunders-Roe Limited, Strain Gauge Division, Technical Information Department.

73. C. Wheatley and J. Buchan. Metallurgia, 1962, 66 p. 91.

74. E.E. Tomashevskii and A.I. Slutsker. Industr. Lab., 1964, 29 (8), p. 1067.

75. P.W. Davies and J.S. Dutton. J. Sci. Instr., 1966, 43 p. 39.

76. G.A. Webster and B.J. Piearcey. Metal Science Journal, 1967, 1 p. 97.

77./

77. C.M. Sellars and A.G. Quarrel.
J. Inst. Metals, 1962, 90 p. 329.

78. J.E. Dorn. "Creep and Recovery" p. 225, American Society for Metals, Cleveland, Ohio, 1957.

79. G.M. Stoloff and L. Davies.
Prog. Mat. Sci., 1966, 13 p. 74.

80. Butcher, Thesis, Cornell University, Ithaca, New York (1962), also reported in Reference 22.

81. D. McLean. Mechanical Properties of Metals, Wiley, 1962.

82. R.W. Baluffi and L.L. Seigle.
Acta Met. 1957, 5 p. 449.

83. D. Hull and D.E. Rimmer.
Philosophical Magazine, 1959, 4 p. 673.

84. M.V. Speight and J.E. Harris.
Metal Science Journal, 1967, 1 p. 83.

85. R.C. Boettner and W.D. Robertson.
Trans. Met. Soc. A.I.M.E., 1961, 221 p. 613.

86. G.W. Greenwood. Phil. Mag., 1963, 8 p. 707.

87. D. McLean. J. Inst. Metals, 1956, 85 p. 468.

88. R.C. Gifkins. Acta Met. 1956, 4 p. 98.

89. C.W. Weaver. J. Inst. Metals, 1960, 88 p. 462.

90. C. Crussard, J. Plateau and G. Henry.
International Creep Conference, Volume 1, p. 91, Institution of Mechanical Engineers, 1963.

91. P.W. Davies, J.P. Dennison and H.E. Evans.
J. Inst. Metals, 1966, 94 p. 270.

92. F.A. McClintock and S. Ali (Editors).
Introduction to Materials Behaviour, Massachusset Institute of Technology, 1962.

93./

93. F.L. Versnyder and B.J. Piearcey.
S.A.E. Journal, 1966, 74 p. 36.

94. P.W. Davies, T.C. Finniear and B. Wilshire.
J. Inst. Metals, 1961, 90 p. 368.

95. Lubahn and Felgar.
Plasticity and Creep of Metals, Wiley.

96. N. Thompson. Adv. Phys., 1958, 7 p. 72.

97. A. Abel and R.K. Ham.
Acta Met. 1966, 14 p. 1489.

98. D.V. Wilson. Acta Met. 1965, 13 p. 807.

99. I. Lemay. Ph.D. Thesis, University of Glasgow, 1962.

100. K.F. Hale. New Scientist, September 22, 1967.

GENERAL BIBLIOGRAPHY

The following books and review articles were extensively used as an introduction to various aspects of the subject matter of this Thesis, in addition to the several points mentioned specifically in the main text.

1) The Metallurgy of Nickel Alloys.

The Nimonic Alloys, W. Betteridge, Arnold, 1959.

Physical Metallurgy of Nickel-Base Alloys, C.H. Lund, D.M.I.C. Report 153, 1961, Battelle Institute, Columbus, Ohio.

2) Precipitation Phenomena.

A. Kelly & R.B. Nicholson, Progress in Materials Science, 10, 1962.

3) Creep and Fatigue.

Plasticity and Creep in Metals, Lubahn and Felgar, Wiley, 1962.

Processes of Creep and Fatigue in Metals, A.J. Kennedy, Oliver and Boyd, 1962.

J.E. Dorn and J.D. Mote, Proceedings of the Third Symposium on Naval Structural Mechanics, Pergamon 1964.

Joint International Creep Conference Proceedings, 1963, London, Institution of Mechanical Engineers.

Fig. 1. Compression Creep Machine.

1) Crosshead with moveable balance weight.
2) Main frame of the Mand Creep Machine.
3) Main frame of the compressive loading rig.
4) Furnace supports.
5) Upper loading ram.
6) Specimen (See Fig. 1a).
7) Lower loading ram.
8) Transducer Assembly (See Fig. 1b).
9) Loading platform.
10) Coupling to the base plate.

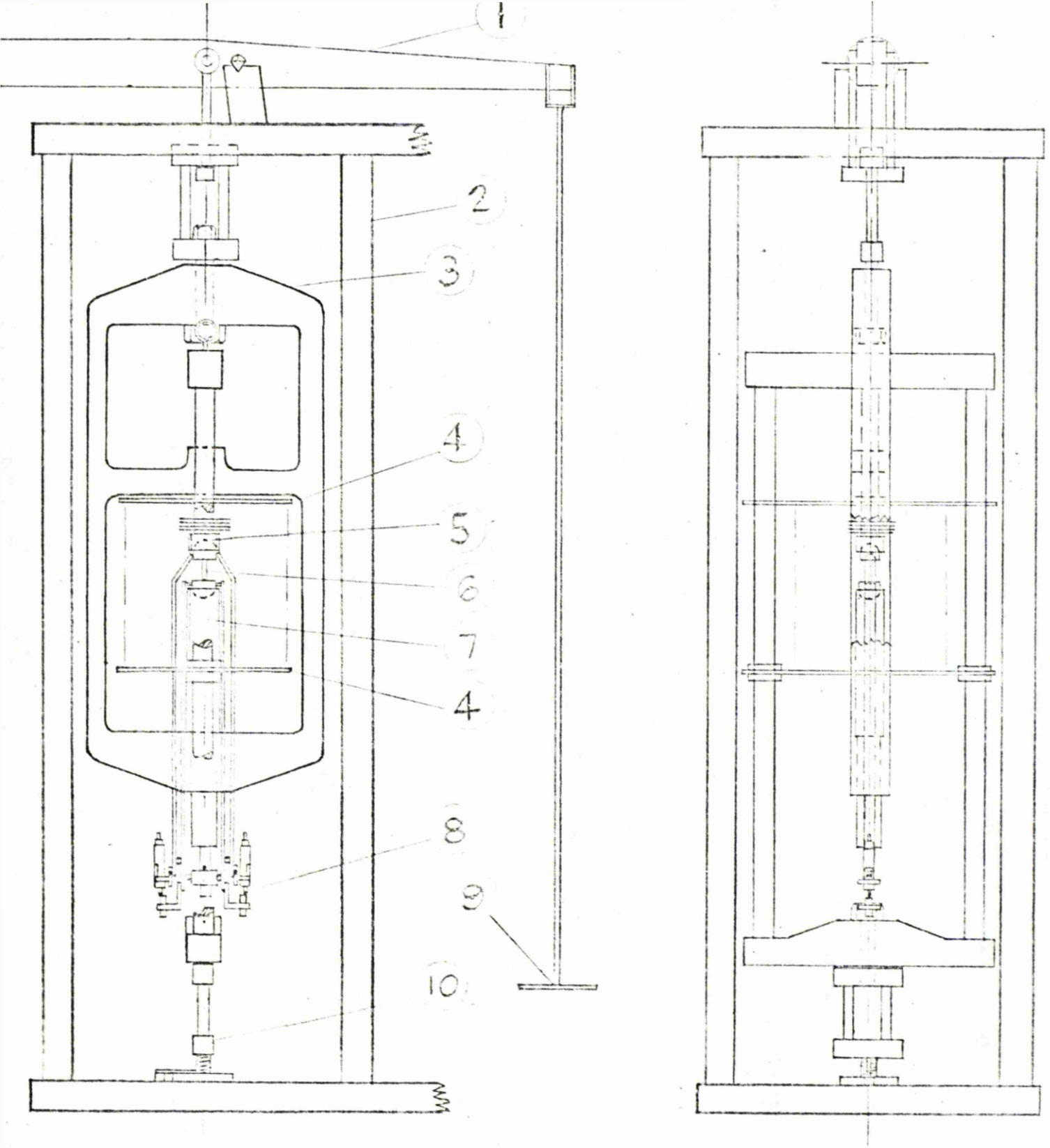

COMPRESSION CREEP MACHINE

FIGURE. 1.

Fig. 1a. Specimen Assembly for Compression Creep Tests.

1) Upper loading ram.

2) Stainless steel heat shields with ceramic spacers.

3) Upper spherical cap.

4) Upper extensometer rod.

5) Thermocouple.

6) Specimen.

7) Thermocouple.

8) Lower spherical cap.

9) Lower extensometer rod.

10) Lower loading ram.

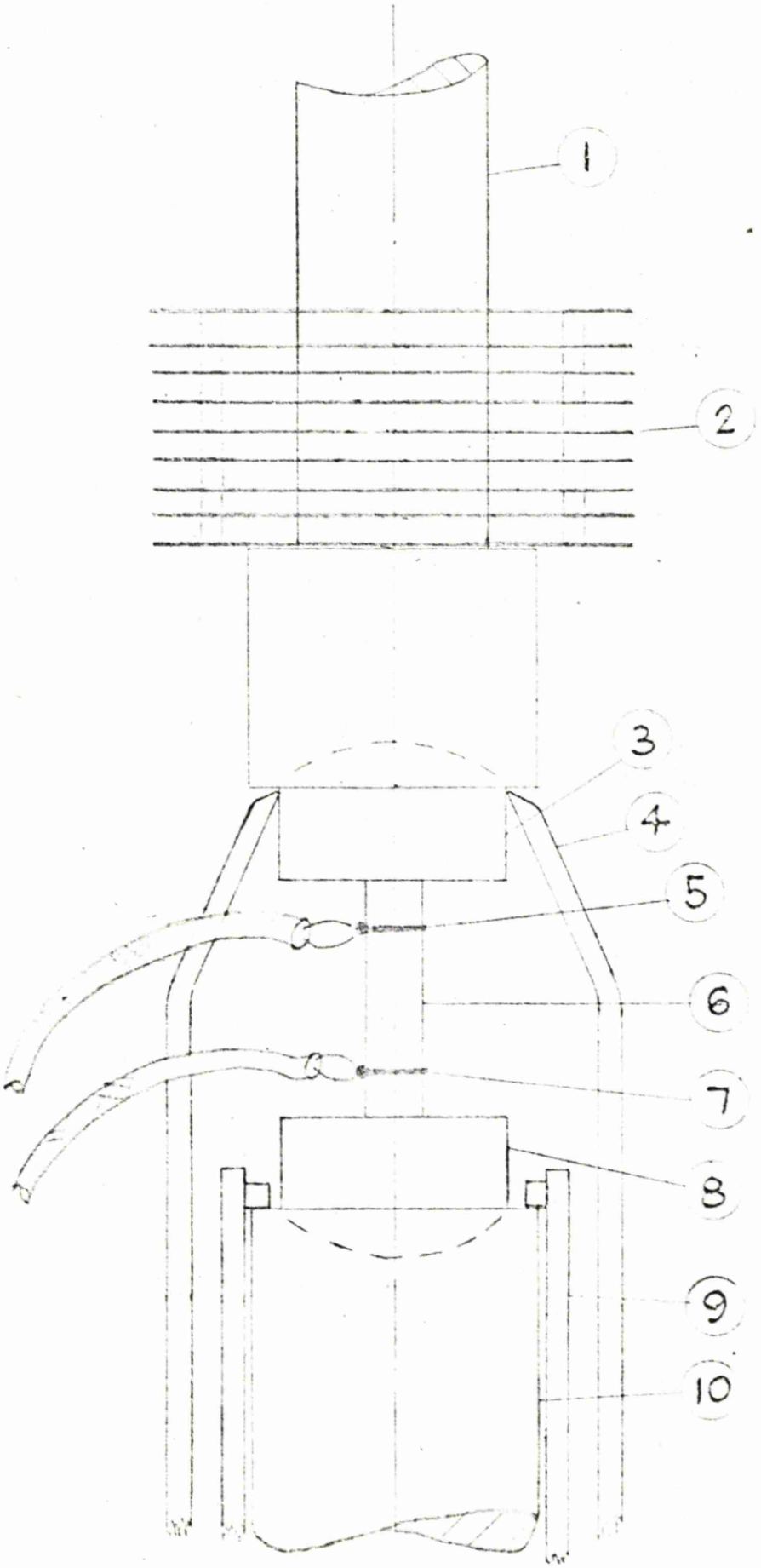

SPECIMEN ASSEMBLY FOR COMPRESSION CREEP TEST

FIGURE. 1.a.

Fig. 1b. Extensometer Transducer Assembly.

1) Support column from main frame.

2) Extensometer rod from top of specimen.

3) Extensometer rod from bottom of specimen.

4) Transducer body.

5) Supporting spring.

6) Transducer mounting block.

7) Transducer core.

8) Micrometer thread for resetting the transducer core.

9) Stainless steel rollers.

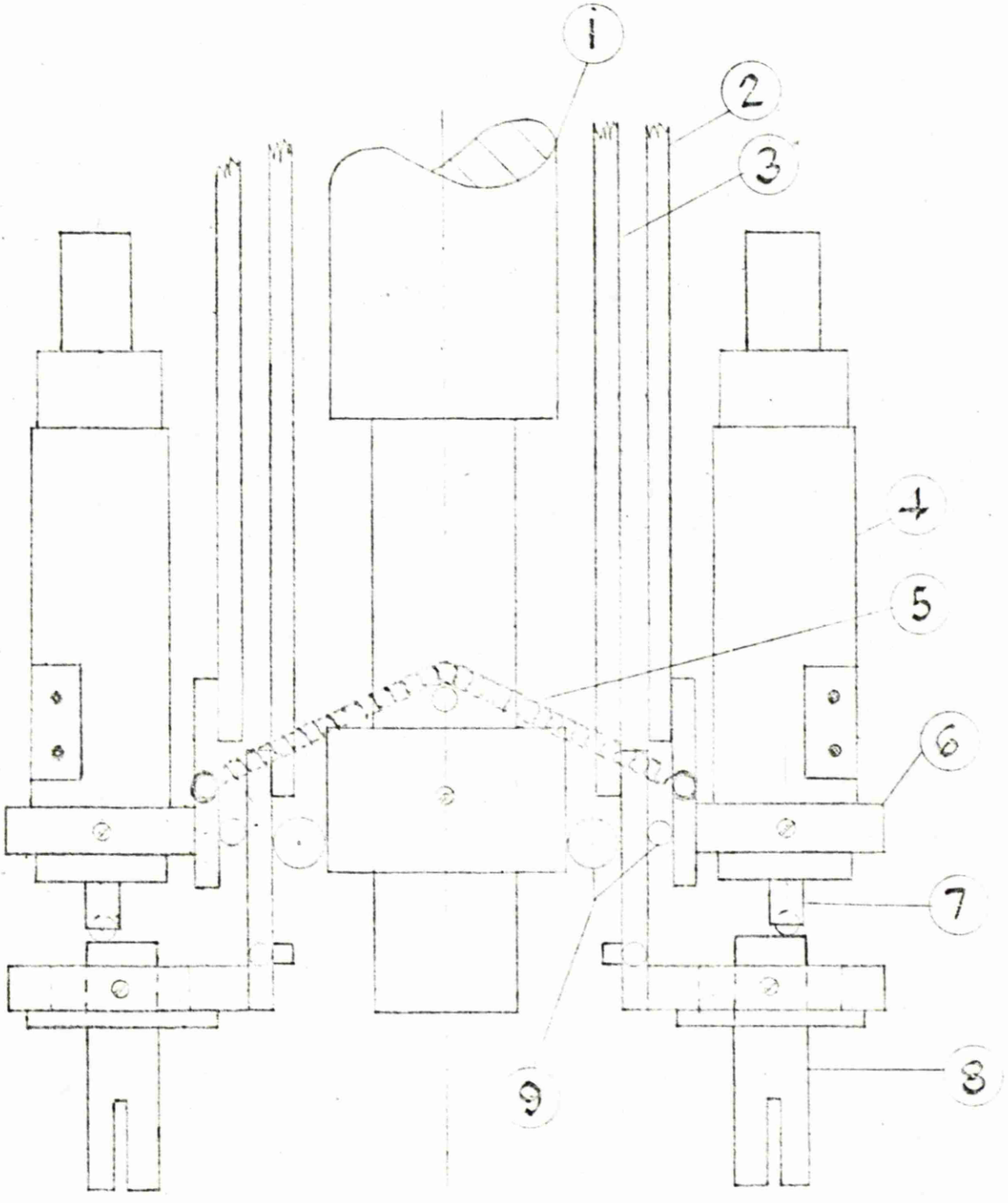

EXTENSOMETER TRANSDUCER ASSEMBLY FOR COMPRESSION CREEP TESTS.

FIGURE 1.b.

Fig. 2. Tensile Creep Machine.

1) Crosshead with moveable balance weight.
2) Universal joint.
3) Main frame.
4) Loading shackle.
5) Furnace.
6) Heat shields.
7) Specimen.
8) Furnace support bars.
9) Transducer assembly.
10) Loading shackle.
11) Universal joint.

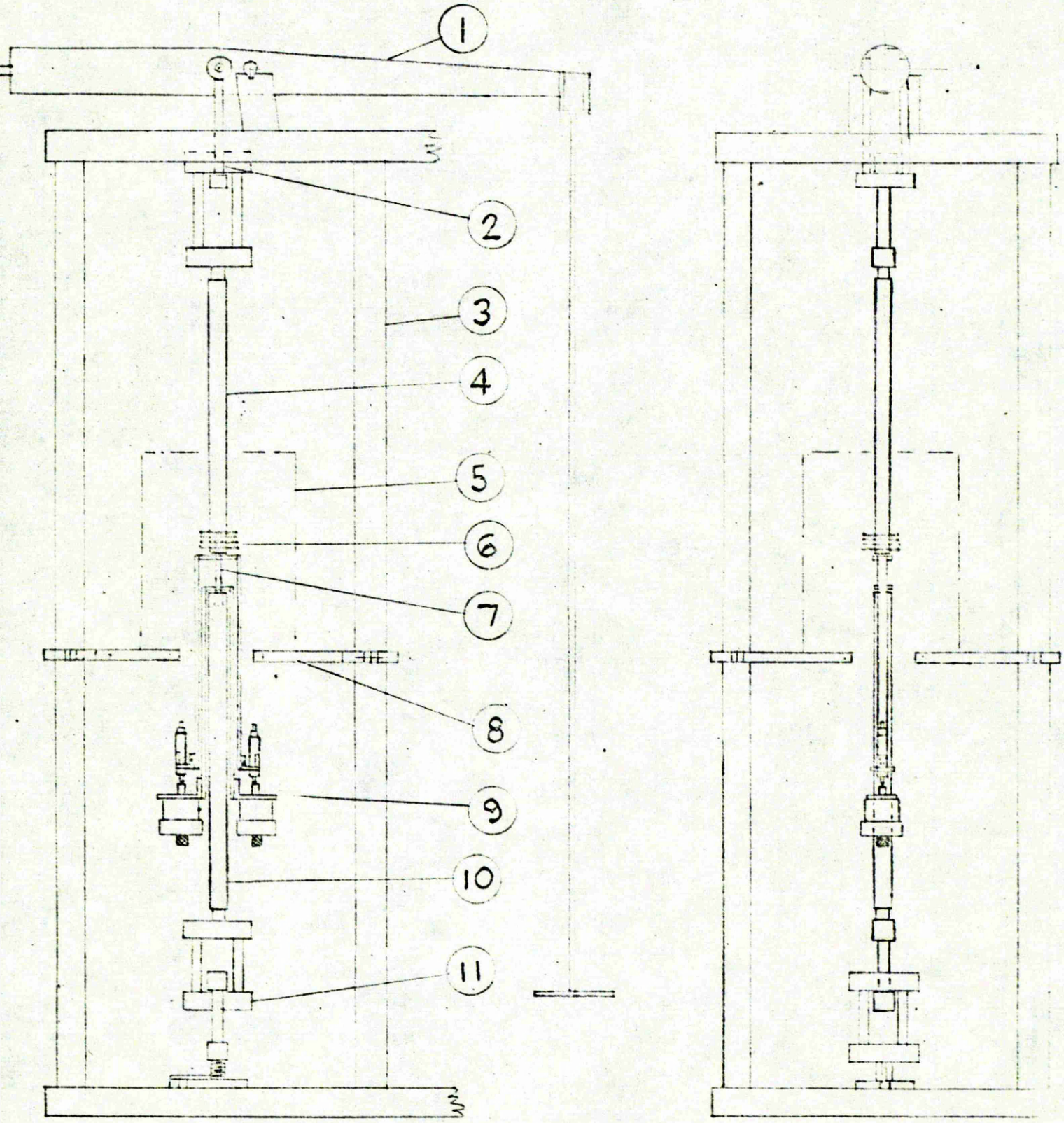

TENSILE CREEP MACHINE

FIGURE .2.

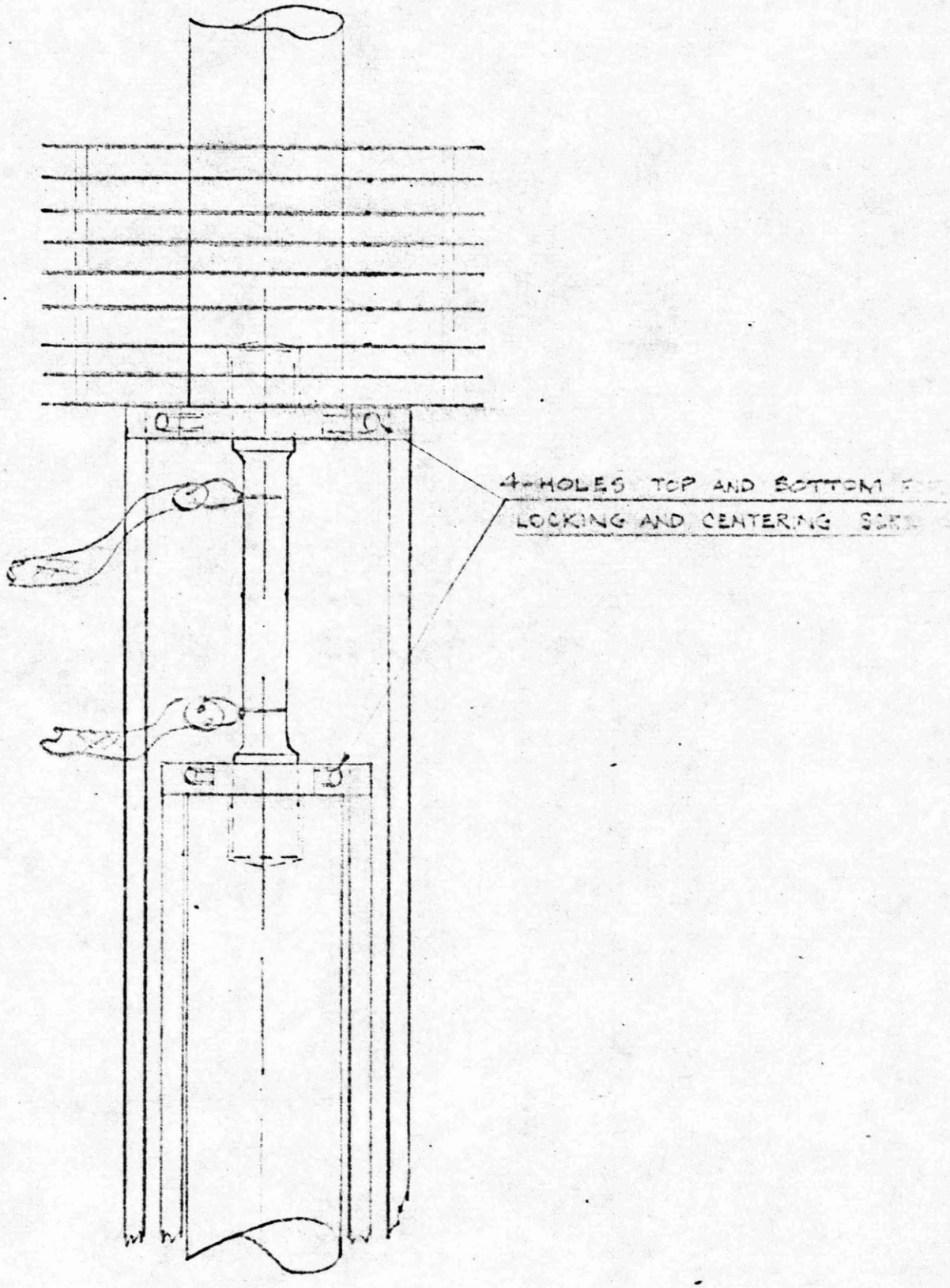

ARRANGEMENT OF TENSILE CREEP SPECIMEN

FIG. 2a

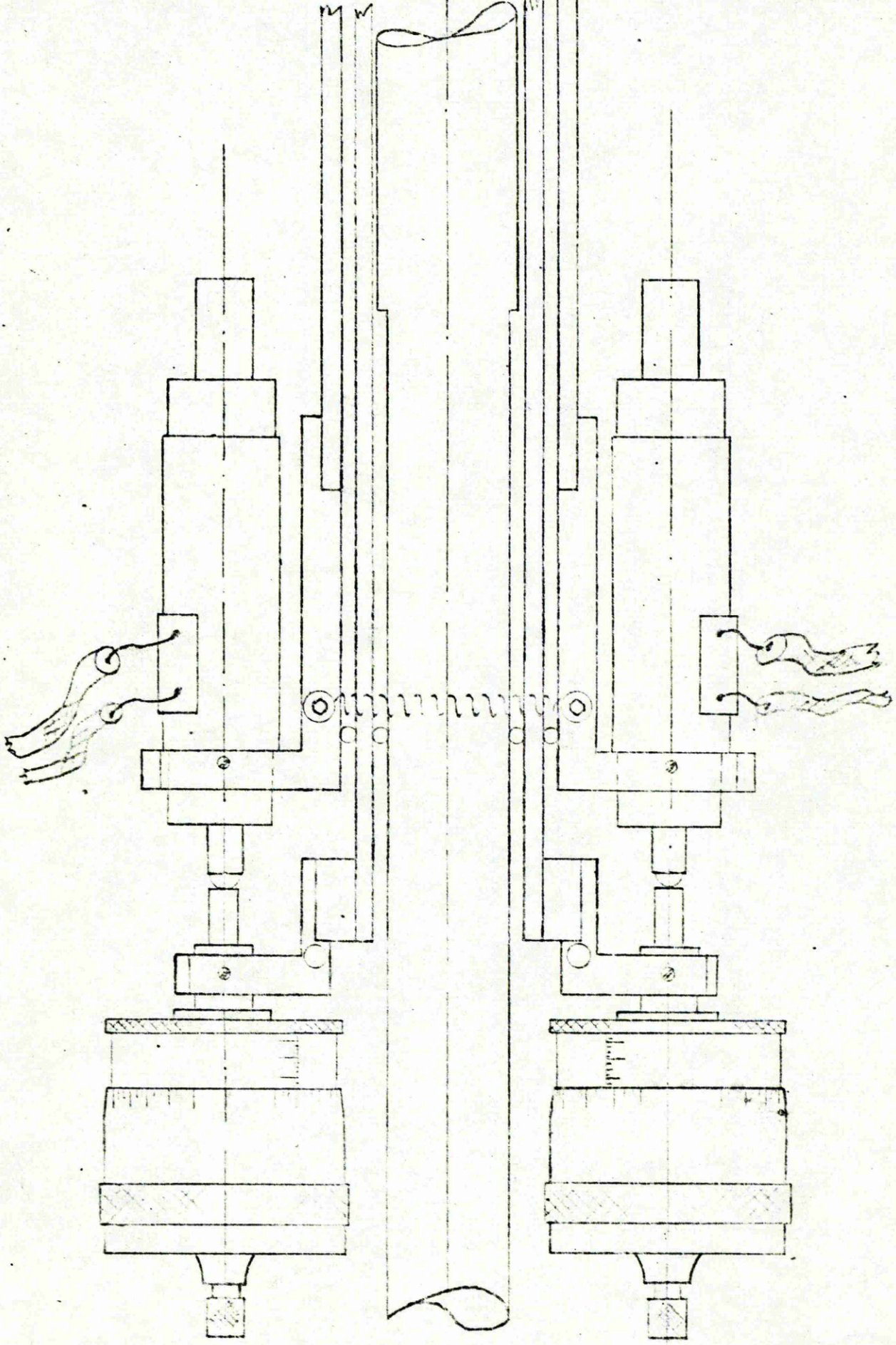

ARRANGEMENT OF TENSILE EXTENSOMETRY

FIG. 2a CONTD.

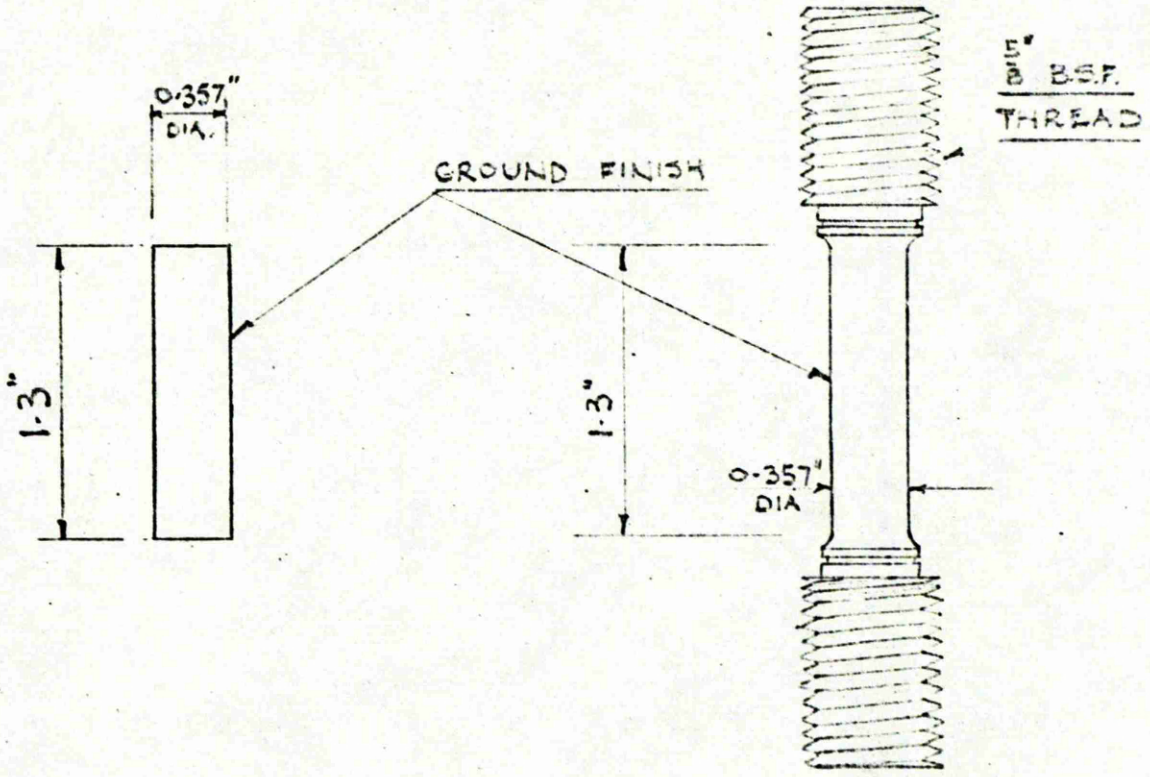

CREEP TEST SPECIMENS

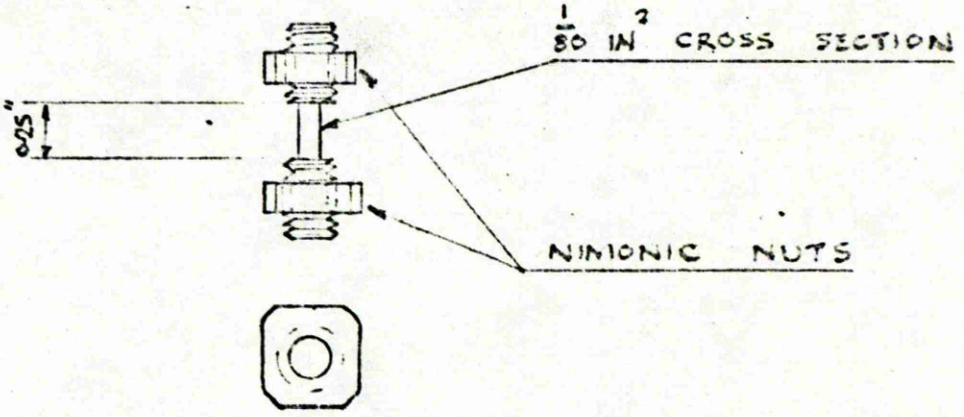

BAUSCHINGER TEST SPECIMEN

FIGURE . 3.

Fig. 4. Furnace.

1) Top Sindanyo End Plate.

2) Shaped firebrick former.

3) Terminal.

4) Top heating resistance winding.

5) Bottom heating resistance winding.

6) Terminal.

7) Bottom Sindanyo End Plate.

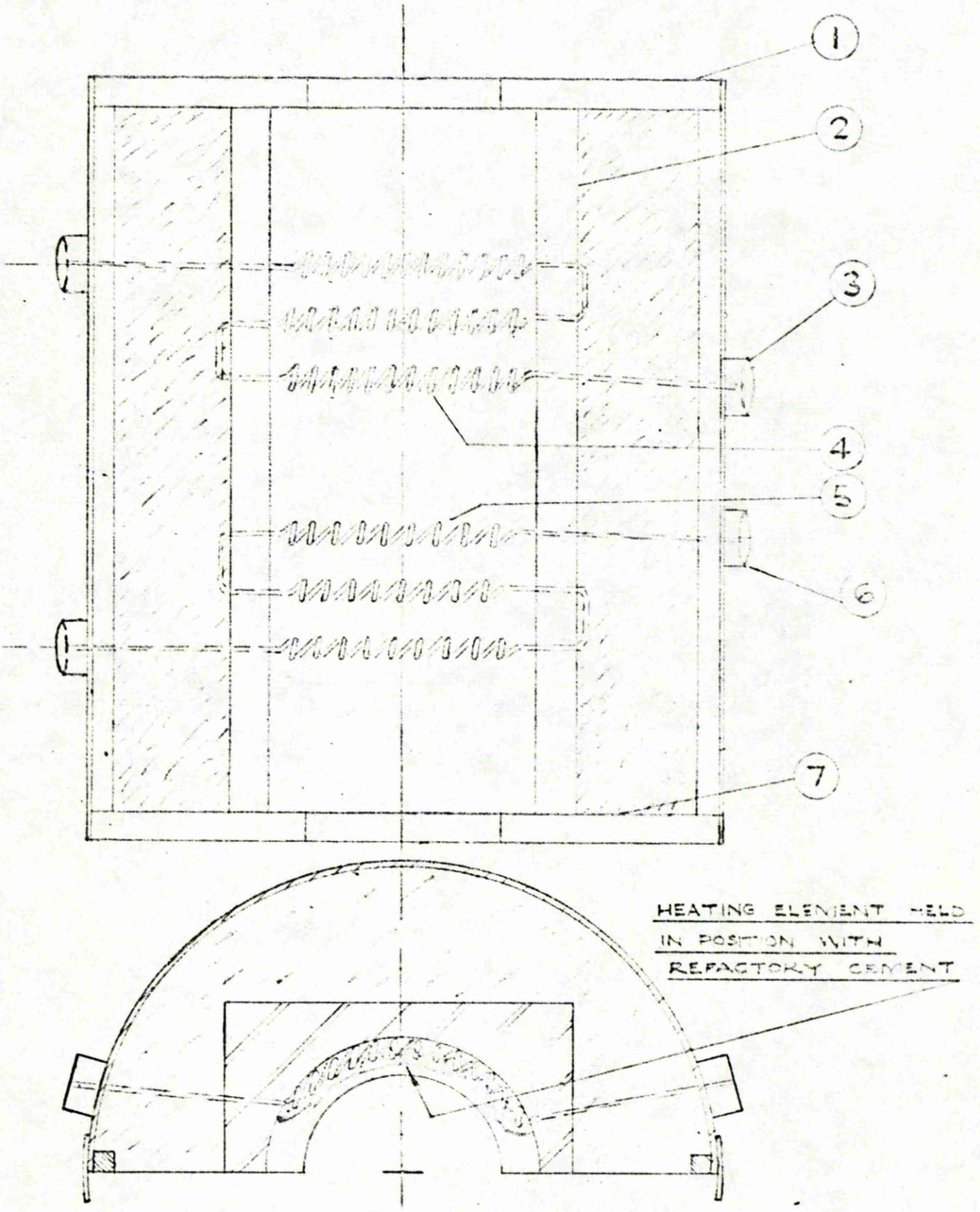

DIAGRAM OF THE SPLIT FURNACE

FIGURE 4.

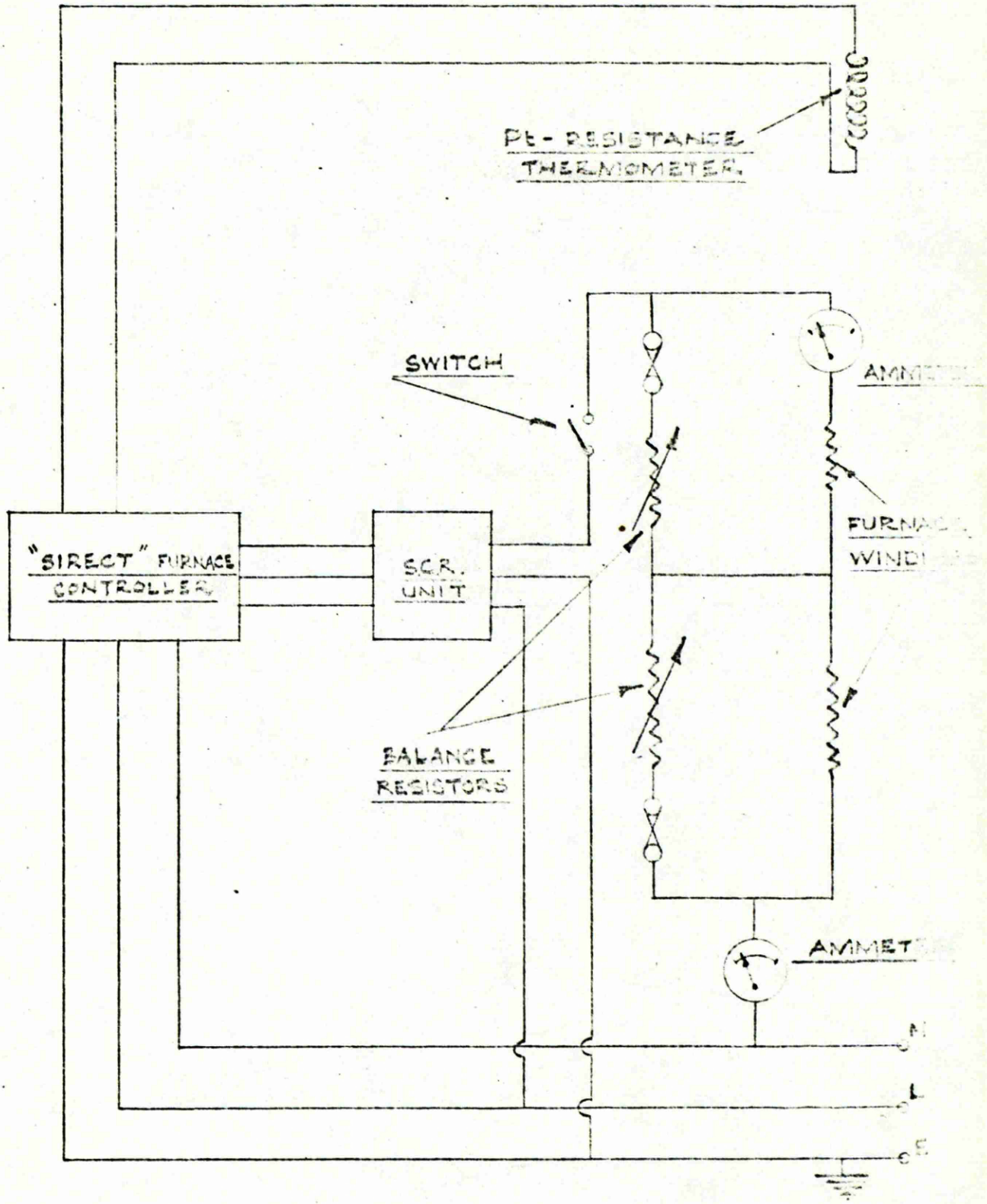

FURNACE CONTROL CIRCUIT

FIGURE 4.a.

Fig. 5. Bauschinger Machine.

1) Coupling to load cell of Instron Universal Tester.
2) Upper loading ram with guiding slot shown.
3) Cooling coils, connected to water supply.
4) Specimen mounting.
5) Main frame.
6) Lower loading ram.
7) Pin securing the lower loading ram to the main frame.
8) Crosshead of the Instron Universal Testing Machine.

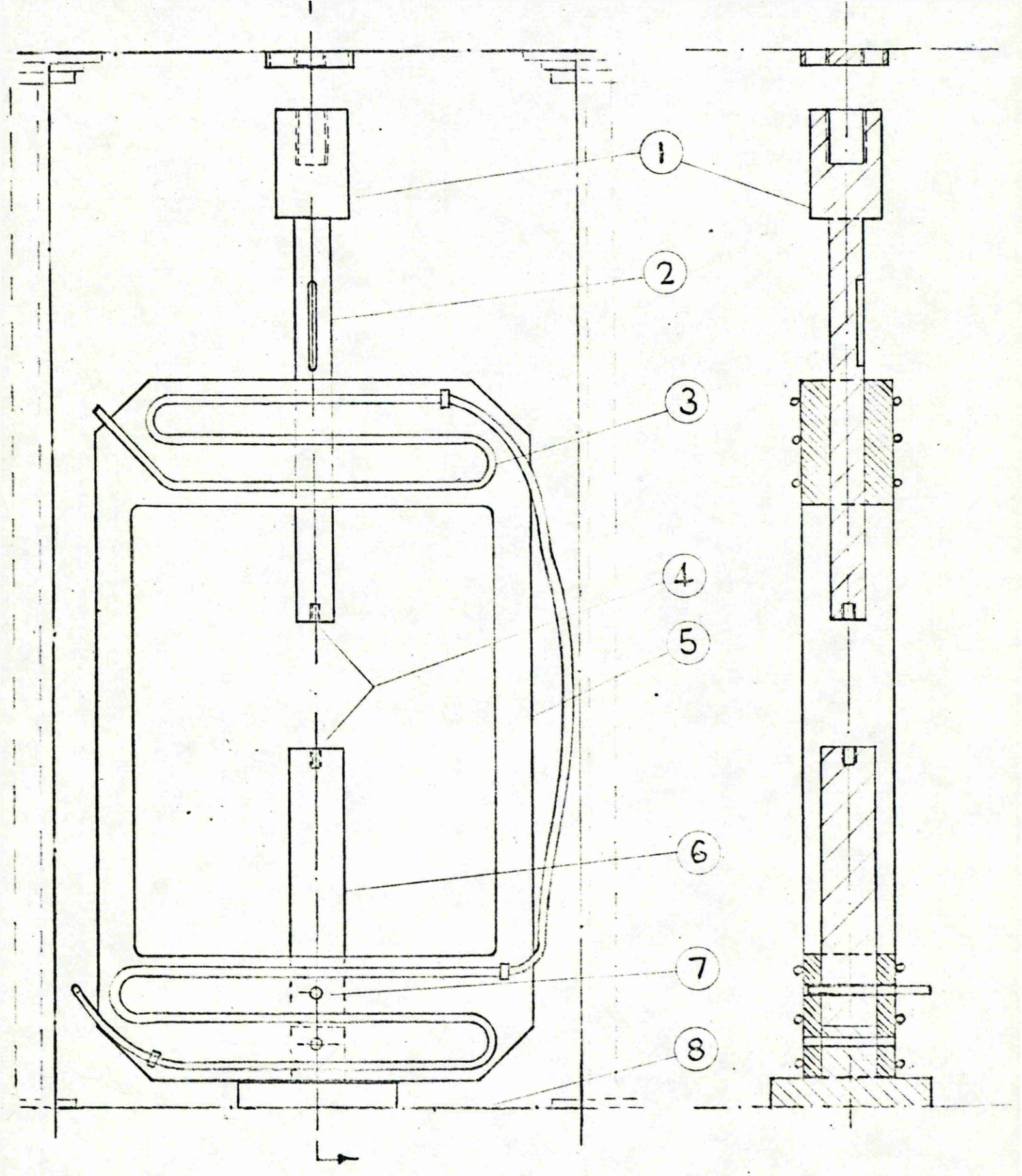

BAUSCHINGER MACHINE

FIGURE 5

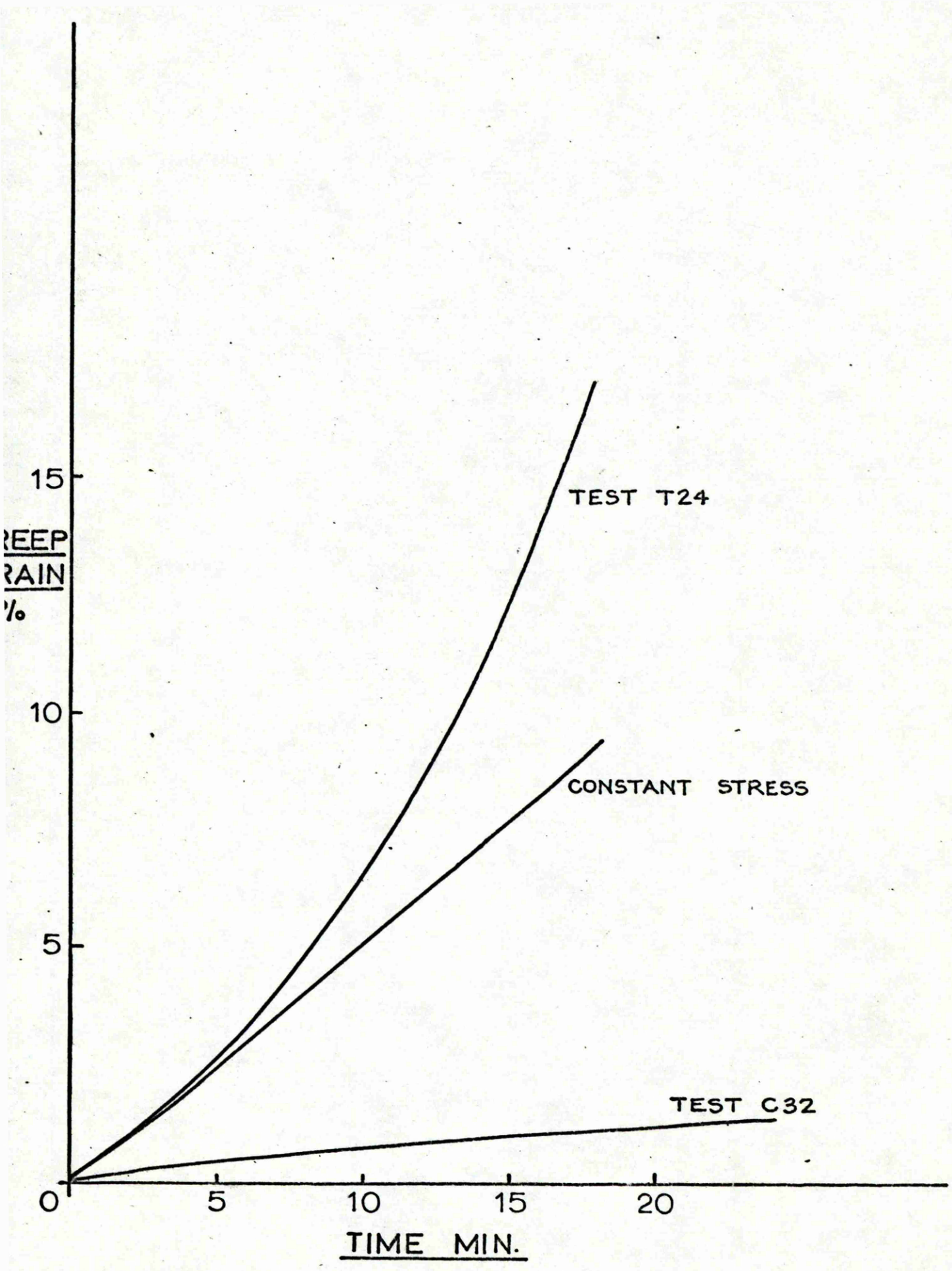

FIG. 6.

Comparative Creep Curves in Torsion and Compression at 1000°C and 20,400 lb.in^{-2}.

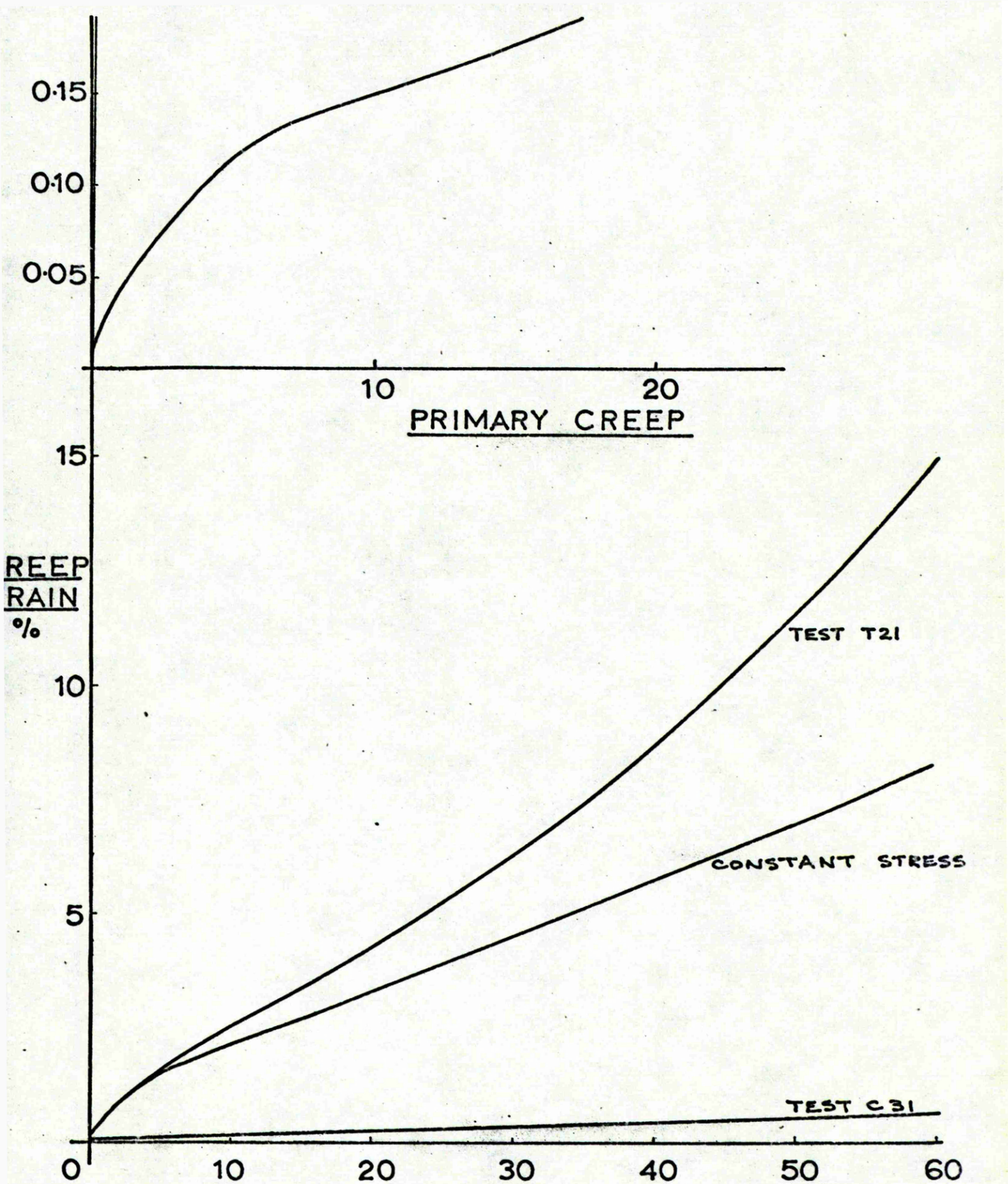

FIG. 7.

Consecutive Creep Curves in Tension and Compression at 1000°C and 17,000 lb.in^{-2}.

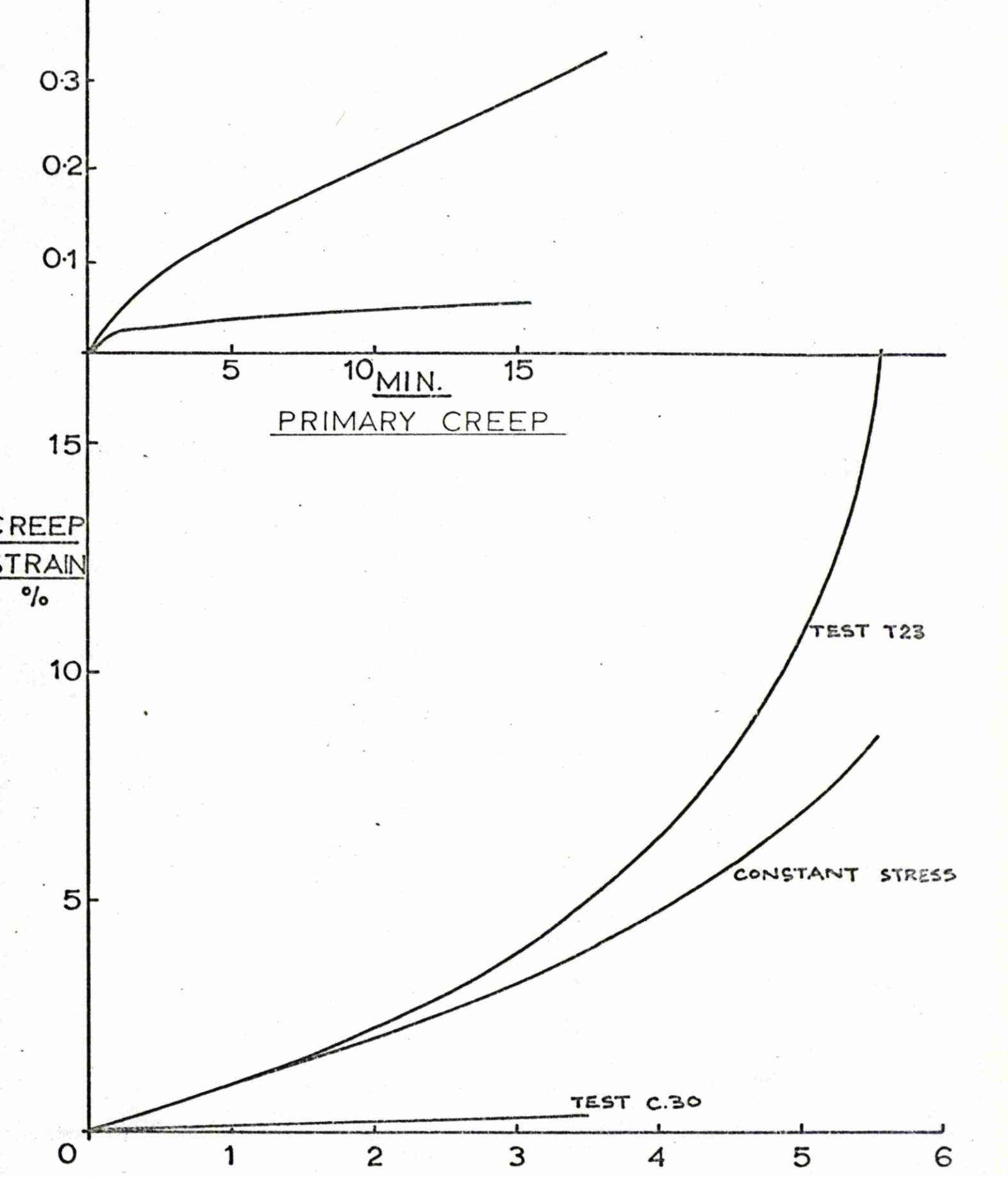

FIG. 8.

Comparative Creep Curves in Tension and Compression at 1000°C and 15,600 lb.in^{-2}.

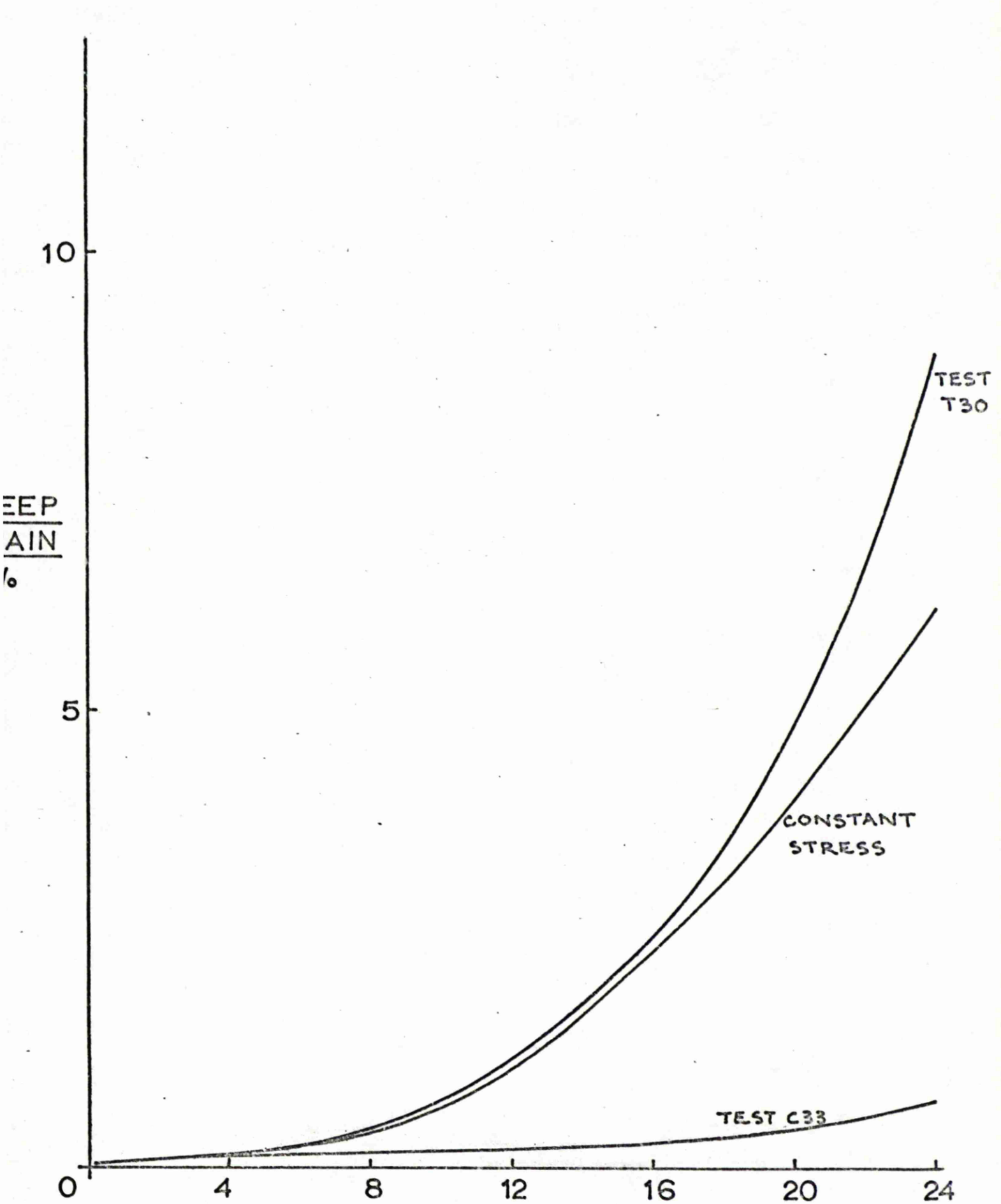

FIG. 9.

Comparative Creep Curves in Tension and Compression at 1000°C and 10,200 lb.in^{-2}.

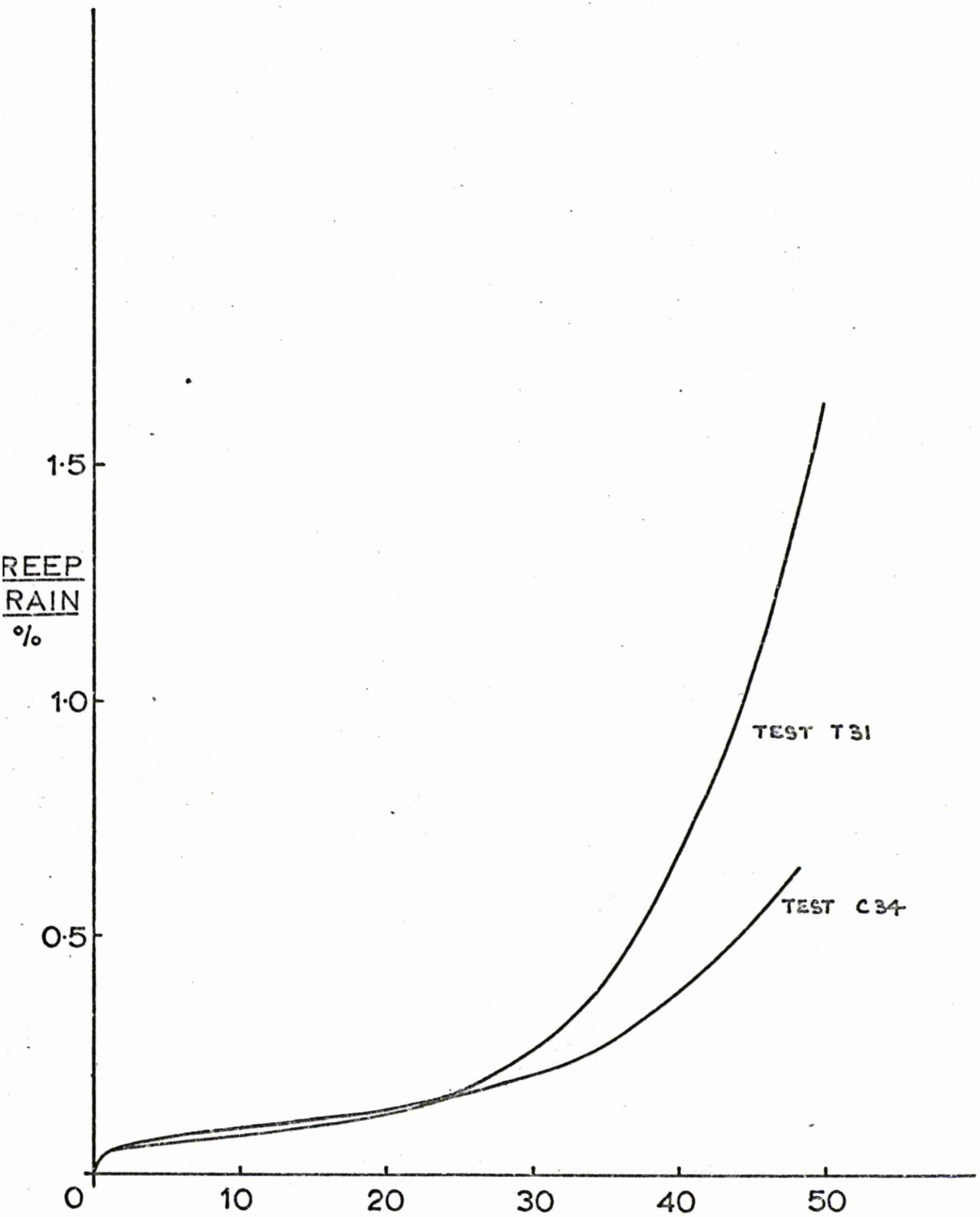

FIG.10.

Comparative Creep Curves in Tension and Compression at 100°C and

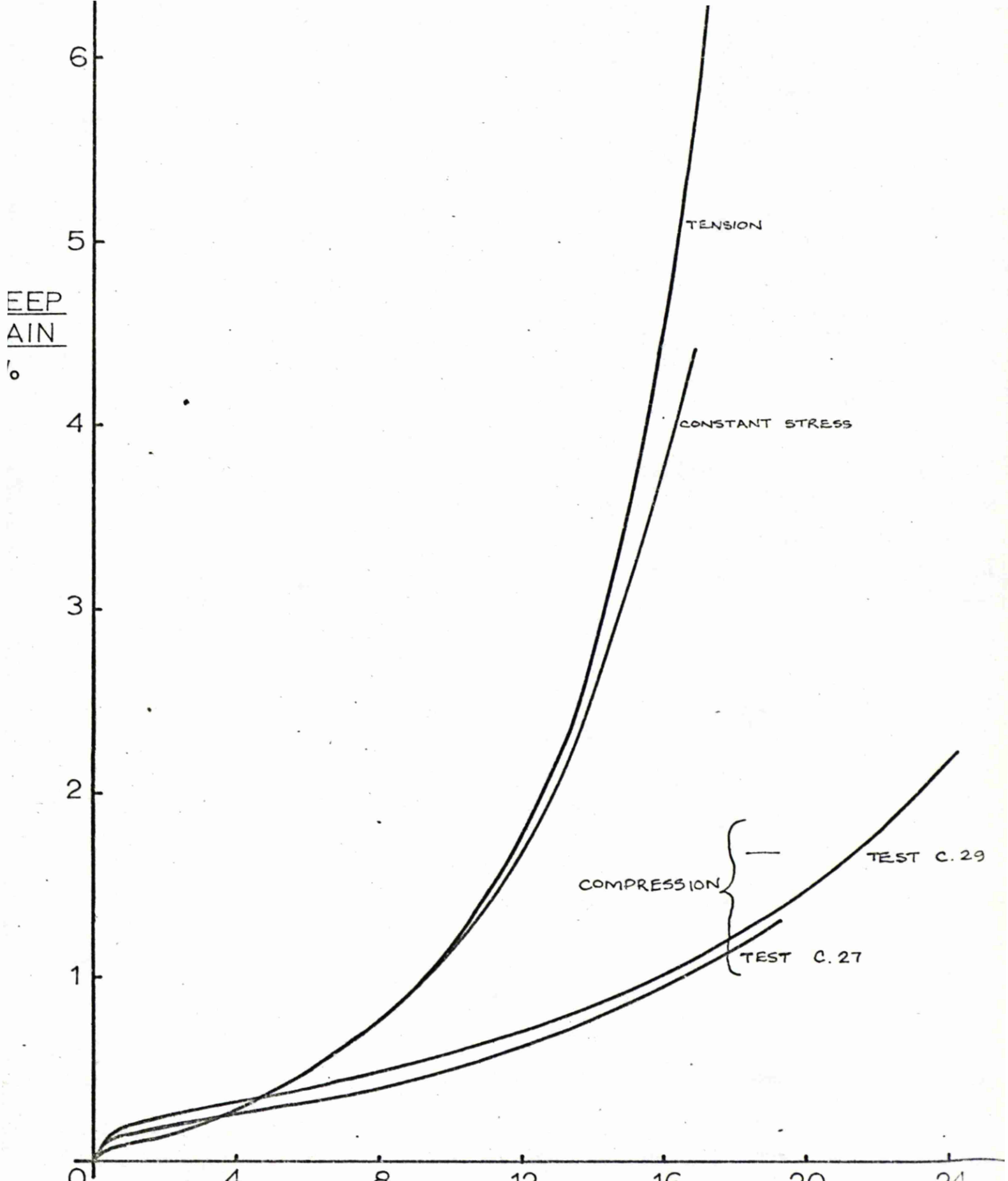

FIG. 11.

Comparative Creep Curves in Tension and Compression at 950°C and 20,400 lb.in^{-2}.

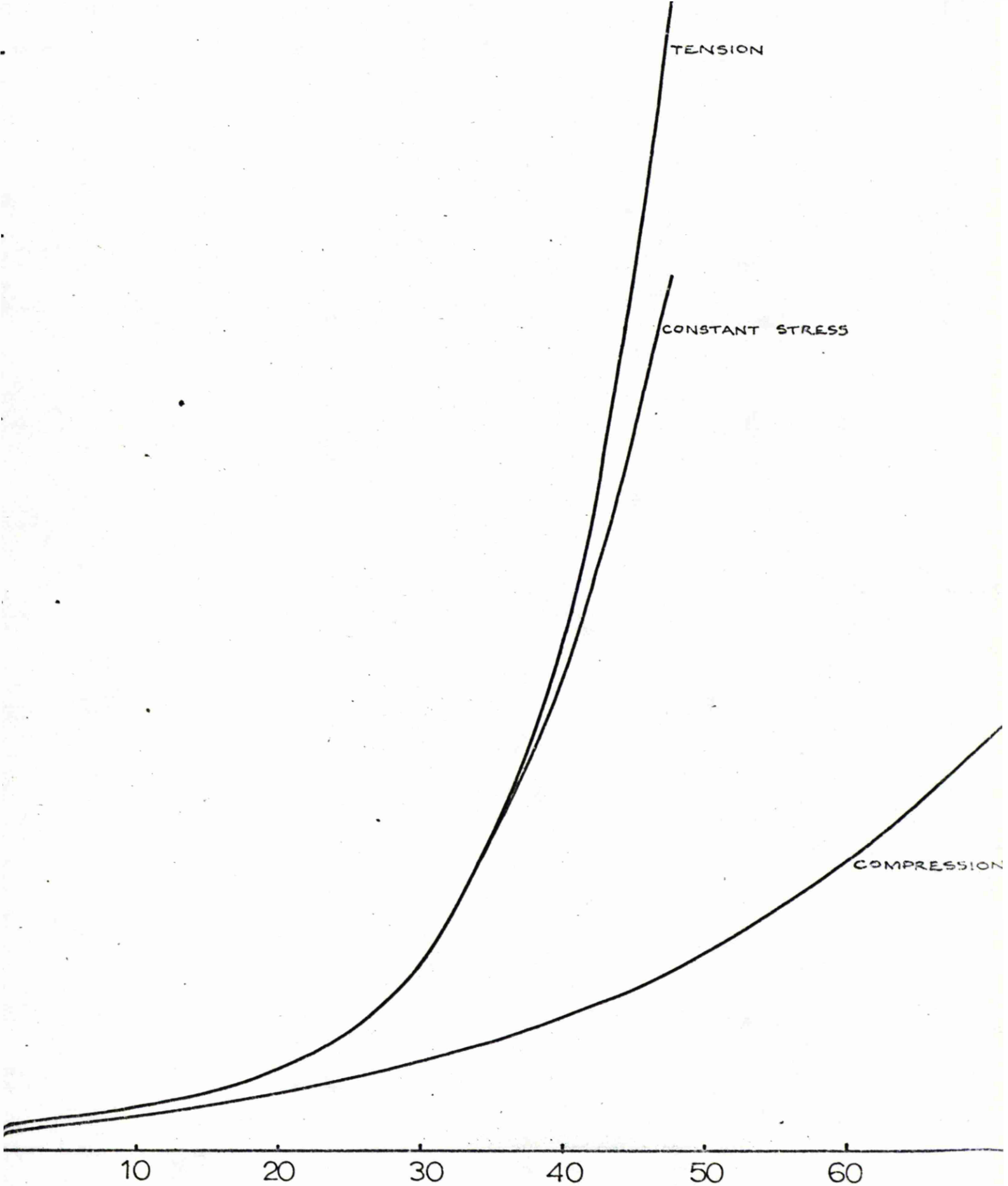

FIG. 12.

Comparative Creep Curves in Tension and Compression at 950°C and 17,000 lb.in^{-2}.

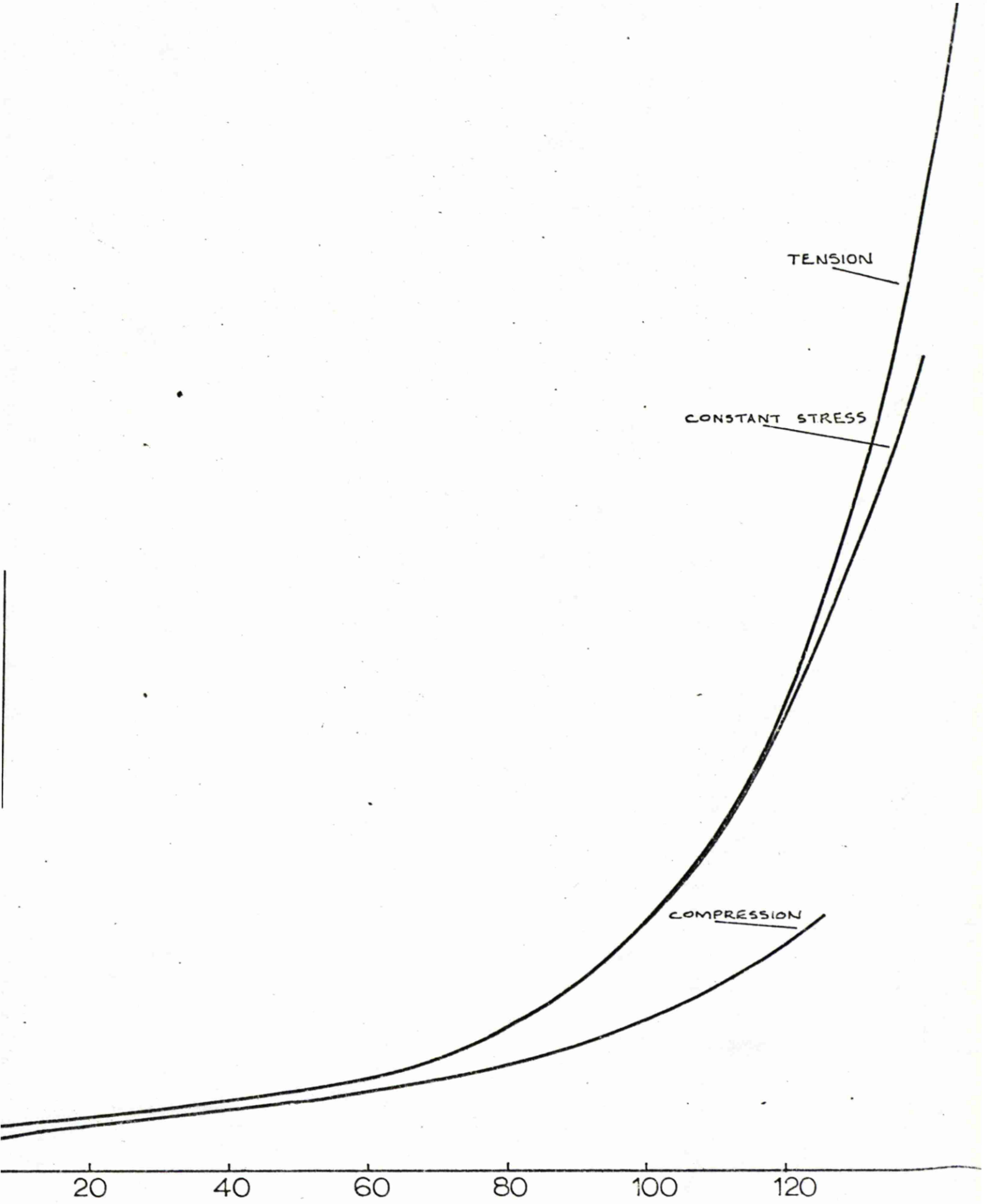

FIG. 13.

Comparative Creep Curves in Tension and Compression at 950°C and 13,600 lb.in^{-2}.

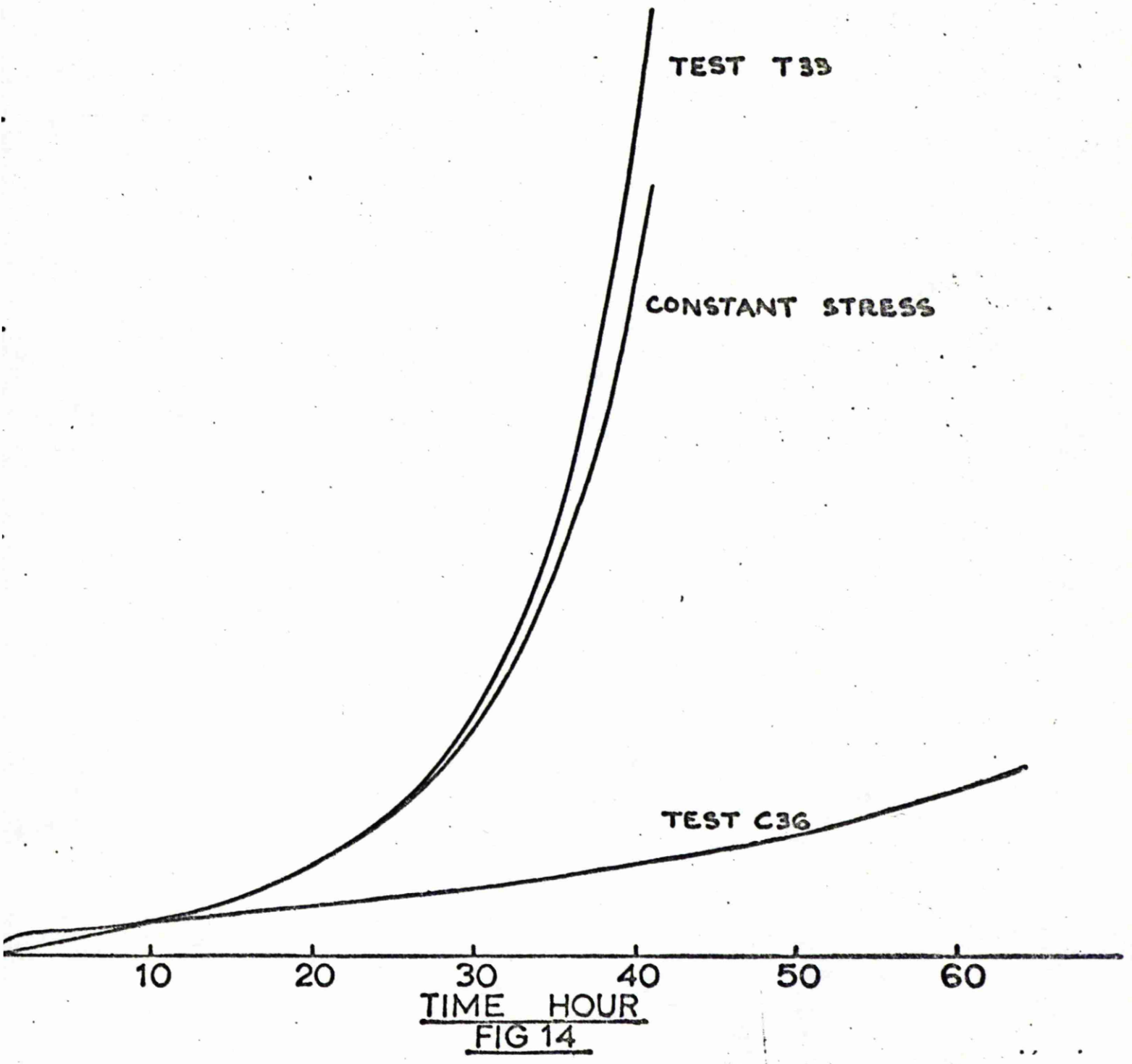

FIG 14

Comparative Creep Curves in Tension and Compression at 930°C and 20,400 lb.in^{-2}.

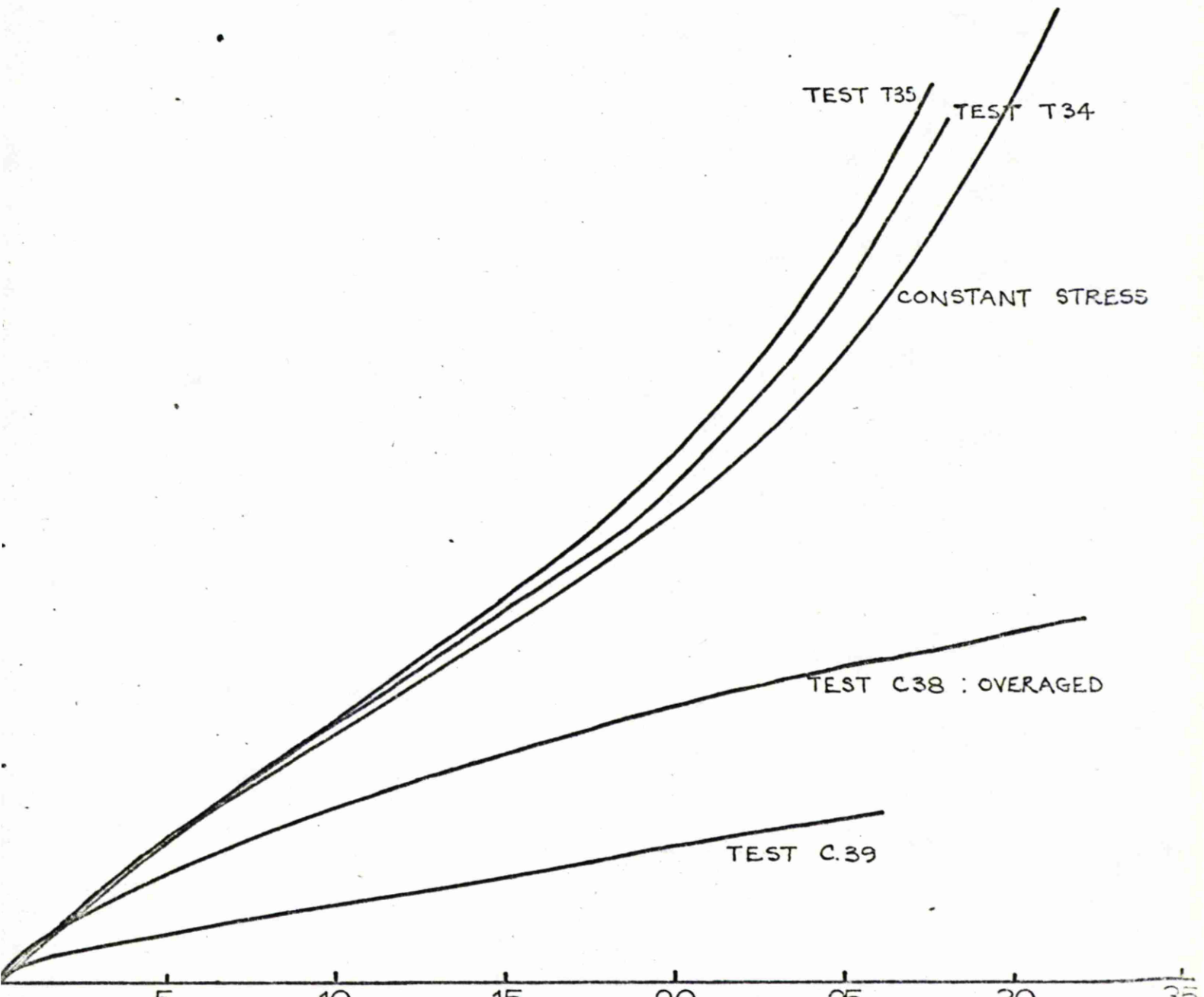

FIG. 15.

Comparative Creep Tests at 800°C and 61,200 lb.in^{-2}.

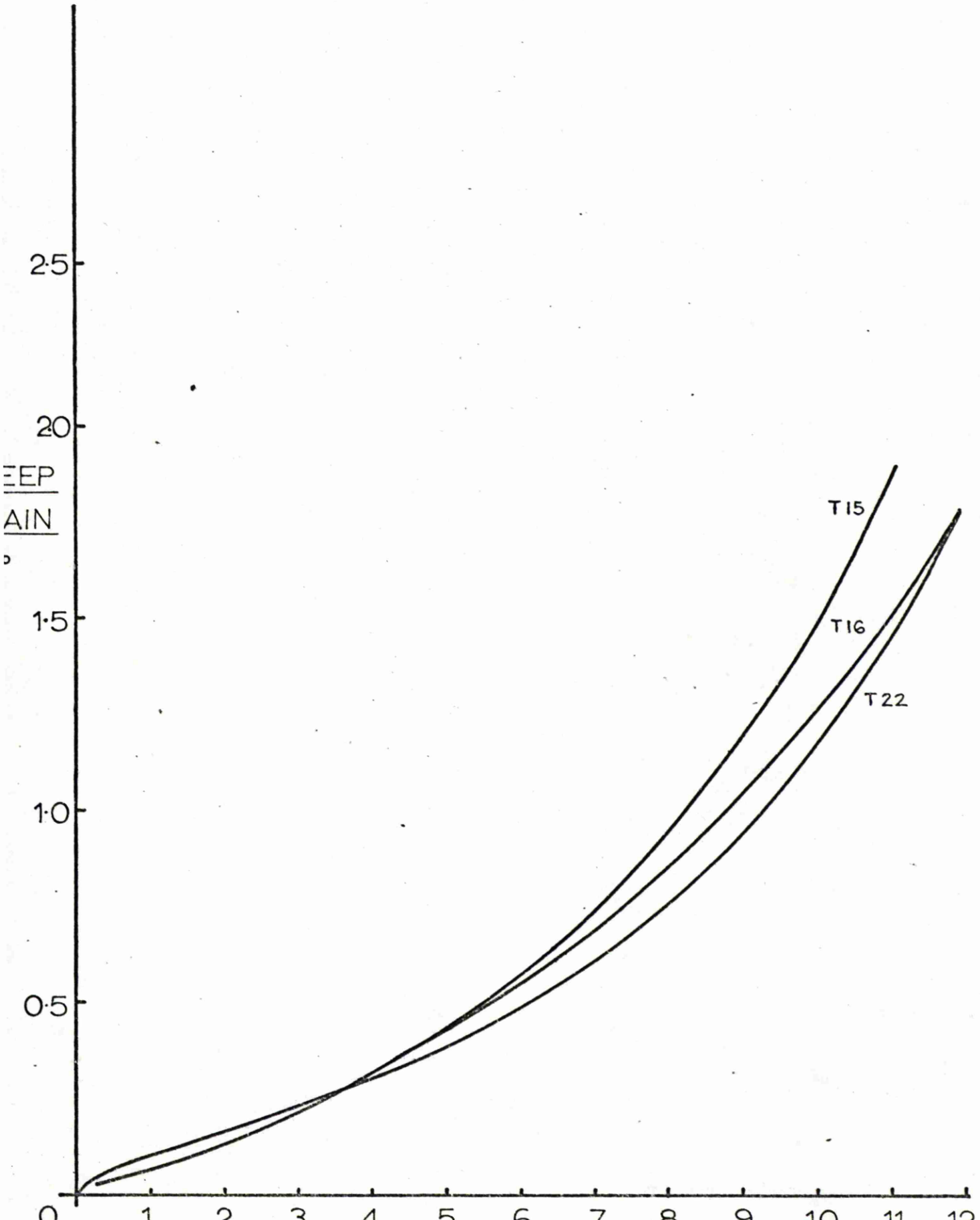

FIG. 16.

Repeated Tensile Creep Tests at 950°C and 20,400 lb.in^{-2}.

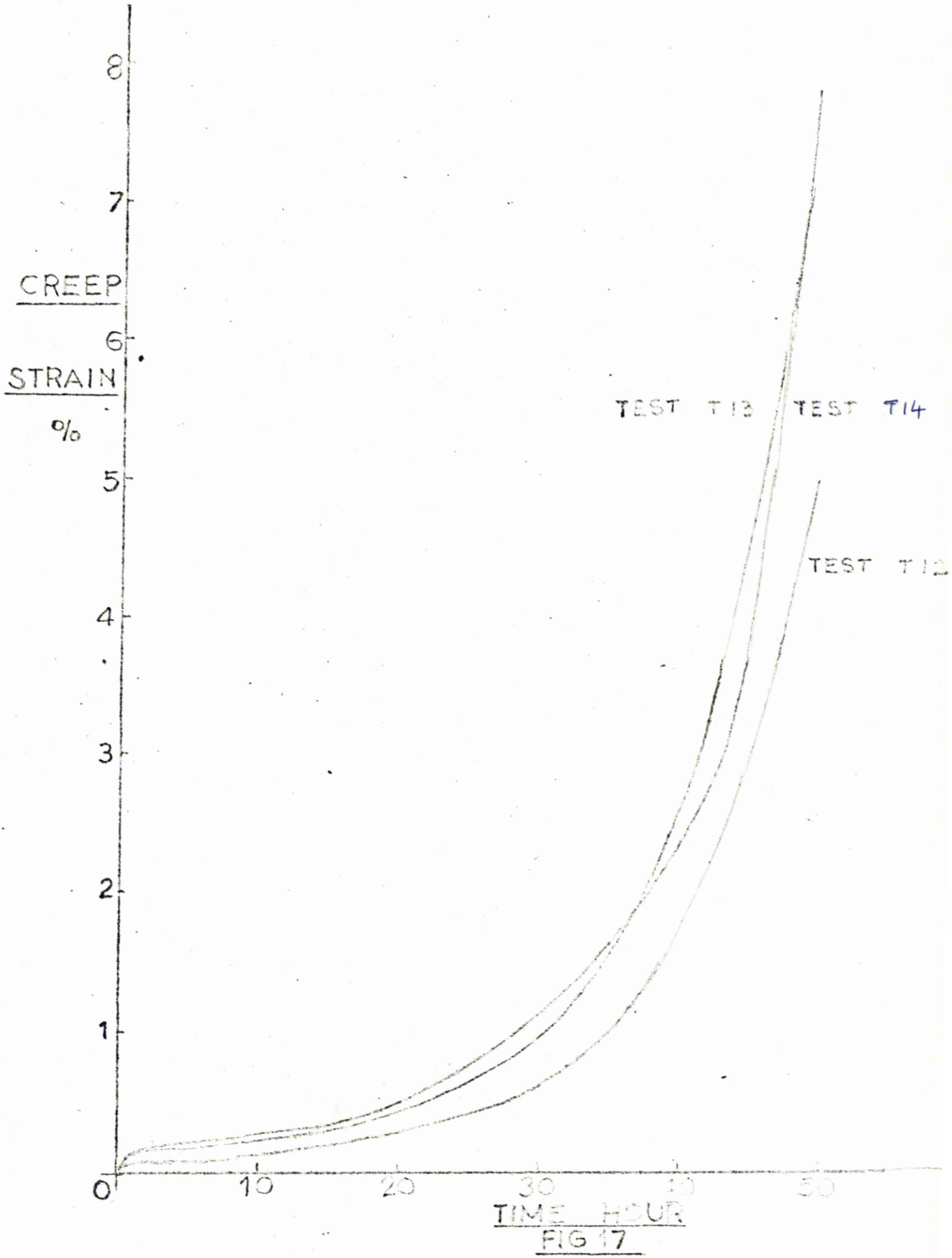

FIG 17

Repeated Tensile Creep Tests at 950°C and 17,000 lb.in^{-2}.

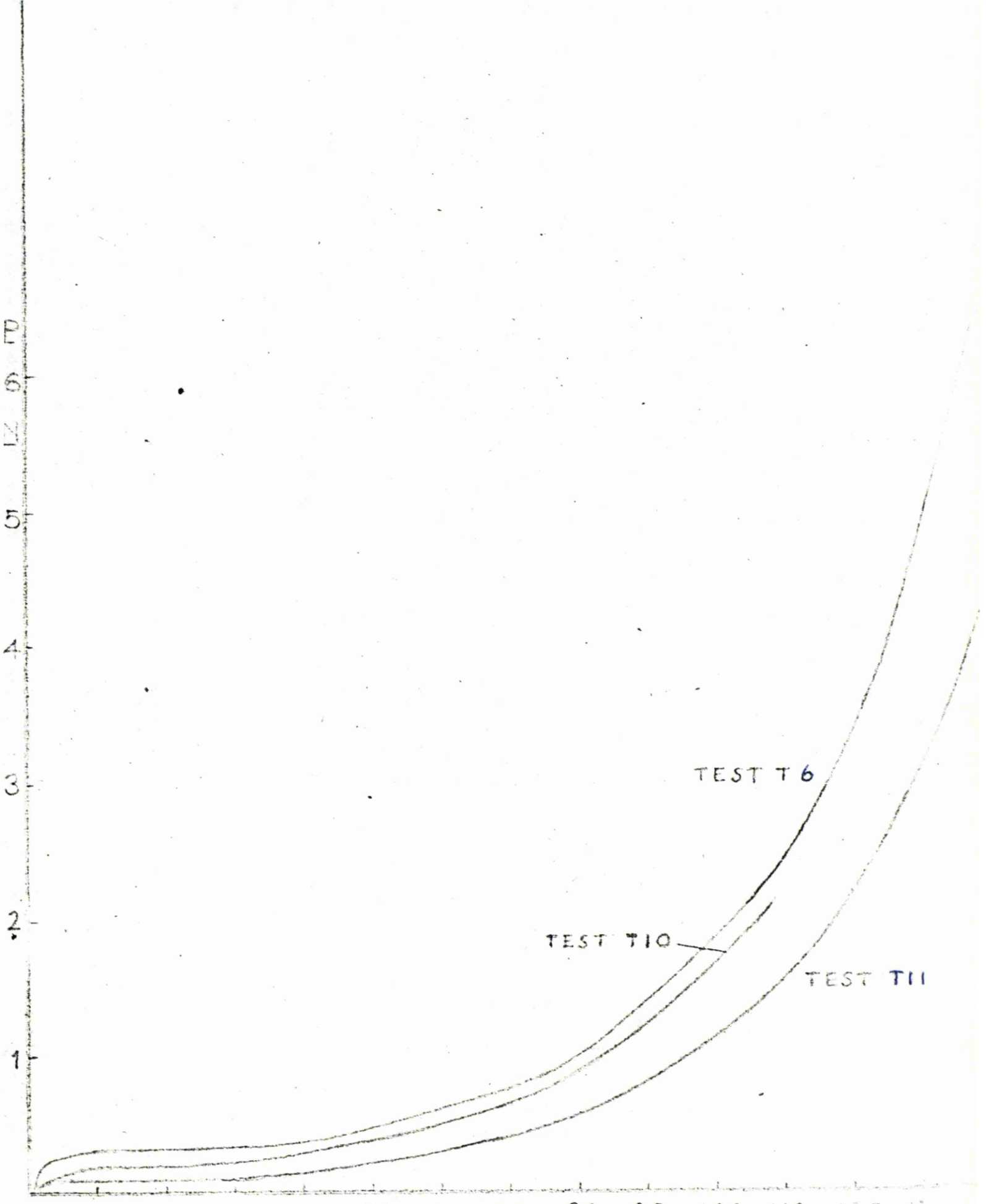

FIG 18

Repeated Tensile Creep Tests at 950°C and 13,600 lb.in^{-2}.

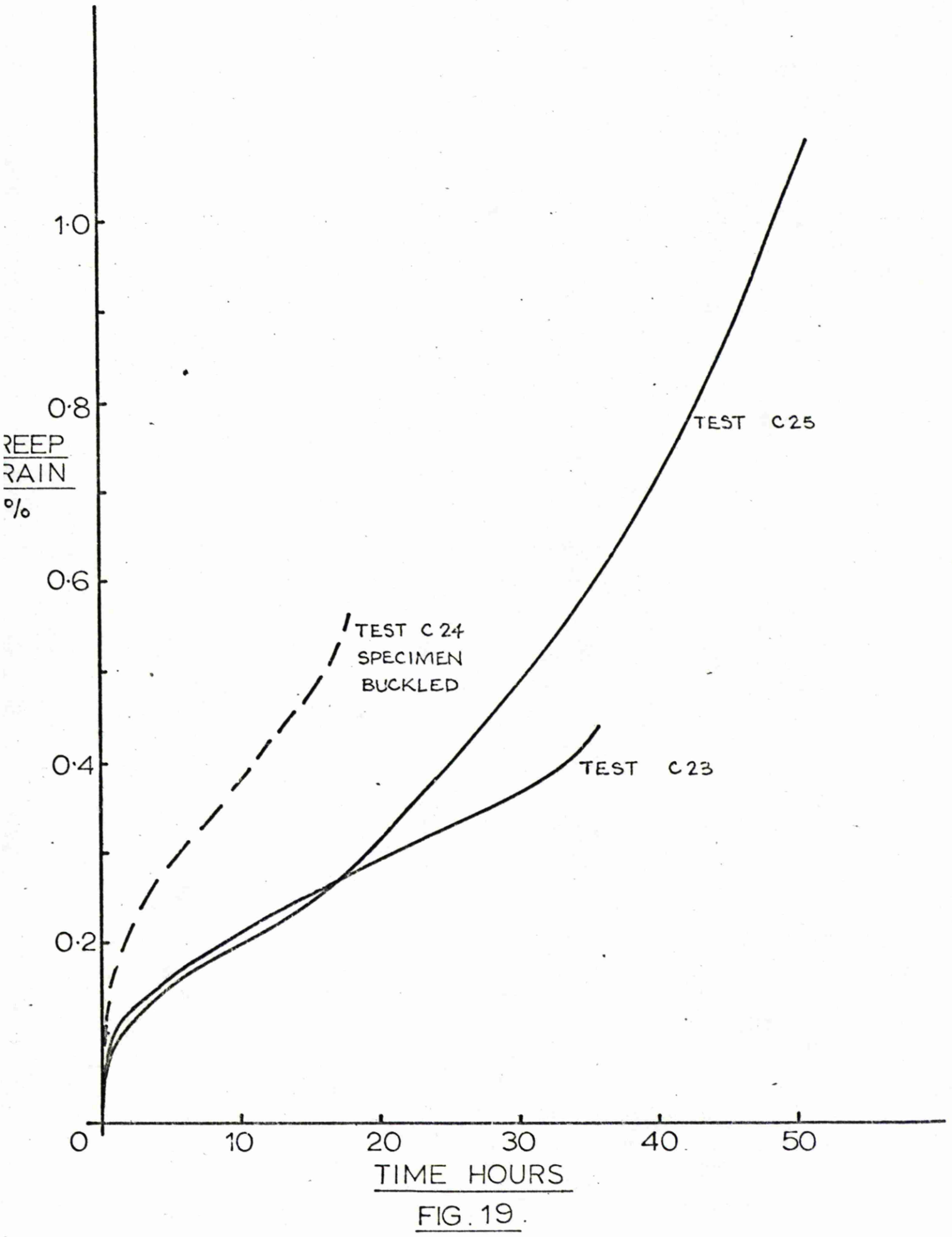

FIG. 19.

Repeated Compressive Creep Tests at 950°C and 17,000 lb.in^{-2}.

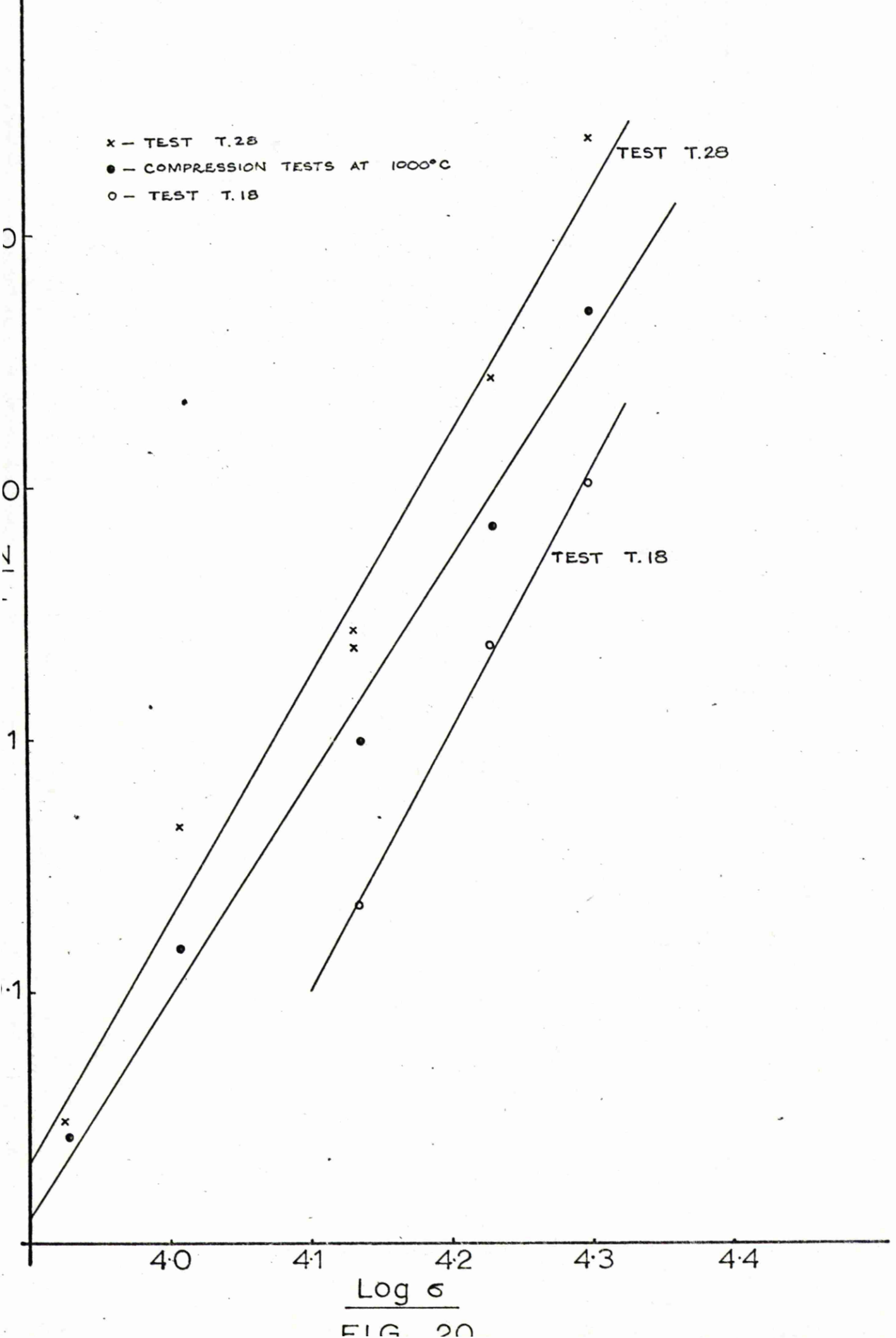
x — TEST T.28
● — COMPRESSION TESTS AT 1000°C
o — TEST T.18
TEST T.28
TEST T.18
0
0
1
·1
4·0
4·1
4·2
4·3
4·4
Log σ

FIG. 20

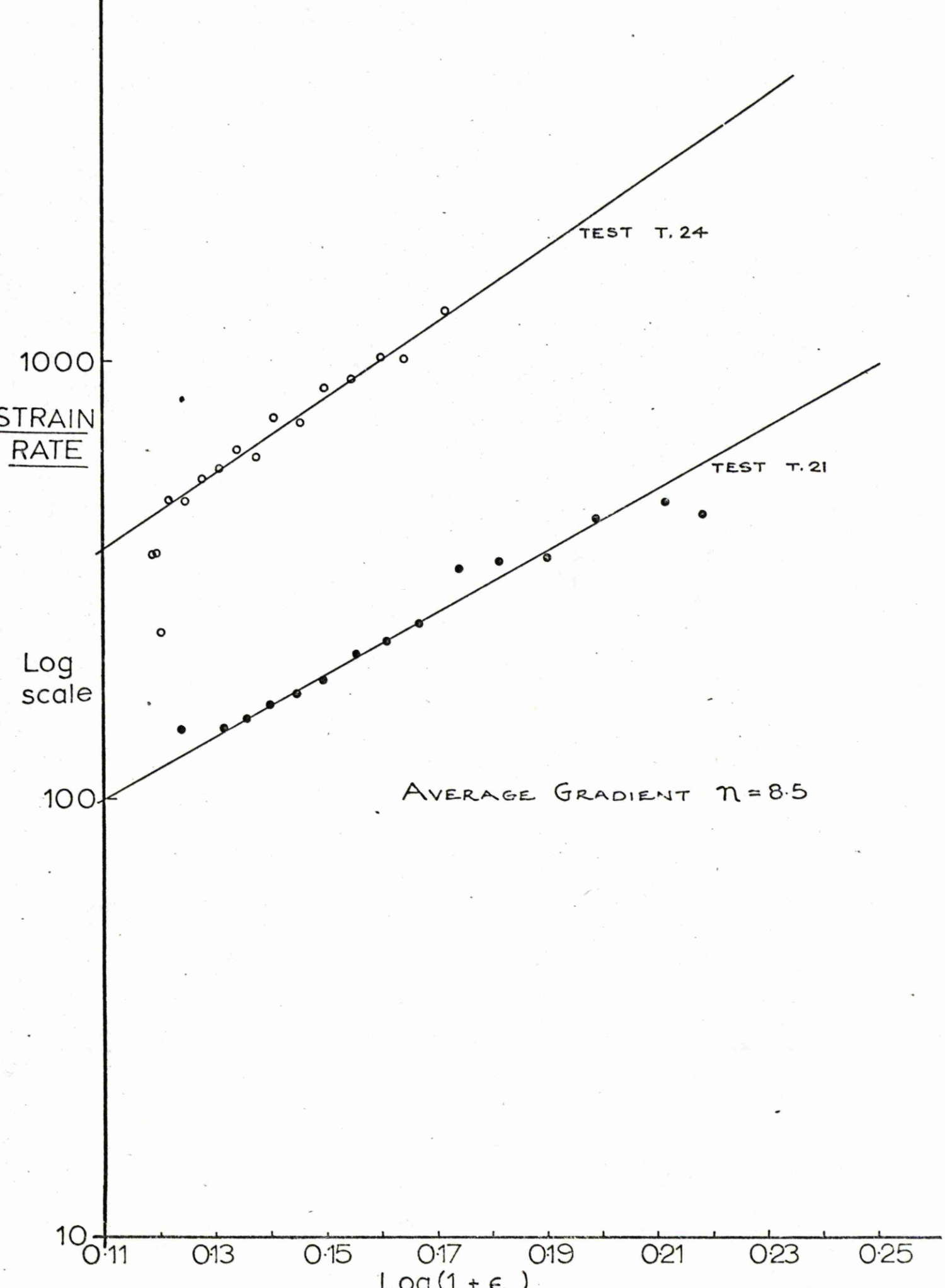
TEST T. 24
TEST T. 21
1000
STRAIN RATE
Log scale
100
10
AVERAGE GRADIENT n = 8·5
0·11
0·13
0·15
0·17
0·19
0·21
0·23
0·25
Log (1 + ϵ)

FIG. 21.

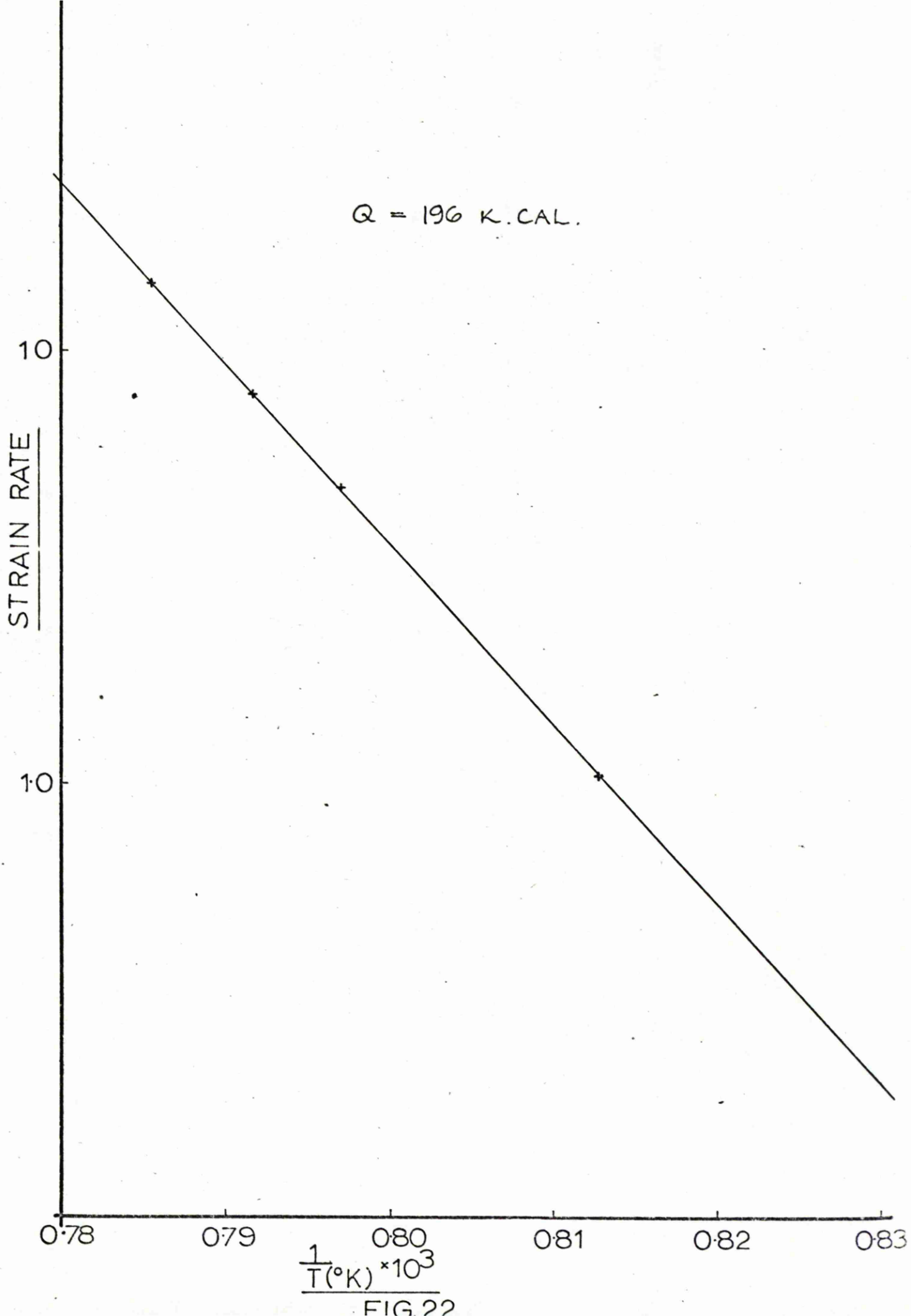

FIG.22

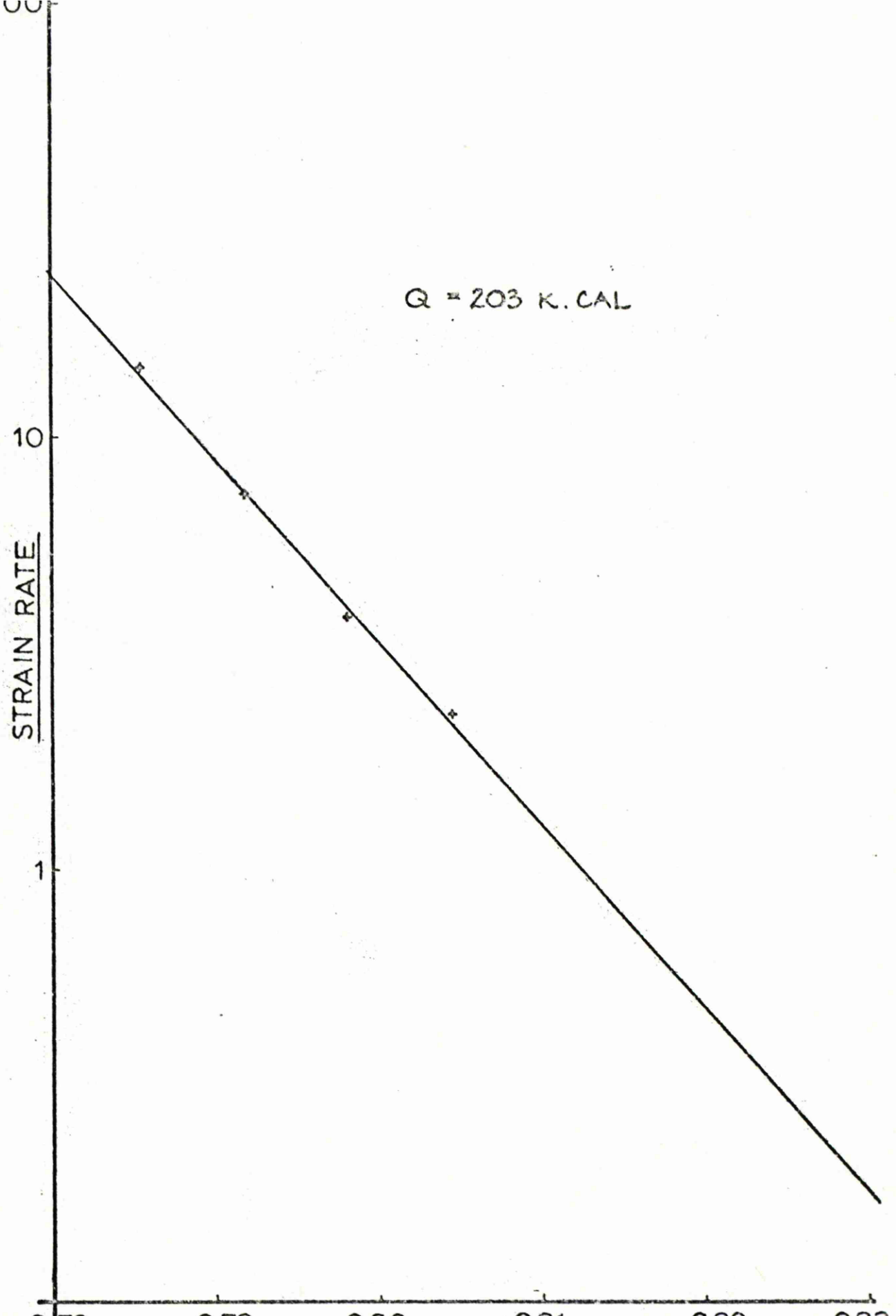

FIG. 23

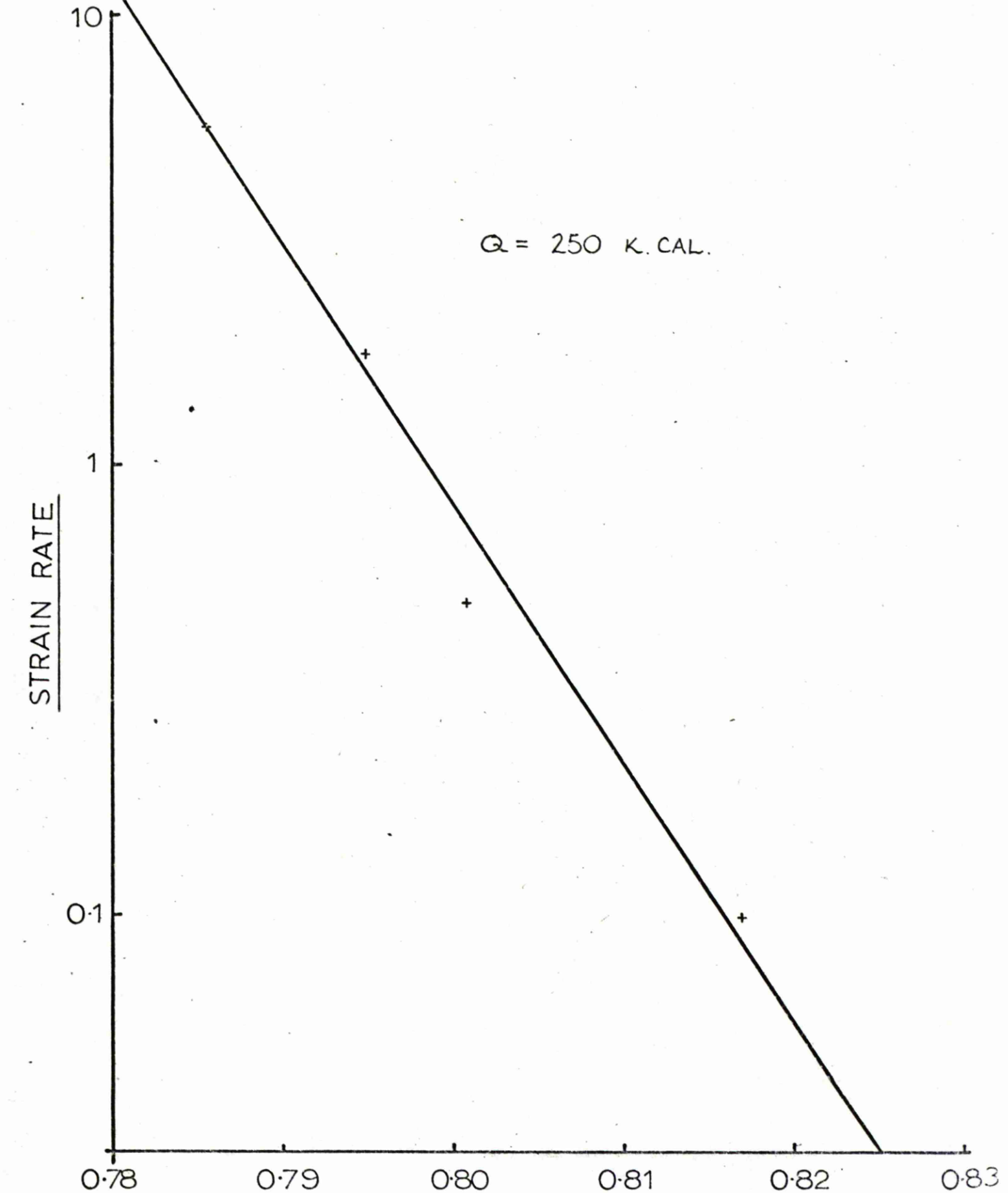
Q = 250 K. CAL.
10
1
0·1
STRAIN RATE
0·78
0·79
0·80
0·81
0·82
0·83
$\frac{1}{T}(°K)^{-1} \times 10^3$

FIG. 24.

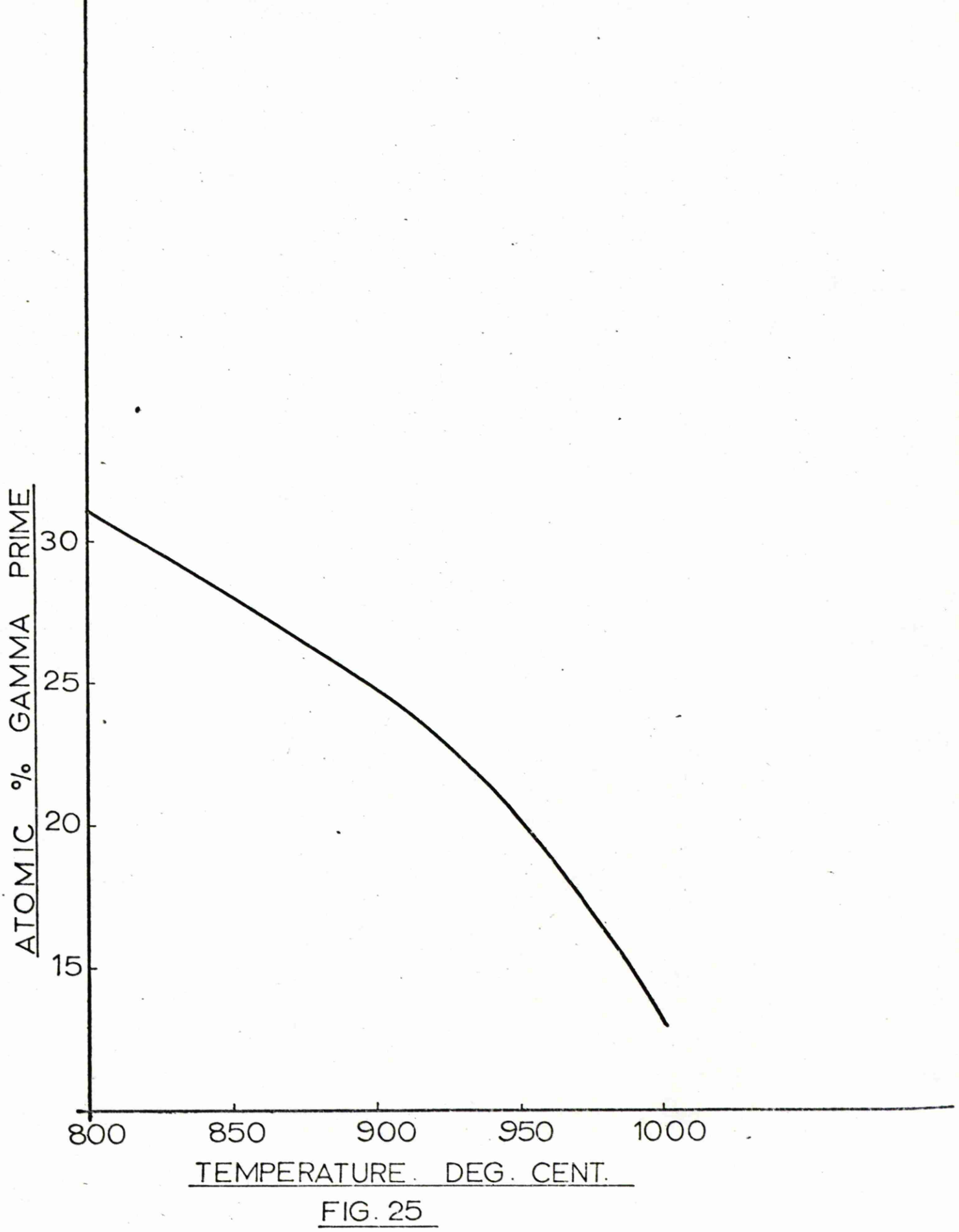

FIG. 25

Variation of the Volume Percentage of Gamma Prime with Temperature.

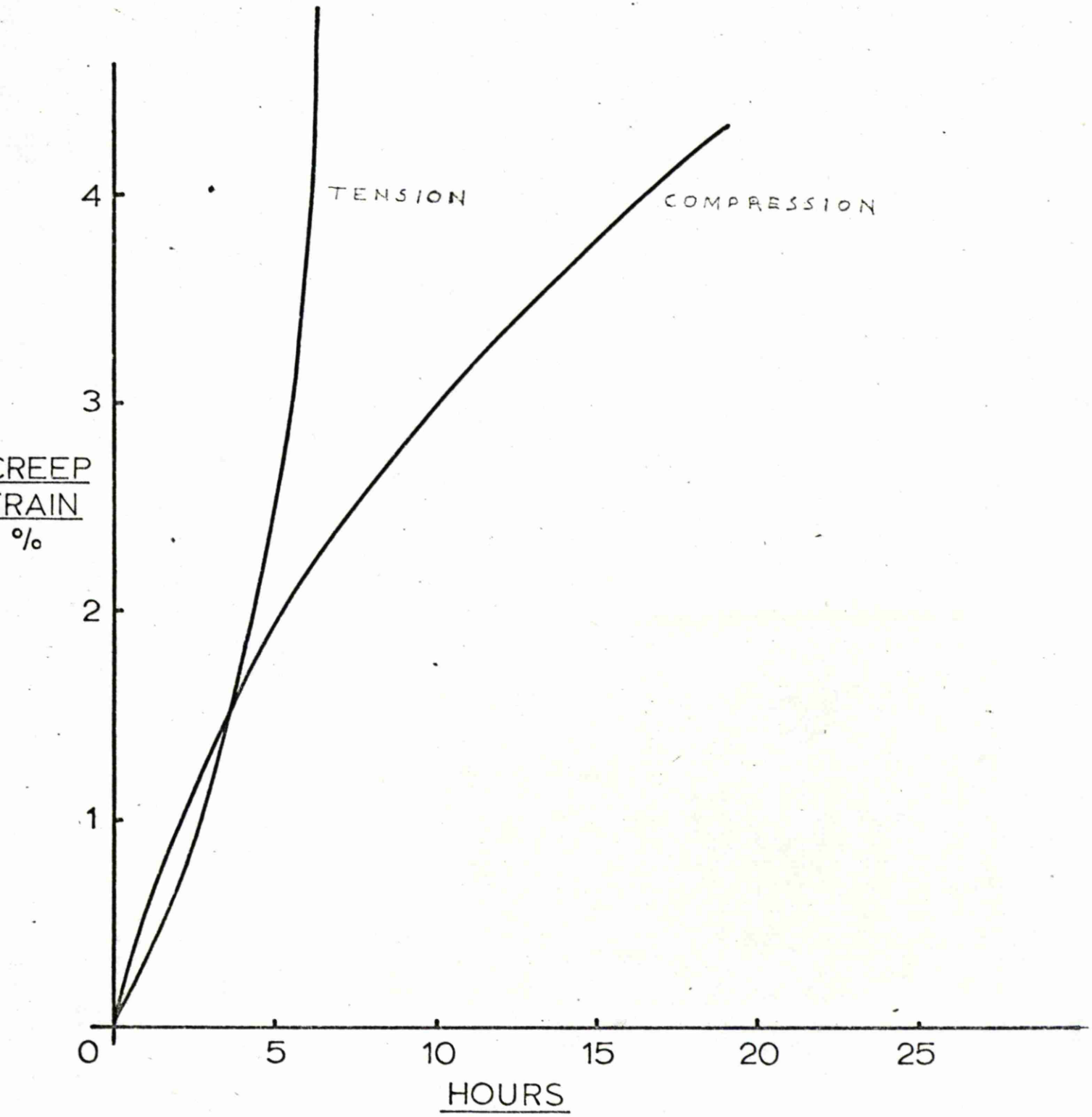

FIG. 26.

Compressive and Tensile Creep Rates in Copper at 580°C and 1,500 lb.in^{-2}.
"Tensile Curve by permission of I. Gillies, University of Glasgow, M.Sc. Thesis, 1967".

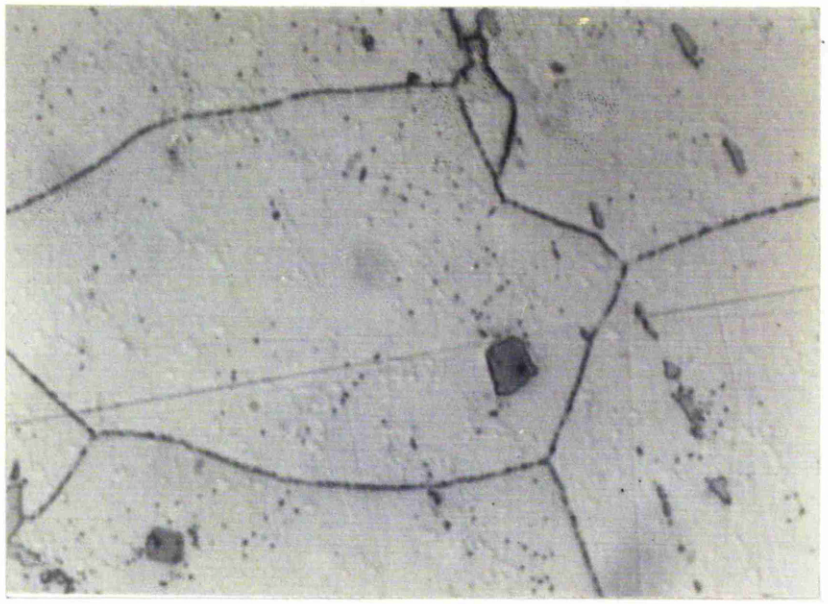

Fig. 27. Nimonic 105 - As Received Material: X 700 Chemical Etch.

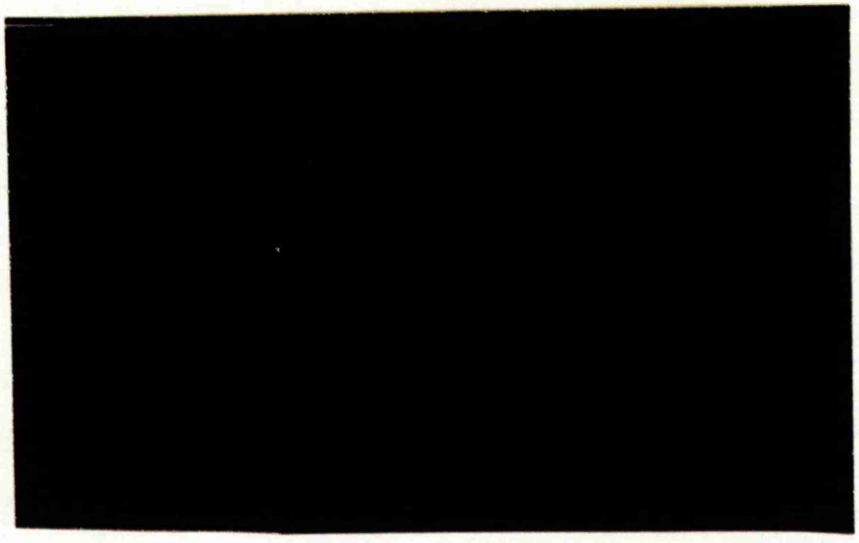

Fig. 28. Specimen Fractured in Tensile Creep - Region Close to Fracture Surface X 400, Chemical Etch.

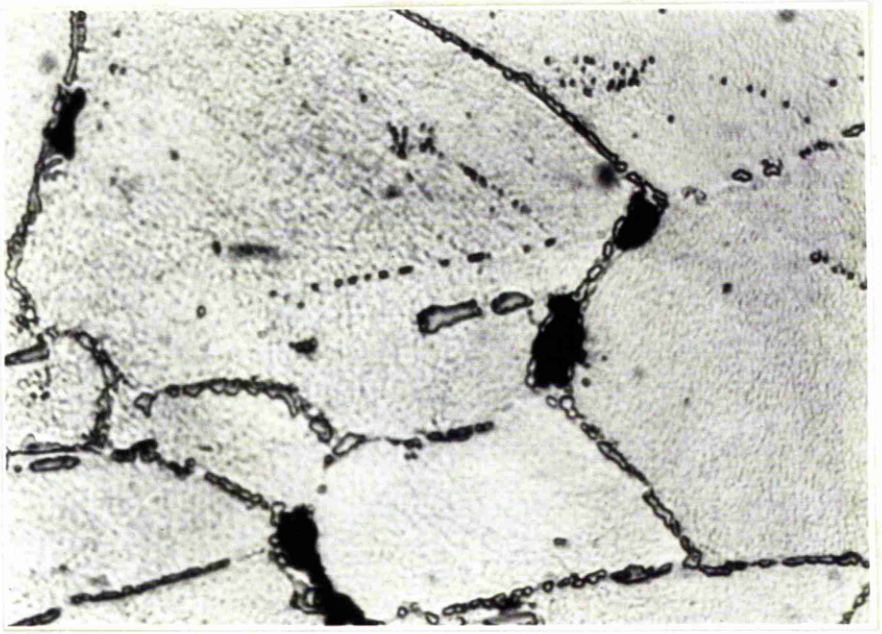

Fig. 29. Cavitation Cracks after 10% Tensile Creep Strain X 1100, Chemical Etch.

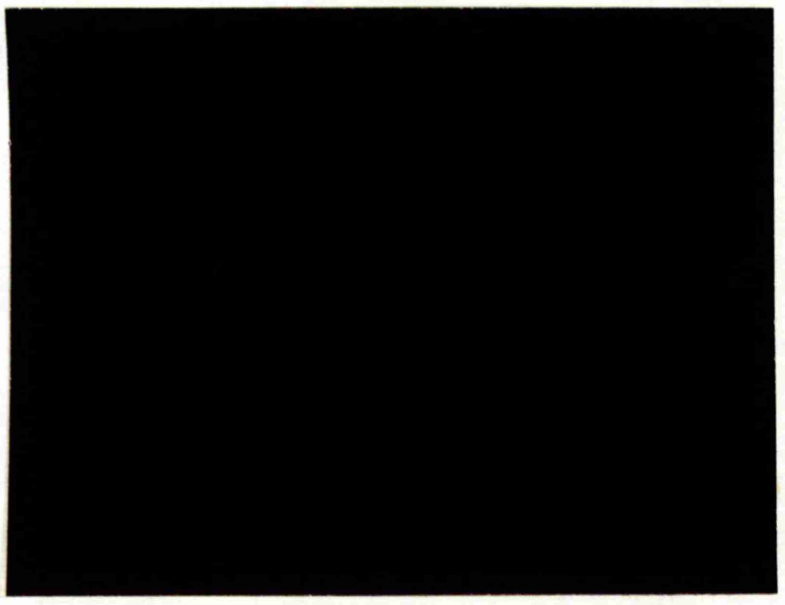

Fig. 30. Isolated Cavitation Crack X 1100, Chemical Etch.

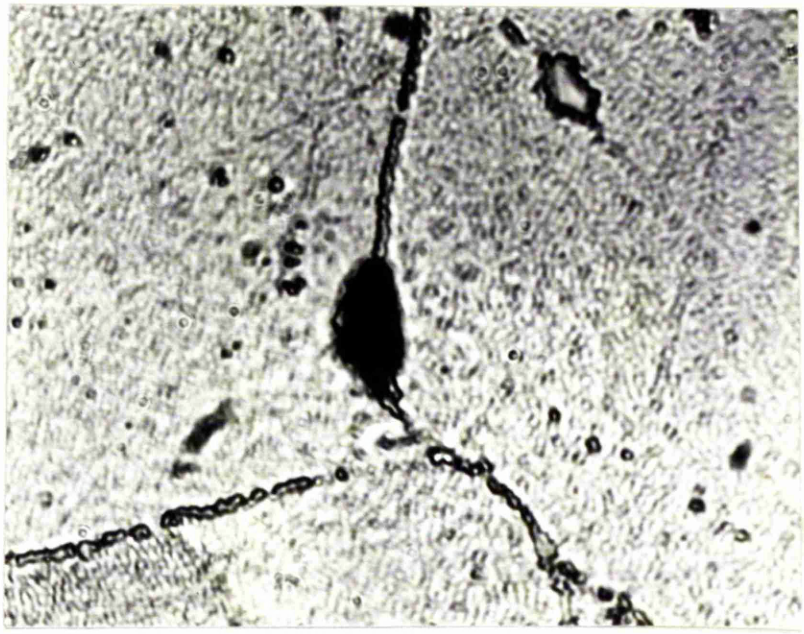

Fig. 31. Large Cavitation Crack X 1000, Chemical Etch.

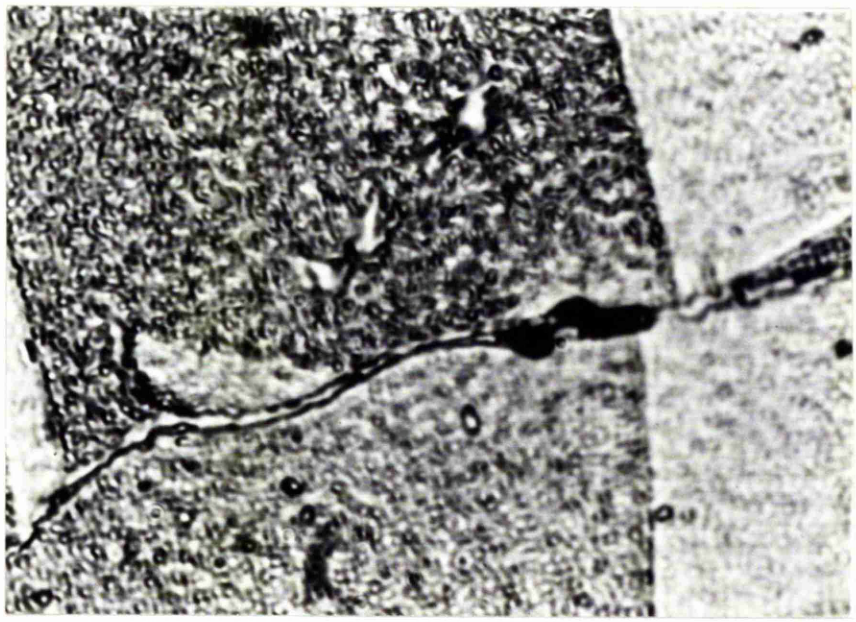

Fig. 32. Small Cavitation Crack X 1100, Chemical Etch.

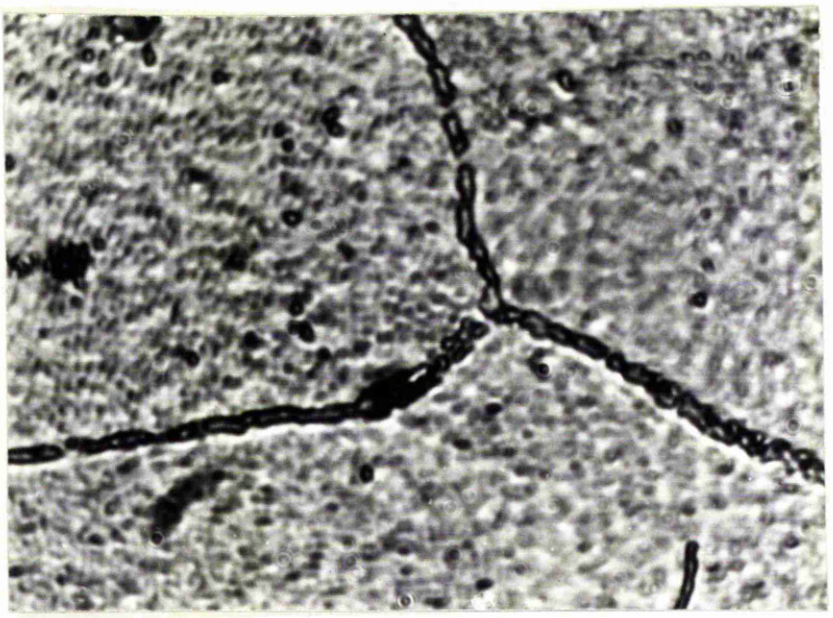

Fig. 33. Small Cavitation Crack, X 1100, Chemical Etch.

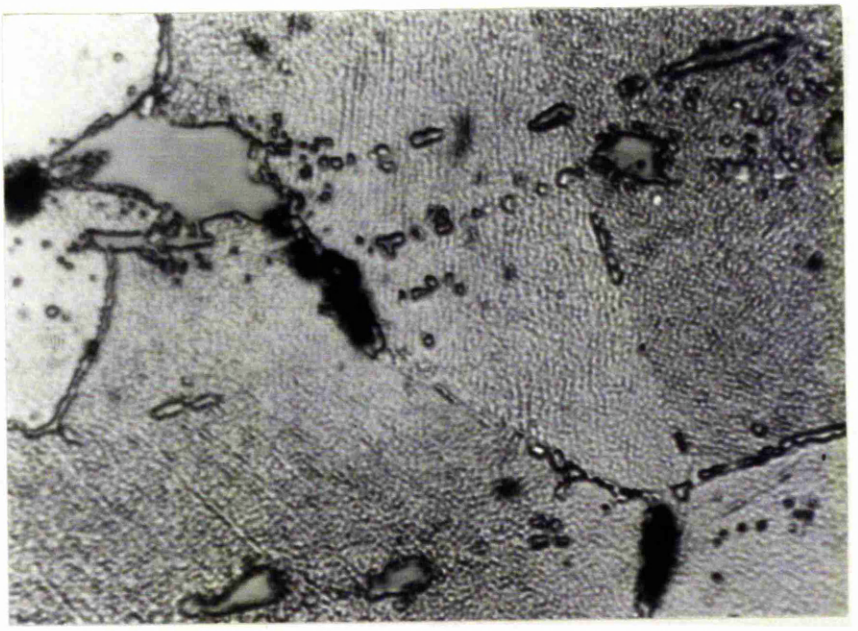

Fig. 34. Cavities Associated with a Massive Grain Boundary Particle, and with a Grain Boundary Triple Point X 1100, Chemical Etch.

Fig. 35. Crack Associated with a Massive Grain Boundary Particle X 1100, Chemical Etch.

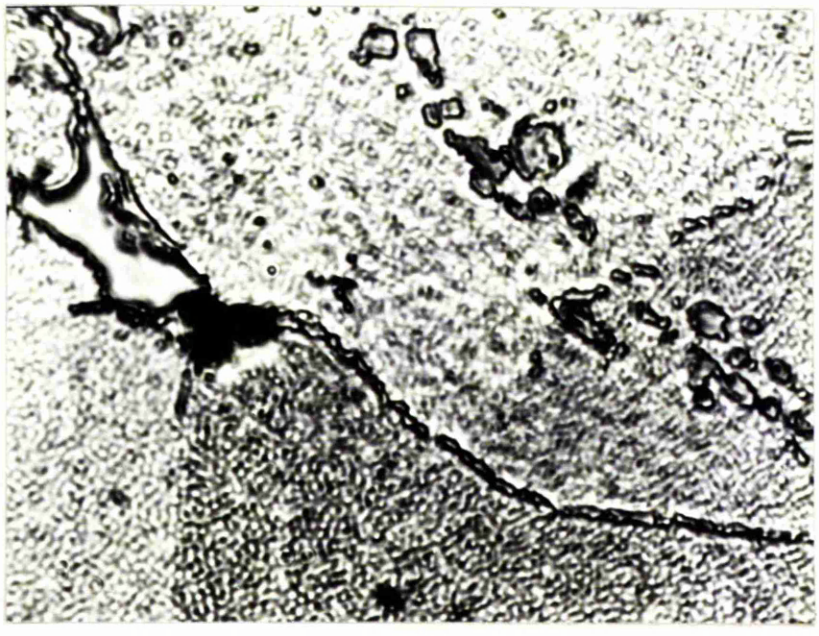

Fig. 36. Cavitation Crack Associated with a Massive Grain Boundary Particle X 1100, Chemical Etch.

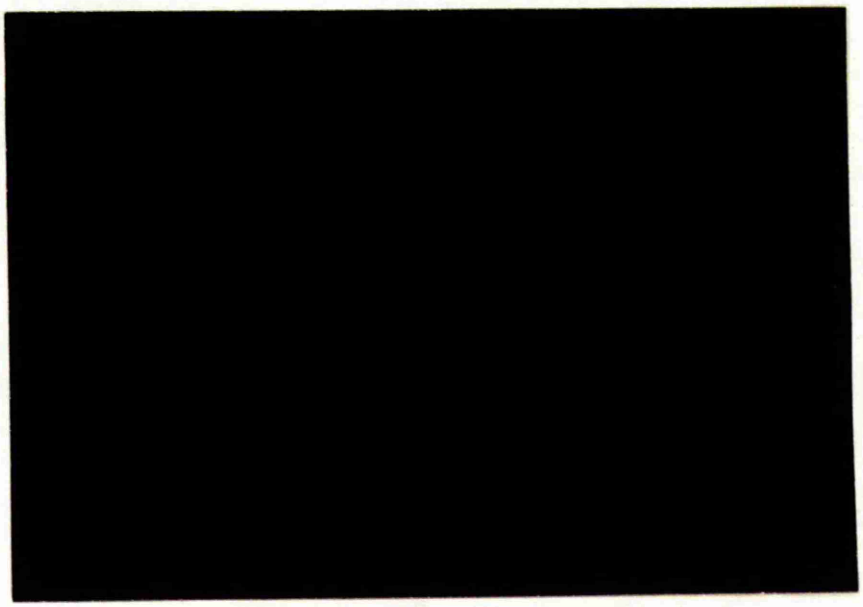

Fig. 37. Cavitation Crack Associated with a Massive Grain Boundary Particle X 1100, Chemical Etch.

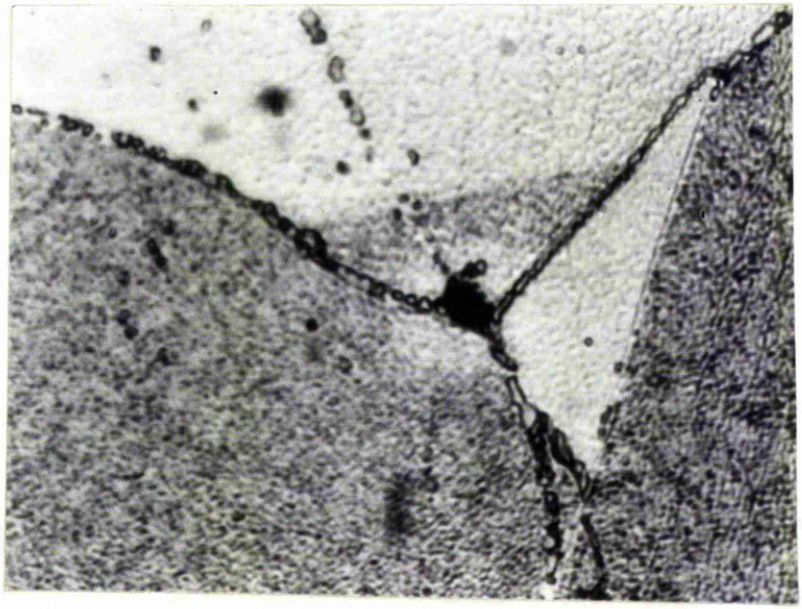

Fig. 38. Cavitation Crack Associated with Grain Boundary Triple Point X 1100, Chemical Etch.

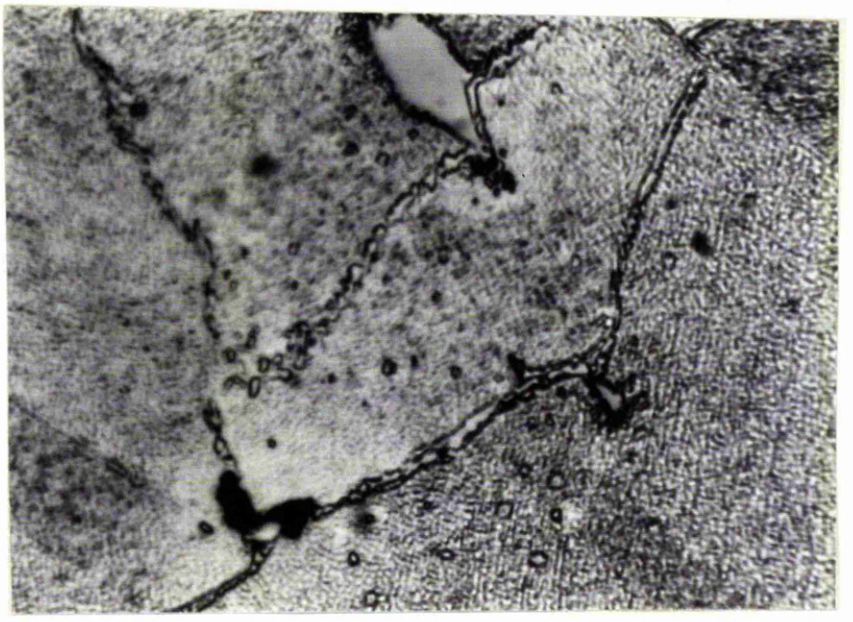

Fig. 39. Cavitation Crack Associated with Two Grain Boundaries X 1100, Chemical Etch.

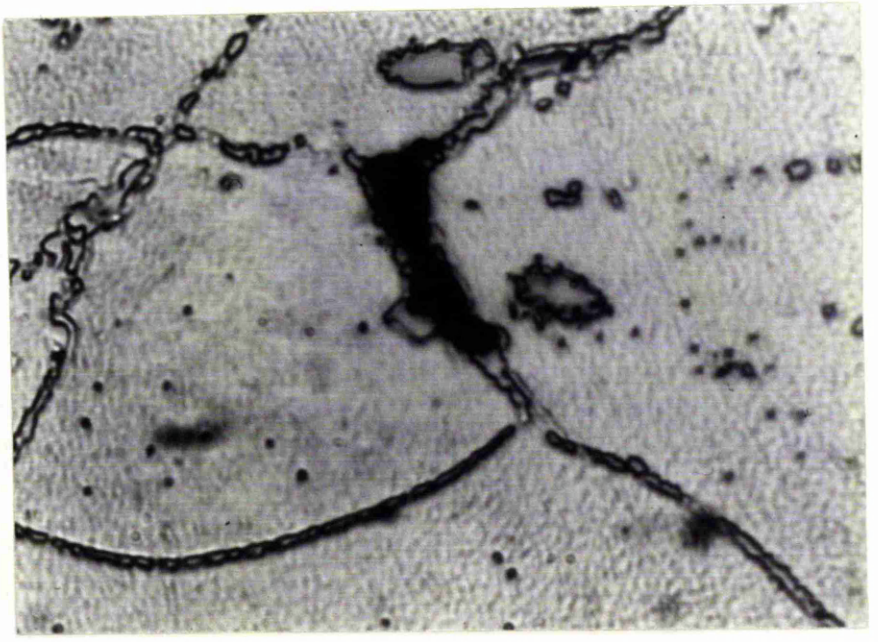

Fig. 40. Typical Wedge-type Crack from the Necked region of a Tensile Creep Specimen fractured at 1000°C X 1100, Chemical Etch.

Fig. 41. Large Wedge Crack from a Necked Region X 600, Chemical Etch.

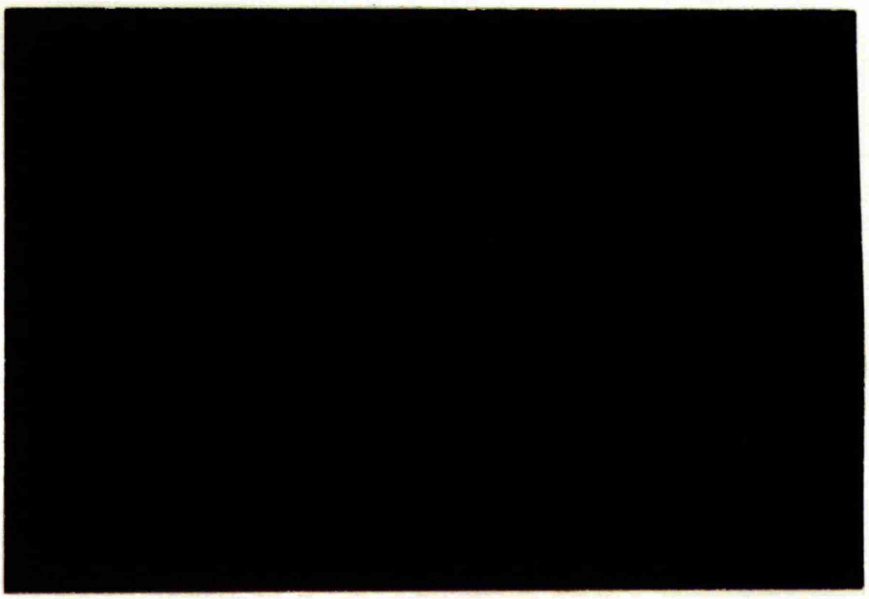

Fig. 42. Fracture Surface of Tensile Creep Specimen fractured at 800°C X , Chemical Etch.

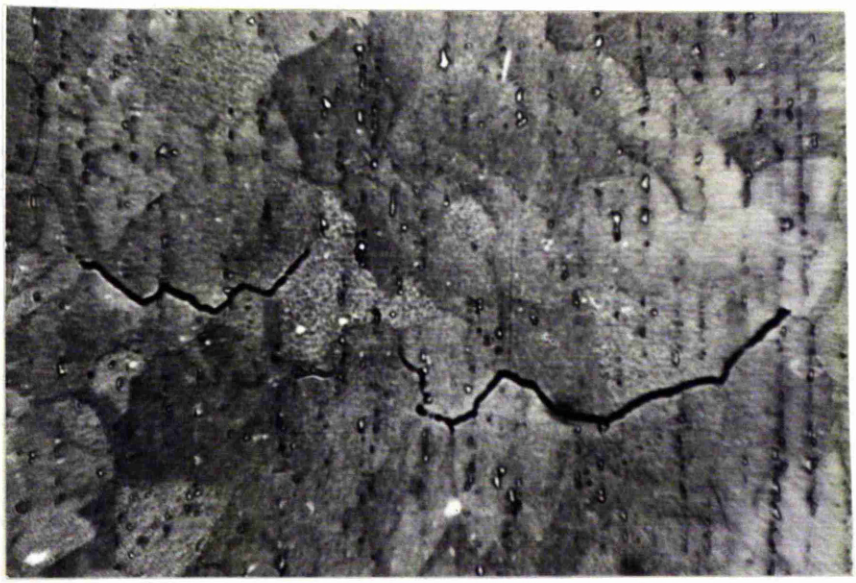

Fig. 43. Unusually Long Grain Boundary Cracks after 4% Tensile Creep Strain at 950°C X 200, Chemical Etch.

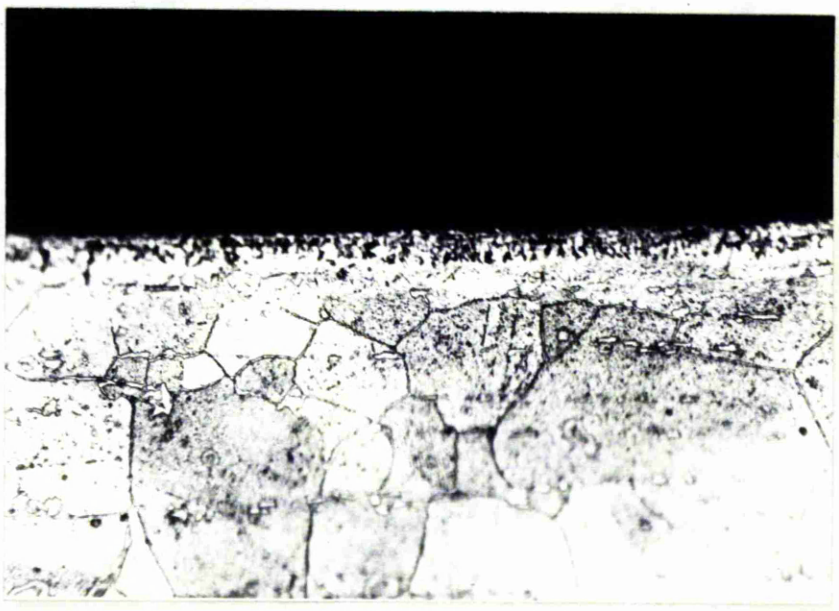

Fig. 44. Effect of Oxidation on the Surface of a Creep Specimen X 700, Chemical Etch.

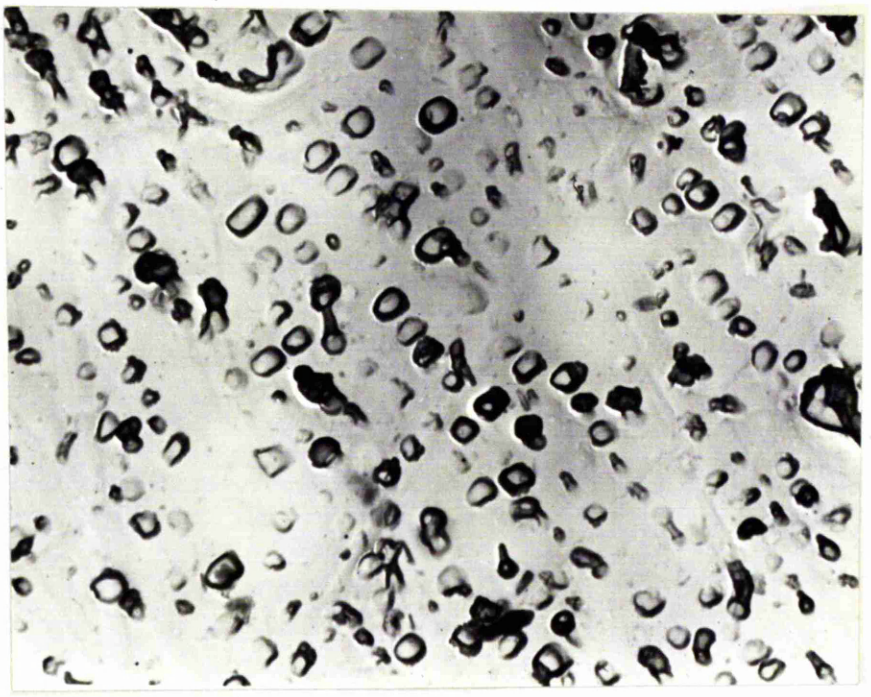

Fig. 45. Replica Electron Micrograph of Tensile Creep Test Specimen after 45 hours at 950°C under a load of 17,000 lb.in . X 8000.

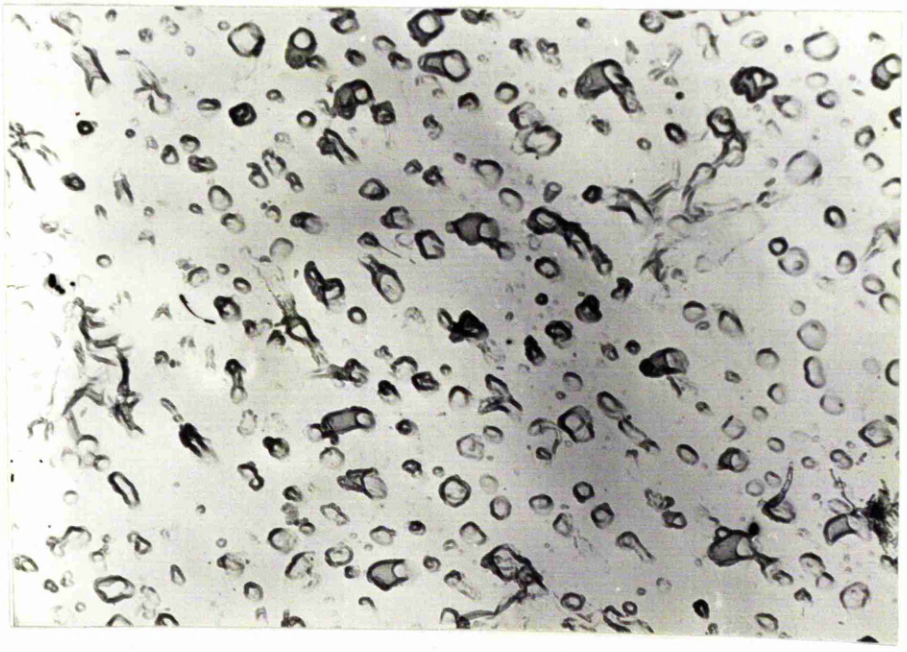

Fig. 46. Replica Electron Micrograph of Compressive Creep Specimen after 37 hours at 950°C under a load of 17,000 lb.in .